TAMPEREEN TEKNILLINEN YLIOPISTO
TAMPERE UNIVERSITY OF TECHNOLOGY

CHRISTIAN STENROOS

PROPERTIES OF ICEPHOBIC SURFACES IN DIFFERENT ICING CONDITIONS

Master of Science Thesis

Examiners: Prof. Petri Vuoristo and
Dr. Heli Koivuluoto.
Examiners and subject approved in
the Faculty of Engineering Sciences
Council Meeting 9.9.2015.

ABSTRACT

TAMPERE UNIVERSITY OF TECHNOLOGY
Master's Degree Programme Materials Science
STENROOS, CHRISTIAN: Properties of icephobic surfaces in different icing conditions
Master of Science Thesis, 108 pages
October 2015
Major: Surface engineering
Examiners: Prof. Petri Vuoristo, Dr. Heli Koivuluoto
Keywords: Icing, icephobic, ice type, ice adhesion, coatings

Icing inflicts serious problems for different branches of industries by decreasing efficiency, productivity and safety. Aviation, off-shore platforms, sea vessels, power network and wind power suffer from the problems that icing causes. Ice accretion causes external loads on the structures, which can collapse structures or danger the safety. For example ice accretion on the aircraft wing decreases its lifting abilities and may result the loss of controlling. Typically ice is hard to remove from the surface. Therefore many methods have been developed in order to melt or detach accreted ice from the surface. The most commonly utilized methods are based on electrothermal heating, where interface between ice and substrate is heated until the ice detaches. Also de-icing chemicals are used on roads and airplane wings.

These abovementioned methods are not environmentally friendly options and therefore different types of coatings for anti-icing solutions have been studied in the literature. Fluorine and silicone containing polymer coatings have been showed to offer icephobic properties. Furthermore superhydrophobic coatings have been studied due to their water repellency and low ice adhesion strengths have been discovered. However superhydrophobic coatings will lose their performance in different icing conditions, which is why it is crucial to study the formation mechanisms of different ice types. Large number of factors such as water droplet size, temperature and wind speed has an effect on icing, its harshness and formation of different ice types. Moreover, influence of different properties on ice adhesion has similar complexity than icing event. Wetting behaviour, surface roughness, surface chemistry and icing conditions have an effect on ice adhesion strength.

The primary aim of this thesis was to study the effect of different icing conditions on the formation of different ice types and furthermore their effect on ice adhesion strength. Ice accretions were performed in the icing wind tunnel in nine different icing conditions. Ice adhesion strength of variety of coatings and surfaces was evaluated with centrifugal ice adhesion test. It was discovered that ice adhesion strength is influenced by the ice type, wetting behaviour and surface chemistry. Nevertheless correlation between ice adhesion strength and the influencing factors needs to be further studied.

TIIVISTELMÄ

TAMPEREEN TEKNILLINEN YLIOPISTO
Materiaalitekniikan koulutusohjelma
STENROOS, CHRISTIAN: Jäänestopinnoitteiden ominaisuudet eri jäätymisolosuhteissa
Diplomityö, 108 sivua
Lokakuu 2015
Pääaine: Pinnoitustekniikka
Tarkastajat: Prof. Petri Vuoristo, TkT Heli Koivuluoto
Avainsanat: Jäätyminen, jäänesto, jäätyyppi, jään adheesio, pinnoitteet

Jäätyminen aiheuttaa vakavia ongelmia eri teollisuuden toimialoille vähentäen hyötysuhdetta, tuottavuutta ja turvallisuutta. Ilmailu, öljyn porauslautat, merialukset, sähköverkosto and tuulivoima kärsivät erityisesti ongelmista, joita jäätyminen aiheuttaa. Jään kertyminen aiheuttaa rakenteiden kuormittumista, mikä voi romahduttaa rakenteita tai vaarantaa turvallisuutta. Esimerkiksi jään kertyminen lentokoneen siipeen heikentää sen nostokykyä ja voi aiheuttaa koneen ohjauksen menettämisen. Tyypillisesti jäätä on hankala irrottaa pinnoilta. Tämän vuoksi useita eri menetelmiä on kehitetty sulattamaan tai irrottamaan kertynyt jää pinnoilta. Yleisimmin hyödynnetyt menetelmät perustuvat sähkötermiseen lämmityselementtiin, mikä perustuu jään ja pinnan välisen rajapinnan lämmittämiseen kunnes jää irtoaa pinnasta. Lisäksi jäänpoistokemikaaleja on käytetty teillä ja lentokoneen siivillä.

Edellä mainitut menetelmät eivät ole ympäristöystävällisiä vaihtoehtoja and sen johdosta erityyppisiä pinnoitteita on tutkittu kirjallisuudessa. Fluoria ja silikonia sisältävät polymeeripinnoitteet ovat osoittaneet jäänesto-ominaisuuksia. Lisäksi superhydrofobisia pintoja on tutkittu laajalti niiden veden hylkimisominaisuuksien takia, ja on havaittu matalia jään adheesiovoimia. Kuitenkin superhydrofobisten pintojen suorituskyky heikkenee merkittävästi eri jäätymisolosuhteissa. Useat eri tekijät, kuten pisarakoko, lämpötila ja tuulen nopeus vaikuttavat jäätymiseen, sen rankkuuteen ja eri jäätyyppien muodostumiseen. Lisäksi jään adheesion vaikuttavien tekijöiden lukumäärä on yhtä moninainen kuin jäätapahtumaan vaikuttavien tekijöiden määrä. Kastuvuuskäyttäytyminen, pinnankarheus, pintakemia ja jäätymisolosuhteet vaikuttavat jään adheesiovoimaan.

Tämän diplomityön päätavoite on tutkia eri jäätymisolosuhteiden vaikutusta eri jäätyyppien muodostumiseen ja jään adheesiovoimaan. Jään kerrytykset suoritettiin jäätävässä tuulitunnelissa yhdeksässä eri jäätymisolosuhteessa. Eri pintojen jään adheesiovoima mitattiin sentrifugaalisella jään adheesiotestillä. Jäätyypin, kastumiskäyttäytymisen ja pintakemian havaittiin vaikuttuvan jään adheesiovoimaan Korrelaatio jään adheesiovoiman ja siihen vaikuttuvien tekijöiden välillä vaatii silti lisätutkimusta.

PREFACE

This master thesis was carried out at the Department of Materials Science, Tampere University of Technology during the years 2014-2015. The thesis was funded by EU-project (FP7) Hydrobond "New cost/effective superhydrophobic coatings with enhanced bond strength and wear resistance for applications in large wind turbine blades" The thesis was supervised by Prof. Petri Vuoristo and Dr. Heli Koivuluoto. I would like to express my deepest gratitude for both of them for their support, guidance and enthusiasm to subject.

Several persons have assisted me in the thesis. I am pleased to express my gratitude to M.Sc. Jari Knuuttila and M.Sc. Annika Lautala for cooperation with coatings. Many persons have also assisted me in the icing test and I would like to thank M.Sc. Riku Ruohomaa, B.Sc. Antti Eerikäinen, B.Sc. Henna Niemelä-Anttonen, B.Sc. Keijo Penttilä and B.Sc. Juuso Pohjola for their help and knowledge. I would also like thank Mr. Mikko Kylmälahti and Mr. Ari Varttila for their assistance. In addition I want to express my gratitude to Dr. Hannu Teisala for meaningful discussions related to this subject. Finally I would like to thank all the staff of Department of Materials Science.

This work would not have been accomplished without the help of my family and friends. For you I am deeply grateful. Last but not least, I would like to thank from the bottom of my heart my beloved Eveliina for her understanding, support and love.

Tampere, September 2015

Christian Stenroos

TABLE OF CONTENT

Abstract ii
Tiivistelmä iii
Preface iv
Terms and their definitions vi
1 Introduction 1
2 Icing issues 3
2.1 Aviation 3
2.2 Offshore and marine 6
2.3 Energy production 8
2.4 Power lines 10
2.5 Tall structures 12
3 Ice accretion on surfaces 15
3.1 Icing event 15
3.1.1 Heterogeneous nucleation theory 17
3.1.2 Severity of ice accretions 20
3.2 Atmospheric icing types 25
3.2.1 Precipitation 25
3.2.2 In-cloud icing 28
4 Methods and materials against icing 32
4.1 Methods against icing 34
4.1.1 De-icing methods 34
4.1.2 Anti-icing 37
4.2 Anti-icing coating materials 40
4.2.1 Polymeric coatings 41
4.2.2 Polymer composite coatings 44
4.2.3 Surface treatments 55
4.3 Summary of the materials and results from literature 57
5 Research methods and materials 61
5.1 Contact angle measurements 61
5.2 Surface roughness 62
5.3 Ice accretion 62
5.4 Ice adhesion 64
5.5 Materials 65
6 Results and discussion 66
6.1 Wettability 66
6.2 Surface roughness 69
6.3 Accretion of different ice types at different temperatures 73
6.4 Results of the ice adhesion tests 79
7 Conclusion 95
REFERENCES 97

TERMS AND THEIR DEFINITIONS

Definitions:

accretion	ice or snow build up on structure
anti-icing	process that prevents ice formation over the protected surface
Cassie-Baxter	wetting state, where air is entrapped between the surface asperities and water droplet i.e. water droplet is resting on the top of asperities
de-icing	removal of accreted ice or snow from a surface
glaze	transparent, dense ice formed in high LWC icing events
icephobic	surface property that minimizes ice adhesion
instrumental icing	period during which ice remains on the structure
mixed	ice type between rime and glaze ice.
peltier	ice adhesion measurement technique, where molded ice columns are pushed with the constant rate until ice de-taches
rime	white, feathery, porous ice type, formed in low LWC ic-ing events
Wenzel	wetting state, where water droplet fill the surface texture
zero degree cone test	ice adhesion measurement technique, where ice is molded on the pile which is pushed until ice detaches.

Greek symbols:

α	original phase
β	new forming phase
Δg	is volumetric phase change free energy of water-ice trans-formation
ΔH	volumetric latent heat from freezing event
$\Delta\mu_{Iw}$	chemical potential difference between ice and water
$\acute{\eta}_1$	collision efficiency of supercooled water droplets
$\acute{\eta}_2$	sticking efficiency of supercooled water droplets
$\acute{\eta}_3$	accretion efficiency of supercooled water droplets
θ	contact angle
ν_i	molar volume of ice phase
σ_{iw}	interfacial energy between ice and water
τ	maximum shear stress,
ω	angular velocity

Latin symbols

A	cross-sectional area/ area of ice
f(θ)	catalytic factor

F	force
F_{water}	flow rate of water
h_{nozzle}	spraying height
m	mass
N	nucleant surface
P_{air}	pressure of compressed air
$P_{water¨}$	pressure of water
r	radius
R_a	average roughness
R_z	mean peak to valley height of roughness profile
S_a	average height of surface (area)
S_z	maximum height (area)
t	time
T_m	melting point of ice
T_w	water droplet temperature
T_{water}	the temperature of water at the nozzles
V	wind speed
w	liquid water mass/unit volume
W_{het}^*	maximum work for heterogeneous nucleation
W_{hom}^*	maximum work for homogeneous nucleation

Materials and chemicals:

Al	mirror-polished aluminum tested in this thesis
Aerosil R805	silicon dioxide, SiO_2, silica
$C_2H_2O_4$	oxalic acid
$C_3H_8O_3$	glycerol
CeO_2	cerium dioxide, ceria
DMPA	dimethylolpropionic acid
FAS-13	1H,1H,2H,2H -perfluoroethoxysilane
FAS-17	1H,1H,2H,2H -perfluorodecyl-triethoxysilane
F-Clean	EFTE, copolymer of tetrafluoroethylene and ethylene
$FeCl_3$	iron (III) chloride
Fluorolink®S10	α,ω- triethoxysilane terminated polyfluorinated polyether
Fluorotelomer V	halfly triethoxysilane terminated fluorinated polyether
GPTMS	(3-glyxidylpropyl)trimethoxy silane
HCl	hydrochloric acid
H_2SO_4	sulphuric acid
H_3PO_4	phosphoric acid
HVIC 1547	silicon rubber
IPDA	isophorone diamine
NH_4HCO_3	ammonium bicarbonate
R2180	silicone elastomer (Nusil technology LLC)

RTV11	room temperature vulcanized silicone rubber (GE Bayern Silicones)
RTV silicon rubber	room temperature vulcanized silicon rubber
PAA	aminoterminated polyacrylate
PC	polycarbonate
PDMS	poly(dimethylsiloxane)
PEG	polyethylene glycol
PEMA	poly(ethyl methacrylate)
PE-PP-copolymer	copolymer of polyethylene (PE) and polypropylene (PP)
PEPE	polyfluorinated polyether
PMMA	poly(methyl methacrylate)
POSS	polyhedral oligomeric silsesquioxanes
PP	polypropylene tape tested in this thesis
PSS	sulfonated polystyrene
PTFE	polytetrafluoroethylene
PU	polyurethane
PU-paint	commercial polyurethane paint tested in this thesis
PVDF	polyvinylidene fluorinde
SH1	F-containing superhydrophobic hybrid coating, Millidyne
SH2	superhydrophobic coating, Ultra Ever Dry®
TEOS	tetraethylotrhosilicate
TiO_2	titanium dioxide, titania
Zonyl 8470	Perfluoroalkyl methacrylic
ZrO_2	zirconium dioxide, zirconia

Abbreviations:

AFM	atomic force microscope
ARF	adhesion reduction factor compared to aluminum
ESEM	environmental scanning electron microscope
DRIE	deep reactive ion etching
IEA	International Energy Agency
ISO	International Organization for Standardization
LWC	liquid water content, typically associated
MVD	mean volume diameter
PECVD	plasma enhanced chemical vapor deposition
PIID	plasma immersion ion deposition
RTV	room temperature vulcanized
SEM	scanning electron microscope

1 INTRODUCTION

Icing inflicts serious problems for different branches of industry in the cold and mountainous parts of the world. It has been reported that icing causes decreased efficiency, safety hazards and structure failures in Scandinavia, Alps, Northern America, Russia, Japan, China and even in South Africa. [1,2,3,pp.2–3] In addition icing has caused serious issues for aviation, which had led into fatal incidents. [4,5] Ice accretion on the airplane wing decreases its lifting abilities, which may result loss of flight control. [6] Besides the aviation, icing causes serious issues for other branches of industries. On the wind turbine blades accreted ice changes the aerodynamic performance of blade and increases loads of the structure, which require standstills that decrease productivity of the turbine. [7,8] Increased loads due to ice accretion may also collapse engineered structures. [3,p.83, 9–11] The most distinct incident related to icing was observed in Canada in January 1998, where ice storm created heavy freezing rain events causing wide destruction on different structures of power network. In total 1,300 high voltage transmission line towers and 35,000 distribution line structures were collapsed or destroyed due to high ice loads. [3,p.83,9] As a result of this catastrophe over two millions people suffered from power outage for weeks and the economic losses were considerable. [9]

Clearly icing possesses life-threatening issues and may results substantial economic losses. Therefore variety of techniques has been introduced to aid ice removal from the surfaces. The basic method that has been utilized to protect surface from icing is based on the electrothermal heating elements, which will melt the interface between ice and substrate facilitating the ice removal.[8,12] Pneumatic boots have been applied on the airplane wings, which performance is based on change of profile shape that results cracking of the ice. Chemicals have been also applied on the surface to melt ice or snow, typically from the airplane wings. Drawback of the chemicals is that they contain harmful chemicals and offer only temporary protection.

Coatings have been presented to offer environmentally friendly option, because no external energy is needed and coatings can be tailored to be free of harmful chemicals. Different coating strategies have been presented, which can be roughly divided into polymeric coatings containing fluorine or silicone compounds and superhydrophobic polymer composite coatings. Their performance as icephobic coatings is based on the hydrophobicity, which is achieved with the proper surface chemistry and roughness. Future aim is to be able to prevent ice formation on the structures.

The aim of this thesis is to study icephobic performance of different type coatings ranging from superhydrophobic to polymer surfaces. Their properties are evaluated in the different icing conditions. Ice accretions are performed in the icing wind tunnel in nine different icing conditions. Ice adhesion strengths are measured with the centrifugal ice adhesion test. The effect of different icing conditions on the icephobic performance of the coatings is inadequately studied in the literature. Therefore, the main goal of this thesis is to study the effect of icing conditions and ice type on the ice adhesion strength. The secondary aim is to evaluate the effect of surface properties (wettability and surface roughness) on the ice adhesion strength. In addition, the performance of icing wind tunnel is discussed in this thesis.

The icing issues in different branches of industry are evaluated in Chapter 2, which works as a motivation for icing prevention and mitigation. The origin of the icing event is discussed in Chapter 3, where ice formation and severity of icing are evaluated. In addition, classification and characteristics of different ice types are discussed in Chapter 3. Methods against icing are stated in the Chapter 4, where different coating strategies and materials are widely expressed. Chapter 5 presents research methods and materials used in this thesis. The results and discussion are in Chapter 6, where wetting behavior, surface roughness, ice accretion, ice adhesion results and their connections are analyzed. Finally conclusions and future recommendations are presented.

2 ICING ISSUES

Engineered structures in the cold climate regions are prone to icing, which causes several problems for different branches of industries. It has been reported that the icing has induced severe problems in the Scandinavia, Northern-America, Northern Russia and also in some parts of Asia, for example in Japan and China. [2,13] The altitude is also great factor in icing event, which is why the icing is a common phenomenon in the mountain areas or in the aviation. The accreted ice causes increased loads on the structures, which can lead to failures in the materials structure or in the worst case the collapse of the whole structure. These failures inflict serious safety problems for example in the aviation and transportation industry. [3]

The icing on the different engineered structures inflicts also other troubling issues than increased loads. Accreted ice can decrease dramatically the functionality of different structures, for example accreted ice drastically weakens the performance of aircraft wing [6]. The decreased performance also affects negatively the safety aspects of different devices. For example the accreted ice on the aircraft wings has led to many fatal accidents. Also the working conditions can be dangerous due to ice loads, for example superstructure icing in the sea vessels hinders the navigation of the ships and also the working environment of the crew on the deck. [14] One of the major issues is related to decline of the productivity in different energy production facilities. For instance ice accretion on the wind turbine blades affect the aerodynamic functioning of the blade and may lead to standstill of the whole turbine in order to prevent larger damages. These standstills will naturally decrease the efficiency of the wind turbines. [7,15]

In this chapter, the main fields that are suffering from the problems caused by icing are presented. These fields include aviation, offshore and marine operations, energy production and also tall structures. In these subchapters the icing problems are evaluated and also some of the countermeasures against the icing are described. More thorough description of the methods and strategies against the icing are presented in Chapter 4

2.1 Aviation

Aviation industry has been used as a typical example of industry, which has battled with icing issues. Problems are related to two different cases in-flight icing and ice or snow accretion at the airports. These problems have caused many accidents during the past decades and some of them have also led to the fatal incidents. According to American Safety Advisor 12 % of all flight accidents were due to the icing weather conditions,

which 92 % where happening in-flight. [6] Anti- and de-icing systems, such as pneumatic boots and piccolo tube heating system, have been developed to prevent the ice accretion, but as the statistics show these systems have failed to demonstrate proper level of functionality. [6,16,pp.26–29]

In-flight icing on the airplane wings can happen in several ways.[6,16,pp.13–14] Firstly the ice accretion can occur before the anti- and de-icing systems are switched on, when the ice accretion is observed by small accretions on the leading edge. The more severe icing is occurring, when airplane encounters high liquid water content (LWC) clouds, which cause runback ice and ridge formation on wing as illustrated in Fig. 1. [18] These ice accretions can be located on the different parts of the wing. This type of icing is considered to be the most dangerous type on the wings, because it dramatically changes the aerodynamic profile of the wing and decreases its lifting ability. The third category contains irregularly shaped glaze ice accretion on the random parts of the wings. [6,17] These ice shapes are formed in the longer contacts with icing conditions. The frost formation on the ground during long standstills is the last category. Formed frost is usually dealt by spraying de-icing chemicals on the wings, but untreated it can decrease the lifting ability of the wings. [6]

Figure 1. *Heavy in-flight icing on the airplane wing. [18]*

Failure in de-icing actions can lead to disaster as happened with Continental Airlines Inc. flight 1713, which was designated to fly from Denver, Colorado to Boise, Idaho. The flight was scheduled flight and the de-icing actions were performed properly before the departure. The delay between the actual take-off time and de-icing was 27 minutes. Shortly after the take-off the plane started to rotate and the flight crew lost the control of the plane leading to uncontrolled crash. The crash site is presented in Fig. 2 [19]. This

accident caused the loss of 28 lives, because the deicing actions were insufficient to prevent icing on the wings of the airplane. Also the investigators stated that delay between the take-off and de-icing was too long. [4]

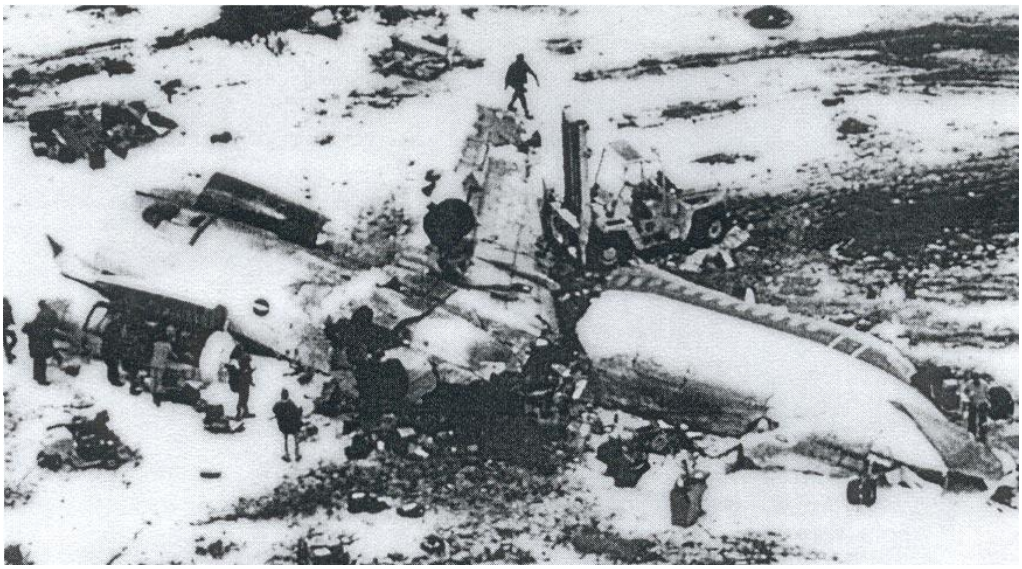

Figure 2. *Crash site of the Continental Airlines Inc. Flight 1713. [19]*

Icing can also inflict severe problems during the flight as the Simmons Airlines American Eagle flight 4184 demonstrated. The airplane encountered icing conditions at 2400 meters. The ice was accreted in the form of ridge on the wing. The location of the accreted ice was behind the de-icing boots, which made removal attempts pointless. The aileron hinge were frozen in the reversal direction, which caused plane to lose flight control and crashed causing 68 people to lose their lives. [5] The remainders of the wreckage are shown in Fig. 3.[20]

Figure 3. *Crash site of Simmons Airlines American Eagle flight 4184. [20]*

As these cases point out the ice accretion the aircrafts possess real thread, which should be encountered by proper actions. De-icing at ground has been performed by spraying chemicals, usually ionic glycol based salts, on the wings as showed in Fig. 4. [21] This method has its vulnerabilities, because it will only remove the accreted ice and snow and offers protection only for short time as the Continental Airlines Inc. accident showed. More permanent solution is needed to prevent this sort of disasters.

Figure 4. *De-icing of the airplane with de-icing chemicals. [21]*

During the flight, pneumatic boots have showed that they indeed can offer de-icing option on the wing. Although this system has its drawback, because it only offers the ice removal for the protected part of the wing i.e. the leading edge. The others parts of the wing are vulnerable for the for example the runback icing or ridge formation. [16,pp.27–28] The runback ice on the wing can also be very harmful, because in the worst case it can decrease lift by 80 % significantly reducing aerodynamic performance. [6]

2.2 Offshore and marine

Icing causes serious problems for marine and offshore industries and its impact has increased due to opening Northern Sea Route through the Arctic Ocean.[12,14,22,23] Northern sea route is now accessible for longer period in the summer months (from June till October), which has increased the marine traffic in the shipping lane. [24] Icing on sea vessel hinders the working conditions that ships' crews are facing. Accreted ice loads can form large and heavy structures on the ships superstructure, which possess a real threat on safety working conditions. Also the heavy loads can change the center mass point of the ships, which severely affect the maneuverability of the vessel. [14,22] The different devices, such as navigation and communication equipment, on the super-

structure of the sea vessels are prone to icing as Fig. 5a) indicates. In addition, the access on the life boats can be hindered due to ice formation. These ice loads are traditionally removed manually by the crew, but the removal is challenging and can in the worst case lead to injuries due to falling ice. Heavily iced ship's deck is presented in Fig. 5 b). [14,23]

Figure 5. *Effect of severe icing on sea vessels' structures. a) Superstructure icing is covering the radar and communication antennas of the small ship [12] and b) heavy icing of the deck. [25]*

Different forms of the icing can occur in the seas. The traditional atmospheric icing produces glaze ice from freezing rain or drizzle and rime ice from the fogs and clouds containing supercooled droplets. Sea spray icing can be paralleled with other atmospheric icing due to its similar icing event. Sea sprays are typically formed by waves contacting different structures (sea vessel's hull, offshore platforms in the sea), which can deliver droplets on the superstructure of the vessel or platform causing superstructure icing. Icing due to sea sprays is considered to possess the greatest threat in marine and offshore operations [12,22] Figure 6 describes icing rates at the starting point of Northern sea route, based on data from the years 1979-2011. [22]

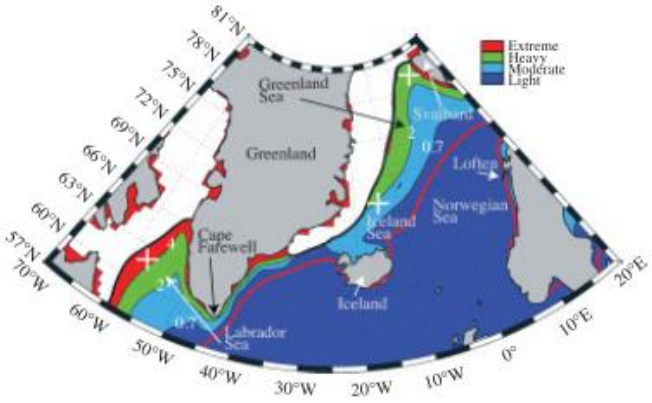

Figure 6. *Icing rates. during the winter months (December, January, February, March) based on data from 1979-2011. [22]*

Anti- and de-icing actions at the offshore platforms and marine vessels have been usually dealt by the crew, which manual de-ices accreted ice or snow with varying tools (etc. hammers, bats). This sort of de-icing is ineffective, personnel costs are relatively high

and also it has been reported to lead into accidents. [12] Anti- and de-icing methods would significantly reduce the safety risks on the functional areas of the off-shore platforms and the sea vessels' decks. It is also vital to guarantee the proper functioning of the communication and navigations systems, which are vulnerable for icing. [12,14]

2.3 Energy production

Icing produces substantial problems for different energy production techniques mostly due to decreased efficiency and functionality. Icing is considered as a problem in wind turbines, hydroelectric turbines and gas turbines, of which the icing on the wind turbine has been experienced to cause the biggest difficulties. [15] Due to great literature impact of the icing issues of wind turbines, this chapter is focused on the icing problems occurring in wind turbines. The heavy ice accretion on the wind turbine blades are presented in Fig.7 and Fig.8 [7,26]

Figure 7. *Iced up wind turbine blade. [26]*

Wind turbines can face harsh conditions, such as erosion, icing, temperature variations, during their operating lifetime. These turbines are often located in coasts, mountains or even off-shore, which makes them prone to different meteorological events like icing. [8,27] Wind turbines can encounter different types of atmospheric icing depending on the conditions. [7,8,15] Different ice types can accrete on the leading edges of the wind turbines, and mainly these ice types are formed from in-cloud icing events. In the in-cloud icing events the clouds and fog containing supercooled droplets will contact with turbine blade, and the icing occurs. Depending on the droplet size in the clouds or fogs rime or glaze is formed on the leading edge and nearby areas of the blades. [28] In Figure 8 the rime ice accretion on the leading edge of wind turbine is presented.

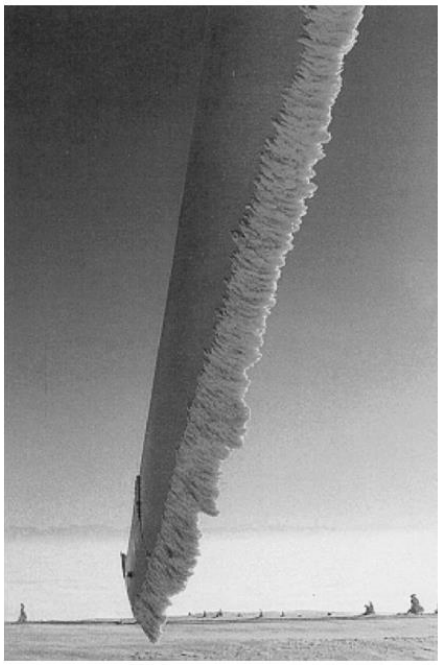

Figure 8. *Severe rime ice accretion on the leading edge of the wind turbine blade. [7]*

Ice formations on the wind turbines inflict severe problems on operation, reduce life time and causes power losses. Ice formed the blades and other parts of the turbine causes increased load on the turbine structure, which can in the worst case lead to failing on the wind turbine. Ice accretion on the leading edge also affects the aerodynamic performance of the wing. Accreted ice changes the aerodynamic balance of the blades, which reduces drag coefficient that increases power losses. Even the small ice accretion on blade will change the surface roughness of the blade and cause power losses due to changed aerodynamic behavior. [7,8,15]

Power losses due to the icing originate from different sources. As mentioned in the previous chapter changes in the aerodynamic profile of the blade can inflict power losses. In some cases the ice formation on the leading edge of the blade can lead to shutdown of the whole turbine. [7] This procedure greatly reduces the efficiency of the whole turbine. Standstill time can be reduced by applying the different de- and anti-icing methods [8,15], which are more thoroughly discussed in Chapter 4.1. By using de-icing methods the accreted ice can be melted during the standstill. Heating resistance based anti-icing methods can be operated during turbine operation. [2,8]

One important aspect concerning the icing in wind turbines is ice fall or ice throw risk. Different size ice pieces can plunge far away from turbine, which causes risk to nearby infrastructure (roads, building, houses). Due to weight and size of shedded ice pieces, they can inflict serious damage to people and structures in the nearby areas. Ice falling off from turbine also hinders the accessibility of maintaining personnel to wind turbine. Proper risk assessment is required in the wind turbine installations. [29]

2.4 Power lines

Different structures of the power network in the cold climates are prone to icing. Overhead lines, insulators and phase conductors are vulnerable to problems caused by icing – flashover due to icing, overloading and ice shedding. In the worst case this can lead to power outages, which has a significant socioeconomical impact. [3,30,31] Canada, USA, Russia, Norway, Sweden, Iceland, Finland and even China and Japan have reported that icing or snow accumulation on the power lines has caused failures in the power distribution systems. [9,30,31] Figure 9 shows the situation, where severe icing events can lead. [32]

Figure 9. *Rime ice accretion on the collapsed overhead line, Ålvikfjellet, Norway. [32]*

Problems that icing causes to power distribution network are substantial both economically and socially. From the engineering point of view, electrical issues related icing is also critical. During the accretion snow and ice act as an insulator between different parts of the insulators. Electrical flashover, illustrated in Fig. 10, can occur, when the accreted ice or snow layers start to melt. Transformation from solid state to liquid state increases highly conductivity of the water layer on the snow or ice, which creates flashover on the insulators. These flashovers can create voltage spikes, or even a complete loss of power. [3,p.322,33,34,pp.2–3] Ice and snow loads have also a mechanical impact on the power lines, which collapse the overhead lines. Ice shedding from the towers and other tall structures is considered as problem, because falling ice might damage lines and insulators and possess risk if lines or towers are located near roads. [35]

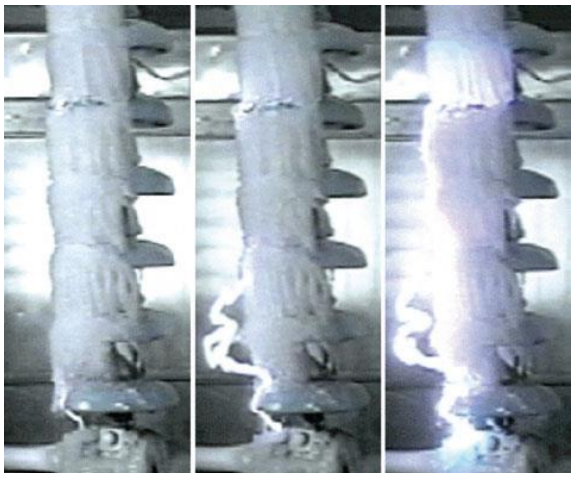

Figure 10. *Flashover over iced up insulator. [36]*

Overhead lines connect different areas and are often located in the elevated areas. Due to large variety of power line locations different ice and snow types can be formed over these structures. Overhead transmission lines, conductors and outdoor substations can face substantial icing events, as was the case in Canada in January 1998. An ice storm created heavy freezing rain events that caused disastrous destruction on the different structures of this power network. In total 1,300 high voltage transmission line towers and 35,000 distribution line structures were collapsed or destroyed to high ice loads. [3,p.83,9] As results of this catastrophe over two millions people suffered from power outage for weeks. [9] Figure 11 shows the collapsed towers as a result of this ice storm. [11] This underlines the importance of need for the research to find ways prevent or battle with the icing issues.

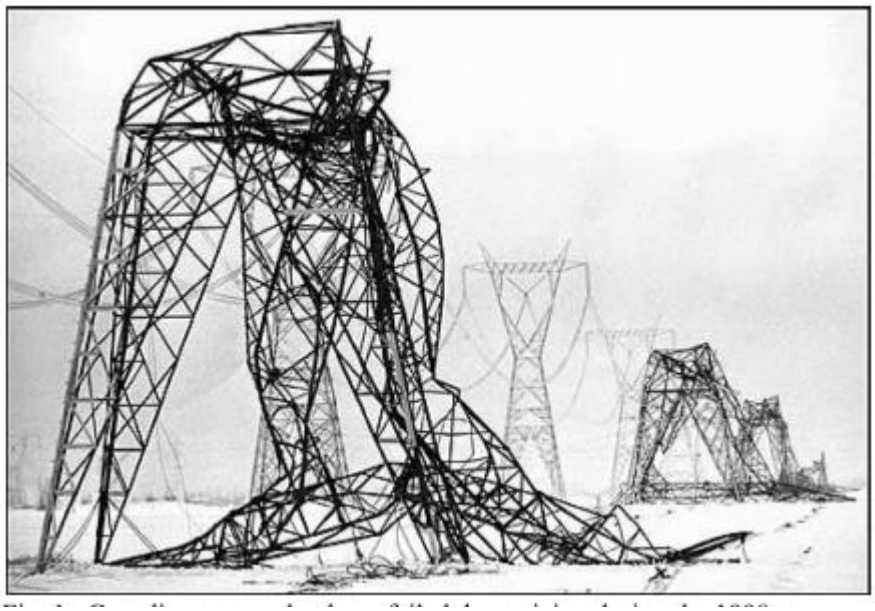

Figure 11. *Part of the destruction from ice storm in Canada 1998. Collapsed high voltage transmission line towers due to heavy ice loads. [11]*

Power network structures can face both precipitation and in-cloud icing. Precipitation icing can occur in the form of freezing rain or as wet snow accumulation. Freezing rain occurs usually near northern coastal areas such as Canada, Norway, Island and USA. Wet snow accumulation has been reported to cause problems in China, Japan, Iceland and other countries in Europa. Wet snow accretion is also problem in countries surrounding the Mediterranean such as Italy, France Slovenia. [3,pp.4–7] In-cloud icing produces rime or glaze ice depending on LWC- content in clouds or fog. In-cloud icing occurs more likely in the elevated areas or for tall structures. [3,pp.4–7,33] Generally rime, glaze and freezing rain have been considered to possess the greatest threat for the reliability of transmission lines. [3,p.33] Even so wet snow accretions have led to failures of transmission line structures in China and in 2008 100km of high voltage transmission was destroyed. [9] In Figure 12, wet snow has collapsed an overhead line in Norway [3,p.2].

Figure 12. *Collapsed overhead line due wet snow accretion.[3,p.2]*

Currently there are not any effective methods against icing on power lines. Different active methods such as heating based on Joule effect or applications based on de-icing chemicals. Both of these methods does not offer effective solution against icing, because heating based system require high amounts of energy and de-icing chemicals are not environmentally friendly. Passive icephobic coatings would offer the best solution, because they do not consume energy during their operative life and does not release any harmful chemicals into the nature. [34,pp.3–4]

2.5 Tall structures

Height has significant effect on icing probability and severity, which has to be considered in the design of different tall structures such as telecommunication and radio masts, wind turbines and tall power line towers.[10,37] In this chapter the focus is on elevated radio and telecommunication masts, which are often exposed to harsh atmospheric icing conditions. In Figure 13, there is presented the tall structure supporting heavy ice load.

***Figure 13**. Rime ice accretion on the mast. Mast's height is 127 m and it is located at the Ylläs, Finland. [10]*

The main problem in icing of tall structure is related to increased loads on the masts. Ice accretion increases total mass that mast's structure has to support and this needs to be taken into an account in the designing stage. [10,37,38] More severe effect on durability of the masts is observed, when the winds are ruled in. The accreted ice increases the surface area of the mast, which increases the effect of wind loads on the structure. [10, 37] Ice also interferes the signal transmissions and receptions. The guy wires, that support the masts, are also prone to icing. Ice accretion on the guy wires causes stretches on the cables, which can lead to breakdown of the wire. In addition ice accretions on the guy highlights the ice fall or ice shedding risk to nearby surroundings (roads, outdoor areas), which might cause the transfer of the mast position [39]. Atmospheric icing events can create heavy ice accretions, over 100 kg/m, on the masts, which can lead into the collapsing of the whole structure. [10,37,38]

One might expect that catastrophical failures of the tall masts do not happen so often. [37] Although during later part of 1990s over 140 radio or telecommunication masts collapsed due icing. Many of these failures were related collapsing of the power line towers and even the tallest and the most expensive masts did collapse during that period. [10,38] Economic impact of these failures is quite significant. The cost of the building of 300 m tall radio and television mast is over 5 M$. During the latter part of 1990s 23 tall 300m mast collapsed due to icing. [37]

There are not at the moment any anti- or de-icing systems, which could be efficiently adapted into the masts. Heating the surface of the mast is not effective way due to high surface area of the mast, but passive solution could offer the solution to this problem. However the current coating solutions do not offer reliable and cost-effective alternatives for icing prevention or mitigation. Due to lack of effective solutions for tall structures, the only countermeasures against the icing can be done in structural designing. By

properly estimating the ice loads, the structures can be designed to withstand the ice masses [38]. ISO 12494 standard “Atmospheric Icing of Structures” classifies accreted ice load into the different categories (R1-R10), which can be taken into account in the designing stage of the mast. Exploitation of the ISO-12494 standard relies heavily on the proper ice detection system, which measures reliably the correct ice loads on the structures. [10] Ice classes are further discussed in the Chapter 3.2.

3 ICE ACCRETION ON SURFACES

Atmospheric icing on the surfaces is very complex phenomena and multiple factors affect the accretion process and ice's behavior on the surface. From climatic point of view, several basic processes, water cycle, wind speed, formation of the clouds, precipitation and presence of different phases (vapor, liquid, and solid) of atmospheric water influence greatly on the severity of icing, accretion rate and ice type. [3,pp.9–10,28,40] Several factors affect also the ice accretion on surfaces, but their connections to ice adhesion are poorly understood. [16,pp.34–35,34,p.15] Surface topography, surface chemistry, wetting behavior and ice characteristics, type, temperature and LWC, have been reported to have influence on ice adhesion, which adds the complexity of icing on the surfaces. [41,42]

Aim of this chapter is to describe icing event and ice accretion on the surface. Heterogeneous nucleation theory and ice accretion model are presented in order to offer background for the accretion process. Icing severity is also evaluated based reports and standards. In addition classification and formation of different ice types are discussed.

3.1 Icing event

Icing event is form precipitation that occurs in the cold climates and it is also a part of hydrological cycle, which is illustrated in Fig. 14. Different stages are involved in the hydrologic cycle, i.e. water cycle, which describes the circulation of water from ground to atmosphere and back to ground. Water is stored in lakes, rivers, oceans, ground water, plants and animals, where it is evaporated by solar radiation into the atmosphere. Warming of ground induces phase change of water from liquid into vapor and vertical current from the ground to atmosphere. The evaporated water vapor in the atmosphere form condensates i.e. clouds due to mixing of air masses that have different humidity. When the clouds reach certain humidity value, the precipitation starts.[43] Depending on meteorological variables, observed precipitation on the ground is in form of rain, drizzle, hail, sleet, freezing rain and snow. [44,45]

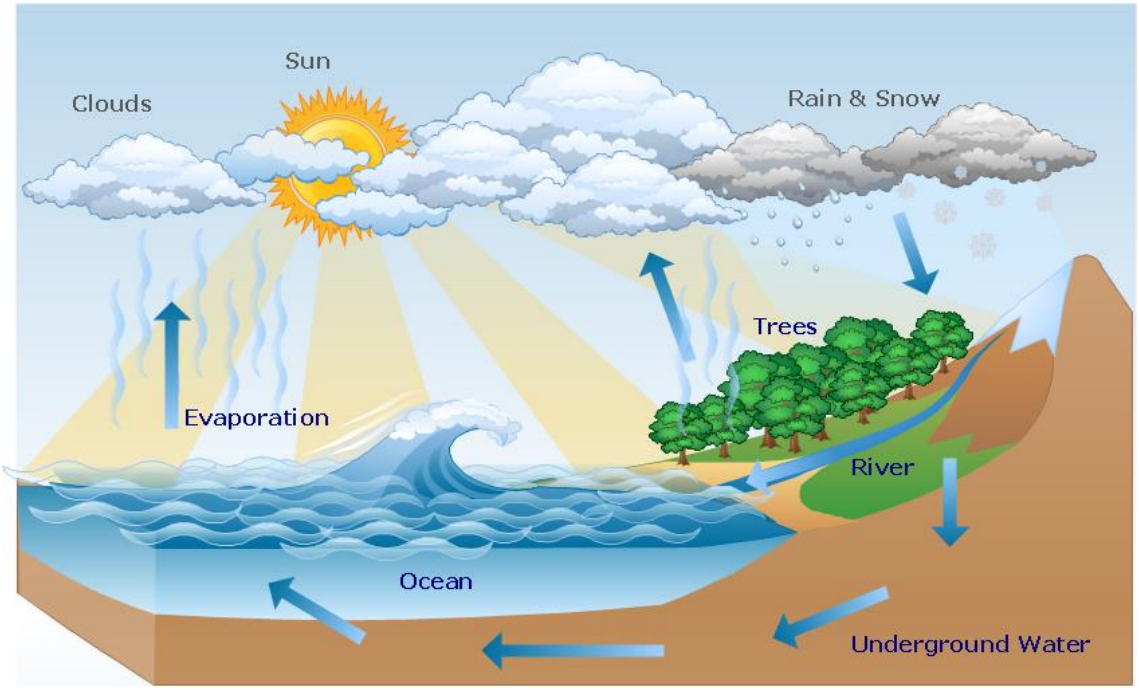

Figure 14. *Hydrologic cycle. [46]*

In order to form ice or snow, the precipitation event should be in the cold climates, where temperatures are subzero. It has been reported that the icing occurs in the Scandinavia, Central Europe, Northern-America, Northern Russia and also in some parts of Asia, for example in Japan and China. Furthermore the altitude also influences on the ambient temperature, therefore icing events are common phenomenon in the elevated areas such as hills and mountains. Therefore it has been recorded that icing events have been occurred in the mountainous area of Spain, Algeria, South Africa, New Zealand and Latin America. [3,p.4]

The liquid water in the droplets can be in form of drop, droplet, hail or snow flake. The significant factor in the atmospheric icing is super cooling of the water droplets, which means that temperature of droplets in the clouds or air is subzero. It is widely accepted that the freezing temperature of the bulk water is 0 °C. [16,p.7,34,pp.11–12] Supercooled water droplets are in metastable state, which means that they are thermodynamically unstable and can easily change their state from liquid water to solid state i.e. ice. [16,p.7] For supercooled water droplets the solid state is the most favorable energy state, which means that water molecules tend to arrange in the lattice. Transformation from liquid water to ice depends on the presence of the nucleating agents according to heterogeneous nucleation theory (discussed in Chapter 3.1.1). [34,pp.11–12,47] If the basal plane structure is similar to ice's structure, it contains the nucleating sites, where ice can freeze. In the freezing process of the ice over the nucleating agent, liquid water starts to form ice crystals. [16,p.7,34,pp.11–12] The crystal structure of ice is hexagonal and crystal growth of ice starts from interface of obstacle surface and droplets outer surface in contact with obstacle. [48,49]

As underlined before, icing is a very complex phenomenon, and quite large variety of meteorological parameters influence on the appearance, properties and accretion rate of the ice. The most significant effect on the ice type is originated from the precipitation type i.e. droplets size distribution and intensity i.e. liquid water content. [3,p.8,40,50,51,52, pp.21–22] In addition the wind and ambient temperature are critical factor that influence the appearance of the ice. Wind's speed, direction and turbulence have an impact on the shape of the ice and also on water droplets movements on the surface. Temperature has the greatest impact on the supercooling rate of the droplets, which determines how rapidly the droplets will cool upon the contact with surface. [3,p.8,40,52,pp.21–22]

3.1.1 Heterogeneous nucleation theory

Firstly, it is widely accepted that supercooled rain droplet is a heterogeneous systems, because it contains solid impurities that can perform as ice nuclei. [53,pp.165–166,54,55] Even on the laboratory scale it is hard the keep water free from any impurities.[55] Secondly, it is observed that the rate of ice formation will increase, if the crystal growth occurs on the solid substrate on the ground instead ice growth in the clouds [56]. Finally, homogeneous nucleation is rare phenomenon outside of some experimental work performed in the laboratory [55]. Therefore it is reasonable to argue that ice nucleation and freezing on the solid surface can be described with heterogeneous nucleation theory, which is widely validated in the literature [47,53,p.221,54–60]

Solid surfaces have always defects and sites on their surface, which can act as nucleating agents in ice formation. In this work we assume that freezing event is occurring on the planar plane. Therefore, the spherical cap model is applied to describe the droplet's state and shape on the solid surface. [53,pp.172–173] In Fig. 15 the spherical cap model is presented, where α can be considered to present water phase and β the new phase i.e. ice.

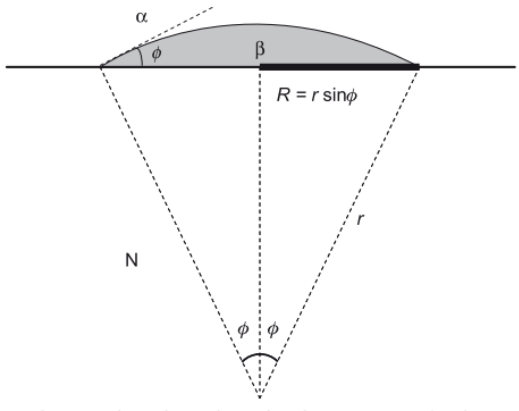

Figure 15. *Spherical cap model. N stands for nucleant surface, α for original phase, β for new forming phase, φ for contact angle and r for critical radius.[53,p.173]*

According to classical nucleation theory, all nucleation have to overcome an energy barrier in order to nucleate [58]. When the energy barrier of heterogeneous nucleation is compared to energy barrier of homogeneous nucleation, it can be concluded that the energy barrier for heterogeneous nucleation is much smaller compared to homogeneous nucleation. [53,p.173,60,61] The reason behind this difference results from effect of the solid surface's nucleation sites. Water droplet's behavior can be described with contact angle, which gives the information about material's tendency for nucleation with water.[53,pp.173–174] In homogeneous system no contact angles exist (there is no solid material), whereas in the heterogeneous nucleation contact angle is formed between the solid surface and water droplet. Therefore, there have been presented term *f(θ)* that takes account the catalytic effect of solid surface in heterogeneous nucleation. In Equation 1 there is presented the relationship between the works of forming the heterogeneous nucleate and homogeneous nucleate.

$$W_{het}^{*} = W_{hom}^{*} f(\theta) \qquad (1),[53,p.173]$$

where the W_{het}^{*} and W_{hom}^{*} are the maximum works needed to form ice nucleus from liquid water, *f(θ)* is the catalytic factor that takes account the contact angle. The equation 1 can be also presented with interfacial energies and chemical potentials as shown in Equation 2 and 3:

$$W_{het}^{*} = \frac{16\pi\sigma_{iw}^{3}v_{i}^{2}}{3\Delta\mu_{iw}^{2}} f(\theta) = W_{hom}^{*} f(\theta) \qquad (2), [60]$$

where

$$f(\theta) = \frac{(1-cos\theta)^{2}}{4}(1 + cos\theta) \qquad (3),[60]$$

where $\Delta\mu_{Iw}$ stands for the chemical potential difference between ice and water, σ_{iw} interfacial energy between ice and water, v_i is molar volume of ice phase and θ stands for the contact angle. Coefficient *f(θ)* can have values between 0 and 1 depending on the contact angle. If *f(θ)* is 1, it represents the homogeneous nucleation. The effect of *f(θ)* on the value of the energy barrier for heterogeneous nucleation is presented in Fig. 16, where contact angle is on x-axis and on y-axis is energy barrier for heterogeneous nucleation.

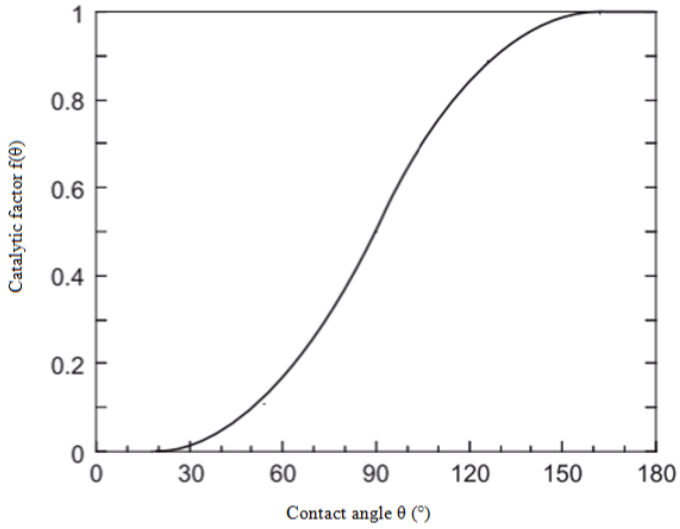

Figure 16. *Relationship between contact angle and catalytic factor. [53,p.174,60]*

Figure 16 points out the energy barrier for heterogeneous nucleation increases exponentially into to certain value with increasing contact angle. This results lower nucleation probability for surfaces with the high contact angles, in other words more energy is needed to start nucleation on high contact angle surfaces.

The maximum work required for heterogeneous nucleation correspond the free energy barrier for heterogeneous nucleation. The Equation 4 takes role of latent heat and temperatures differences inside droplet into account:

$$\Delta G^*_{het} = \frac{16\pi\sigma^3_{iw}T^2_m}{3\Delta H^2(T_m - T_w)^2} f(\theta), \qquad (4), [58]$$

where ΔG^*_{het} is energy barrier for heterogeneous nucleation, T_m is melting point of ice in normal conditions, T_w water droplet temperature and ΔH is a volumetric latent heat from freezing event.

Critical radius for curvature of supercooled water droplet on the solid surface can be calculated with the equation 5,

$$r^* = -\frac{2\sigma_{iw}}{\Delta g}, \qquad (5) [53,pp.221–222]$$

where σ_{iw} is interfacial energy between ice and water and Δg is volumetric phase change free energy of water-ice transformation. In order to supercool water to nucleate, the critical radius of the droplet should suitable with the defect sizes or cavities on the surface i.e. the surface roughness influences on the nucleation according to this theory.

The heterogeneous nucleation theory of ice offers a background for freezing event. Theory is applicable on at the pretty static situation, because it does not take a stand for

dynamic behavior of the supercooled water droplets. In the real icing event in the nature, the droplets have certain amount of velocity that they will impact on the solid surface. The theory underlines the usage of the hydrophobic materials as icephobic coatings, because hydrophobicity should increase the energy required for nucleation to start. [47,59–61] However after ice formed on the surface, nucleation should proceed in accelerated manner.

3.1.2 Severity of ice accretions

During the past decades there has been a great interest on modelling the ice accretion on different manmade structures. These models have used in the assessment of mechanical loads that accreted ice inflicts on the certain structure, which can be taken into account in the designing phase. [3,p.8,40,62,63] As discussed previously in Chapter 2, the ice storm in Canada gives a perspective how severe destruction and related economic losses can occur in severe icing events.

Ice accretion model should describe how main parameters in the icing event have been taken into consideration. The main parameters in the icing event, that have influence accreted ice's shape, density and rate of accretion, are LWC of rain, droplet size distribution, temperature, wind speed and direction and in addition relative humidity. [3,p.8, 40,52,p.40]

Lozowski & Makkonen (2005) [62] state that proper ice accretion model should include the following six factors:

1. Consider how air flow goes around the icing obstacle.
2. Impingement of supercooled droplets.
3. Internal and external heat load which affect the sticking probability of the droplets.
4. Behavior of unfreezed liquid on the surface after an impact.
5. Ice properties; growth direction, shape, density, roughness and icicle formation.
6. Response of the iced structure i.e. growth, twisting. [62]

Multiple ice accretion models have been presented in literature, which take a stand for accretion of different ice types rime, glaze, hoar frost, wet snow and sea spray icing or the impact on different engineered structures such as power network lines, wind turbines and tall structures etc. [10,38,62,64–70] For clarity reasons and the scope of this thesis, only the Makkonen model is presented, which is widely used in the literature as a standard model for ice accretion [62,63,71]. ISO 12494 standard " Atmospheric icing of structure" proposes that Makkonen model [67] can be used to describe ice accretion on the cylinder-shaped icing structures. As discussed, the shape of the icing structure has an effect on flux dynamics of the air flow, which is why this model does not give accurate estimates for different shaped structures. Formula of Makkonen model is presented

in the following at the Appendix C of ISO-12494-standard for accreted ice mass (m) vs. time:

$$\frac{dm}{dt} = ή_1 ή_2 ή_3 \cdot w \cdot A \cdot V \qquad (6), [63]$$

where $ή_1$, $ή_2$, $ή_3$ are correction factors that have value between 0 and 1. These factors point out the correct amount of ice accretion that different processes in the icing event reduce from the maximum amount. Factor $ή_1$ stands for collision efficiency of the water droplets or snow flakes, $ή_2$ describes the sticking efficiency, which is mainly related to wet snow growth, $ή_3$ signifies the accretion efficiency, which considers the either dry or wet growth of the ice and its impact on the ice accretion load and rate. Liquid water mass/unit volume is marked with w, wind speed V and cross-sectional area with A.

Collision efficiency denotes the ratio of water droplet hitting the icing object and its value can be considerably less than 1, because the smaller droplet have tendency go around the object with air flow's streamlines. [3,p.87,63] This situation is illustrated in Fig. 17.

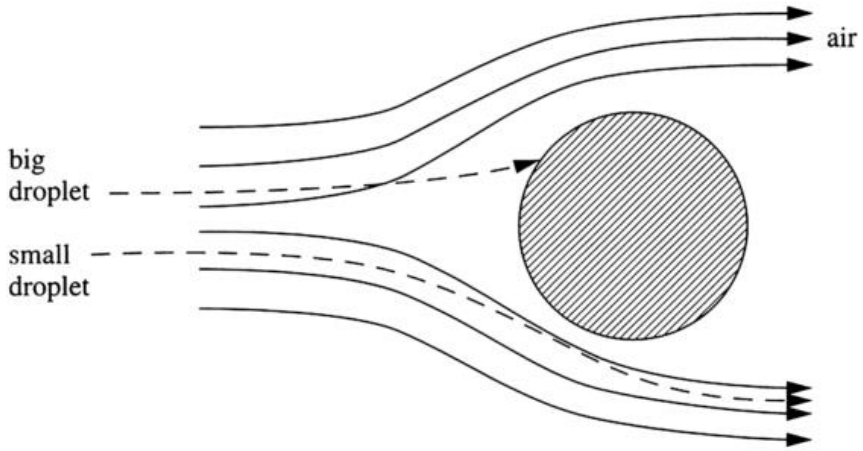

Figure 17. *Streamlines of the airflow and possible trajectories of the droplets. [3,p.87]*

The second correlation factor $ή_2$, sticking efficiency, describes the amount of droplets that stick and form ice on surface after their collision. In the right conditions it is possible that the droplet can bounce off from surface. The third factor $ή_3$, accretion efficiency, considers whether the accretion is in dry or wet mode. Dry ice accretion is related to formation of rime ice, as illustrated in Fig. 18,a). In dry ice accretion, the accretion efficiency has a value of 1, because all the droplets hitting the surface freeze immediately upon the impact. Wet ice accretion is observed in the icing events, which LWC water content is high, for example in the freezing rain events. Wet mode of ice formation presented in Fig. l8b). [3, pp. 88-89]

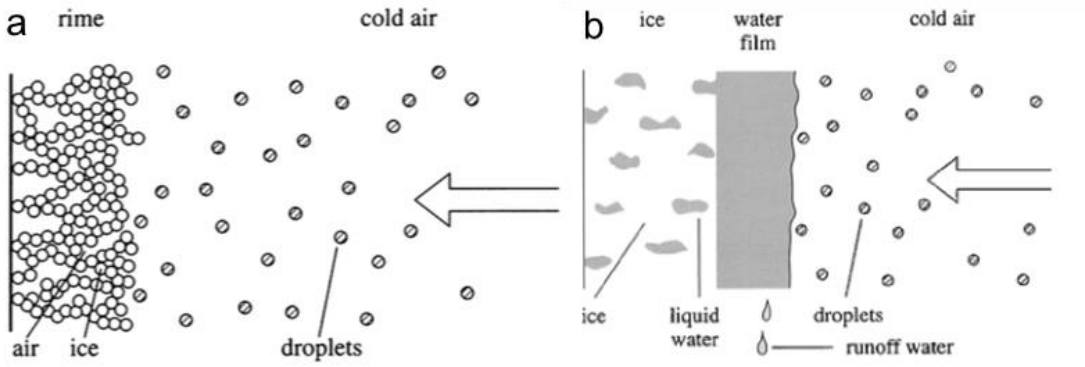

Figure 18. *Schematic presentations of ice accretions a) rime ice and b) glaze ice. [3, pp. 88–89]*

Makkonen model is an useful tool when assessing to possible ice loads on different structures. Although the model relys heavily on avaibility of the meteorological data, such as LWC, MVD, temperature, wind speed, which are measured only in the research centers. Although lack of observed input data, it is possible to produce quite accurate small grid weather forecast, which can be used as input data. [40,52,p.40,62]

Ice accretions models give valuable data, which can used in the assessment of the site's icing conditions. IEA Wind and ISO 12494 have presented tables of icing severity i.e. "ice classes" of the site, which can be used, depending on the application, to evaluate production losses and ice loads that have to be considered in the structural design.[2,pp.16–17,63] The crucial factors in these classifications are duration of the icing event, its severity and annual frequency of the event. [2,p.20,63]

The IEA Wind ice classification system is applicable for evaluation of icing class of the site. By determination of the severity of icing, classification system gives an estimate of annual power losses for the wind turbine.[2,p.17] The different ice classes according to IEA Wind are presented in Table 1.

Table 1. *IEA Wind's ice classification system.[2]*

Ice class	Meteorological icing (% of year)	Instrumental icing (% of year)	Production losses (% of annual production)
5	>10	>20	>20
4	5-10	10-30	10-25
3	3-5	6-15	3-12
2	0.5-3	1-9	0.5-5
1	0-0.5	<1.5	0-0.5

Figure 19 shows map of icing severity utilizing the IEA's ice classes. The in-cloud icing data is collected over 20 years from 4000 observation station. As discussed previously altitude increases icing severity and this map shows the situation at 350 m.[72]

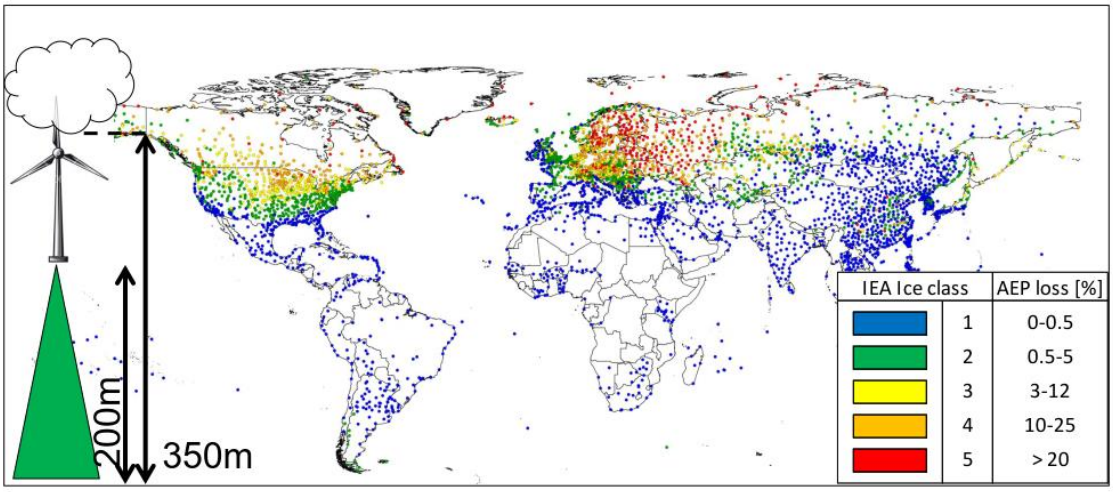

***Figure 19**. Icing severity map of the places prone to in-cloud icing.[72]*

Meteorological icing denotes the duration of the icing event i.e. the ice accretion time on the wind turbine. Instrumental icing is the time that ice stays on the surface. Ice class is measured with icing of the unheated anemometer. The time that anemometer is disturbed by icing corresponds the meteorological icing values. Based on these measurements the production losses can be estimated. [2,p.17] According to IEA's suggestions the anti- or de-icing is cost-effective solution, when ice class of the site is 3 or higher. [72]

ISO 12494- standard "Atmospheric icing of structures" has also classified icing severity on different structures, such as towers, mast, cables etc. Although it does not concern icing of overhead transmission lines, whose withstanding of the ice is evaluated in the IEC 60826 "Design criteria of overhead transmission lines". ISO 12494- standard presents ice classes for both rime and glaze ice accretion, because their density differs. In order to recognize valid ice class for the site, there are options; 1) collect meteorological data as an input data for ice accretion model to assess ice loads like in these studies [66,73], 2) measure accreted ice masses on the site (kg/m), which were performed for example in these studies [10,38]. Ice classes for glaze ice, having the density of ice 900 kg/m^3, are presented in Table 2.

***Table 2**. Ice classes for glaze ice (density 900 kg/m^3). [63]*

Ice class	Ice thickness (mm)	Masses for glaze ice (kg/m)			
		Cylinder diameter (mm)			
		10	**30**	**100**	**300**
G1	10	0.6	1.1	3.1	8.8
G2	20	1.1	2.8	6.8	18.1
G3	30	3.4	5.1	11.0	28.0
G4	40	5.7	7.9	15.8	38.5
G5	50	8.5	11.3	21.2	49.5
G6	To be used for extreme ice accretions				

Ice class for glaze ice accretion can be determined whether by measuring the thickness of accretion or by measuring ice load (weight on distance, kg/m). Class G6 is for extremely severe icing site. The similar classification for rime ice is presented in Table 3. [63]

***Table 3.** The ice classes for rime. [63]*

Ice class	Ice mass (kg/m)	Rime diameter (mm) for object diameter of 30 mm			
		Density of rime (kg/m^3)			
		300	**500**	**700**	**900**
R1	0,5	55	47	43	40
R2	0,9	69	56	50	47
R3	1,6	88	71	62	56
R4	2,8	113	90	77	70
R5	5,0	149	117	100	89
R6	8,9	197	154	131	116
R7	16,0	626	204	173	153
R8	28,0	346	269	228	201
R9	50,0	462	358	303	268
R10	To be used for extreme ice accretions				

For rime ice it is vital to take on account the role of density on the weight of ice accretion. Wet snow accretions are considered in this table for rime, because its density is in same range than rime ice. These classification systems require either reliable meteorological data for ice accretion models or measurement on the site. Site assessment is a critical step when the engineering structures are built in the icing climates [2,7,8,52,72,74]. With the proper provision and designing many of the icing issues can be hindered, which is a start in the prevention of expensive problems that icing inflicts.

3.2 Atmospheric icing types

Atmospheric icing includes all the meteorological processes where falling supercooled rain droplets or wet snow flakes impinge on the structure. As a result of this droplet bombardment ice or snow will accrete on the structure.[2, p. 12,3, p. 4,16,28,34, p. 13, 40,42,45,50,52, p. 13,56,63,70, 75, 76, 77, p. 6] Icing types can be divided into two categories, precipitation and in-cloud icing, depending on their meteorological conditions such as LWC, MVD, and temperature. [3, pp. 4–5, 16, 51, 63, 77, pp. 6–10] The LWC content in in-cloud icing is usually low varying between 0.1-0.9 g/m^3 and high in precipitation altering between 1-10 g/m^3. In addition the droplet sizes in the in-cloud icing varies between few µm to 50µm and for precipitation icing; freezing drizzle around 100 µm and freezing rain from 100 µm to several mm. [50] It can be concluded that in-cloud icing takes place with the low LWC and small water droplets. Instead precipitation icing occurs in events, where the LWC is high and water drops larger. Atmospheric icing types can be divided in the different categories based on the formation mechanism and droplet size. Precipitation icing is formed from falling droplets or snow flakes and in-cloud icing is occurring in the clouds or fog contacting with structures. In Figure 20 classification is illustrated.

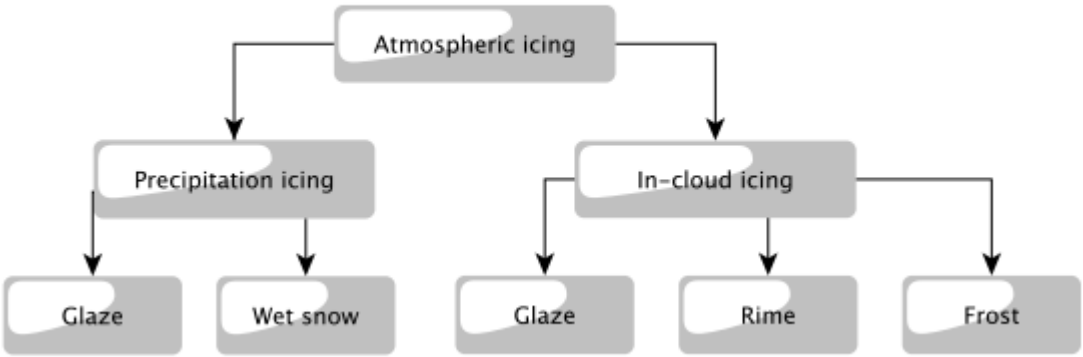

Figure 20. *Classification of atmospheric icing.*

3.2.1 Precipitation

Precipitation icing can take place with two different ways by freezing rain and drizzle or wet snow accretion. In the precipitation icing the droplet size is larger compared to in-cloud icing and the LWC content is also higher. In other words, in precipitation icing falling rain droplets or snowflakes impinge the icing surface and on the contrary in in-cloud icing microscale droplets in clouds or fog collide with the surface.[8,63]

Emergence of sufficient climatic conditions for precipitation icing starts from creation temperature gradient inversion. Typically the temperature decreases with the increasing

altitude. However during winter months, this situation is disturbed. Solar radiation heats the ground, which gets warmer during the days. When the sun is set, warm ground starts to heat air layers above. Although air is not very good heat conductor, which for the air layers near the ground remains colder. The air layers in higher altitude are in fact warmer, possibly over 0 degrees, than the ground regime. These air layers are described in Fig. 21, where falling snow flakes or ice particles from the clouds enter the warm regime (over 0 degrees) and melt into the form of rain drops. Because of the colder air layers near the ground, these rain droplets start to cool down i.e. supercool. [3, pp. 4–6, 44, 45, 77] Supercooled droplets are in metastable state once they hit the surface and their state is disturbed which drives the droplets to freeze. [42]

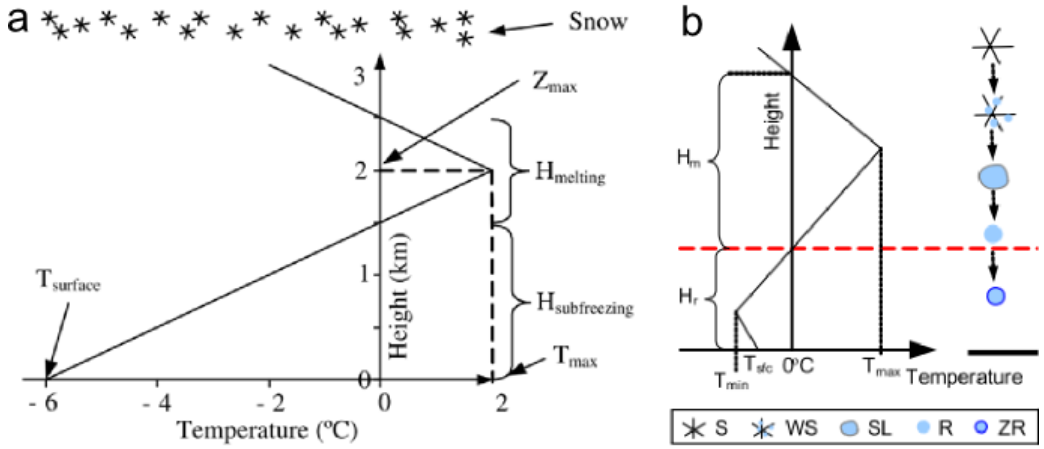

Figure 21. *The effect of altitude and temperature on precipitation. a) Temperature change of precipitation against altitude [44] and b) change of precipitation type with decreasing altitude. S stands for snow, WS for wet snow, SL for slush, R for rain and ZR for freezing rain. [45]*

Precipitation falling from the sky can be in different forms; rain drops, ice pellet, slush or snowflakes depending on the rate of melting on the warm regime, which is visualized in Fig. 21. According to form of precipitation, different kinds of accretions are observed on the surfaces. When the freezing rain or drizzle is concerned the glaze ice is observed, which formed from in wet i.e. high LWC precipitations where the droplet sizes are also larger. In formation process, the supercooled rain droplets collide with the surface and start freeze upon the contact. Although due to high LWC content, the part of the water droplet does not freeze immediately in the impact, but remaining liquid can run along the surface and then freeze. [3, 44, 45, 77, p. 7] These kinds of impingements create dense, transparent and homogeneous structure, which adheres tightly to surface. Typical features of the glaze ice are also formation of the horns and icicle formation due to run-back water streams on the surface, as presented in Fig. 22. [63] In addition glaze ice's cohesive forces are higher compared to other ice or snow types [42].

Figure 22. *Illustrations of glaze ice accretions. a) Freezing rain accretion [78] and b) transparent glaze ice on tree branch [79].*

In general the glaze in the freezing rains or drizzles is formed at temperatures ranging from -6 - 0°C.[2, p. 12] Even so formation of glaze is possible down to -10°C with any wind speeds. Due to the high water content, glaze accretions add mass to icing structures quite quickly and icing events last usually some hours. Glaze ice can cause severe problems to different structures due to its high density and high accretion rate.[34, pp. 13–14, 52, pp. 13–14, 63] As mentioned in the Chapter 2.4, the worst catastrophe caused by freezing rain was recorded in Canada, where thousands of power network structures collapsed due to high glaze ice accretions.

As explained before, the precipitation can be occurring with different degrees of melting. Another precipitation type that inflicts issues for different engineering structures is wet snow. Wet snow accretions are formed, when partly melted, high LWC snowflakes collide with surface. Typical temperature for wet snow formation is between 0 °C and 3°C. As described in Fig. 21a) the falling snow or ice particles melt, when they enter in to the warm (over 0 °C) zone of the atmosphere.[2, p. 12, 80] Depending on the degree of melting rain, slush or wet snow is formed. In the wet snow formation there is only a little of melting involved and on the contrary in the freezing rain there is complete melting in the warmer zone. The accreted wet snow will actually freeze on the surface, when temperature falls below 0 °C after accretion event. [2, p. 12, 63, 80, 81] Typically wet snow accretions last hours and the precipitation rate is between 2- 5mm/h, but in the worst case event can last up to 24 hours and the precipitation rate can doubled compared to typical values. [3, p. 140]In Fig. 23 there is presented wet snow accretion on the collapsed overhead line.

Figure 23. *Wet snow accretion on the collapsed overhead line. [80]*

When comparing the wet snow to dry snow accretion, the key difference is that wet snow has very high LWC values [63]. Partial melted, high water containing snowflakes are sticking very effectively on the surface and on the top of each other. However the mechanical forces the snow are weak due to porous structure.[81] Density of wet snow is in a range of 300-600 kg/m^3 and it is mainly composed of liquid water, ice granules and air pockets.[2, p. 12, 3, p. 121] The whole structure is connected together by the capillary forces.[3, p. 121] Wet snow accretion cause mainly problems for the overhead lines and collapsed structures have been reported in [80, 81].

3.2.2 In-cloud icing

Micron sized droplets and low LWC values are typical characteristics for in-cloud icing, which occurs when clouds or fog contacts solid obstacle. Therefore the in-cloud events take place at the high altitudes and cold climates. The supercooled droplets will freeze upon the contact with the surface, and create either rime or glaze ice depending on the droplet size, temperature and LWC.[3, p. 7, 77, p. 8] As described in the freezing rain event, glaze ice is formed in the events that have high LWC values and containing large droplets. The droplets in the in-cloud icing events are on the tens of microns and in the freezing precipitation above 100 microns.[50] Opposite ice type for glaze is rime ice, which is formed in the dry in-cloud icing events. Rime ice has a porosity in its structure and it can be either soft or hard rime depending on the level of porosity. In addition, the last type of ice which can be formed in the in-cloud icing event is hoar frost, which in the sublimation process from supercooled water vapor directly into solid ice. Hoar frost

is not considered in this thesis, because it is light, low adhesion ice type that does not produce any serious problems for majority of structures. The only exception is the overhead lines, where it can cause inflict corona discharge that produces power losses. [3, p. 7, 63, 65] The model for hoar frost formation is presented by Makkonen [65].

The glaze ice formation in the in-cloud icing is rather similar compared to freezing precipitation. During the contact of water droplet with the surface, the part of the liquid droplet does not freeze immediately, but the remaining liquid can run along the surface. Finally it will freeze, but the runback water creates typical characteristics such as icicles formation and horns i.e. runback ice. Glaze ice is typically formed in the temperatures between -6°C - 0°C [2, p. 12, 63], but some authors have claimed that the formation can happen temperatures down to -14 °C [56]. Wind speed has also an effect on the formation of certain ice type and the graph for effect of wind speed and temperature in the formation of different ice types is presented in Fig. 24 [63]. Droplet size in the in-cloud glaze icing is some tenths of micrometers and LWC varies between 1-10 g/m^3 [50]

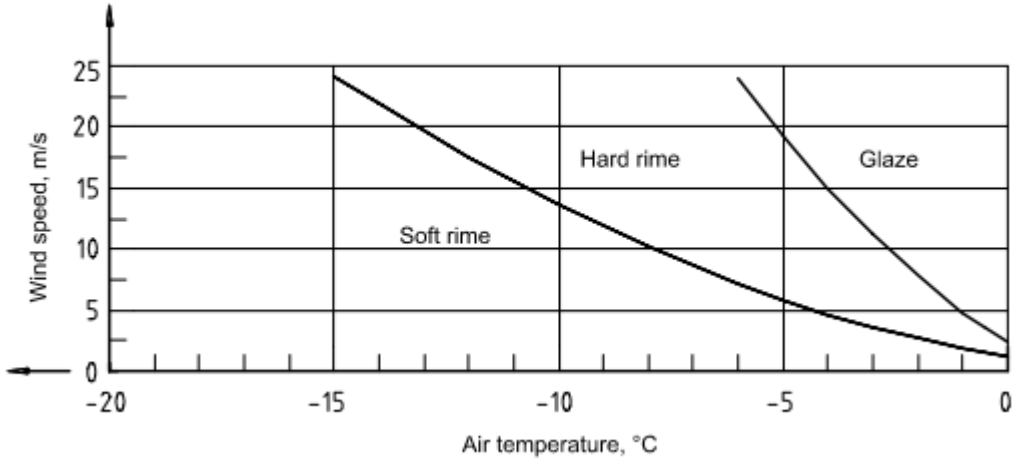

Figure 24. *The effect of wind speed and temperature in the formation of different in-cloud ice types. [63]*

Rime ice is generally formed on the elevated and exposed areas such as mountain or hill tops. Variety of structures, tall structures and wind turbines, suffers from rime ice accretion, which can last even days. [3, p. 7, 63] In the rime icing event, the droplet size inside of the cloud is small and droplet sizes can be as low as few micrometers. The LWC is just few tenths of g/m^3 [50], usually around 0.4 g/m^3 [16, p. 8]. The rime ice is formed in the wide temperature range from -20 °C to 0 °C [2, p. 12], but typically it is associated with the colder temperatures below -10 °C [42, 56]. In Fig. 25 there are presented the rime ice accretions on the mountain tops.

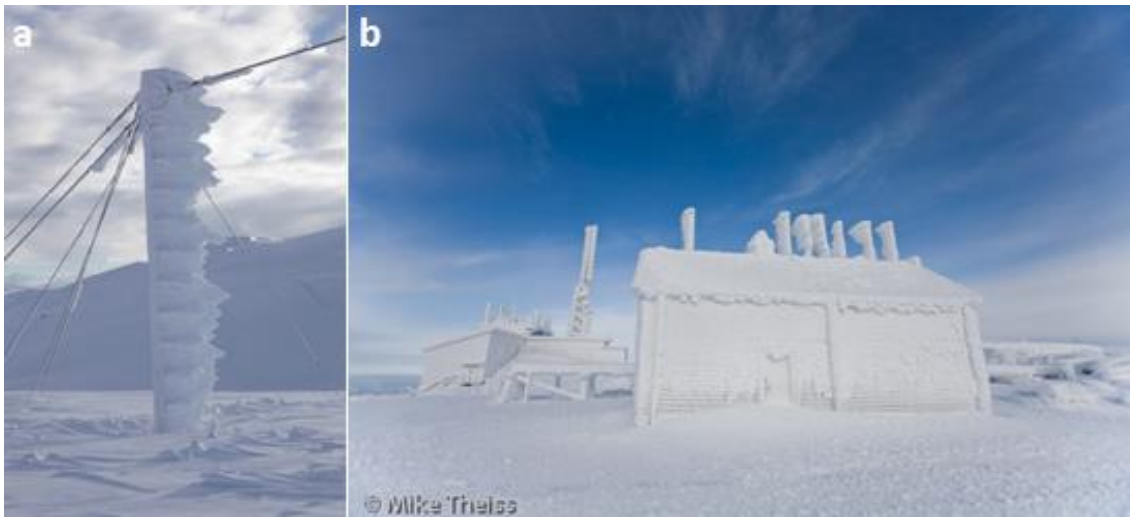

***Figure 25**. Examples of the rime ice accretions, a) Rime accretion on the power network structure Ålvikfjellet, Norway [32] and b) rime accretion on building on the top of the Mt. Washington, USA. [82]*

Formation of rime ice differs from other icing due its small droplet size, low temperature and low LWC. In the rime icing event small supercooled droplets impigne with surface and freeze immediately upon the impact remaining their spherical form. This creates air pockets inside structure, which can be observed as a milky, white and opaque color. Depending on the porosity level either soft or hard rime is formed. Hard rime is formed in the warmer temperatures with higher LWC content, which makes it adhere tightly on the surface. Instead soft rime is fragile and does not form strong adhesion with the surface. Soft rime has a feathery structure with needles and flakes pointing out to wind direction. [63] In the Table 4 there is presented a comparison table between all the atmospheric icing types.

There are some variation between different authors for formation temperatures of different in-cloud icing types. Acccording to Farzaneh (2008) [3,p.33] only rime ice is formed in the in-cloud icing events and temperatures determines whether hard rime or soft rime is formed. Soft rime is formed in the colder temperatures [3, p. 33] It is also stated by some authors that the rime ice accretion takes place temperatures below the -10 [42], but some authors claime that rime icing happens temperatures below the -15 °C [16, p. 8, 56]. At the very low temperatures, starting from below -20 °C down to -40 °C, icing is not relevant phenomena to observe, because the LWC decreases close to zero and droplets starts to transform into ice pellets. [8, 16, p. 8, 77, p. 8] The sticking capability of the ice pellet is poor and no ice accretion is not formed in the impigment of ice pellets.

Table 4. *Characteristics and properties of the different atmospheric ice type. P stands for precipitation icing and I for in-cloud icing.* *[2, p. 12, 3, p. 33, 16, p. 8, 42, 63]*

Ice type	**Icing type**	**General characteris-tics**	**Adhesion/ Cohesion**	**Density (kg/m^3)**	**Tem-perature (°C)**	**MVD**	**LWC (g/m^3)**
Glaze	P	transparent, dense	Strong	900	-10 – 0	100 µm-2mm	up to 1.2
	I				-6 – 0	30-50 µm	1 – 10
Wet snow	P	White, eccen-tric	weak (form-ing), strong (freezed)	300-600	0 – 3	several mm	1 – 10
Hard rime	I	Opaque, rough	strong	600-900	-20 – 0	5-30 µm	around 0.4
Soft rime	I	White, feath-ery, fragile	low to me-dium	200-600	-20 – 0	5-30 µm	under 0.4

Glaze and hard rime are the most tightly adhered ice types, which densities are also high. These ice types can generate high ice loads on different structures, which can lead to severe problems. [2, 63] Wet snow and soft rime have quite similar appearance, but there is a significant difference in the LWC values; wet snow has very high and soft rime very low values. It can be concluded that the precipitation icing event have high LWC and naturally higher droplet size. On the other hand in-cloud icing event have lower LWC values and significantly smaller droplet sizes. [50, 77,pp.8-10]

4 METHODS AND MATERIALS AGAINST ICING

Several methods have been developed to prevent or diminish the icing on the different structures. There are multiple problems in the different field of industry, but many of them have also common problems, where different techniques attempt to offer solutions. The motivation behind the research of the anti- and de-icing methods is to improve safety aspects, operating environment, durability or efficiency. Prevention of the disasters, like 1998 ice storm in Canada that collapsed thousands of power network structures, is in the center of focus. In the worst case icing can cause the loss of lives, as was the case the in 1987 and 1994. [4, 5]

The driving factors behind the rapid increase in the research have been the opening of the Northern Sea Route, increase in the wind power production in cold climates and long-lasting problems in the aviation, offshore, marine and power networks. Increased traffic on the Northern Sea route and altogether of artic region, have risen up the problems that this challenging environment causes i.e. ice loads and hazardous working environment.[3, p. 83, 9, 11] At 2013 there was in total 318 GWh installed wind power, of which 60 GWh was in cold climates. International Energy Agency (IEA) defines cold climate as a climate, where temperatures are subzero and icing is occurring. Many of the planned installation are focused on the mountains and uphill areas, where he operating conditions are changing swiftly. Operation in the cold climates possesses many challenges for cost-effectiveness, maintenance and safety. The icing affects greatly on the aerodynamic profile of the wind turbine blade, which inflicts extra loads on the blade's structure and also on the rotor. This problem greatly shortens the durability of the blades. [2] Due to these challenges and increase in the production, there is clear need to research materials and methods to fight against the icing.

Icing is phenomena, which will happen eventually in the right climatic conditions. Therefore researchers have had difficulties to find surfaces that would completely repel ice nucleation and further on accretion [3, p. 231]. On this account focus of research in icing mitigation has been generally divided into two groups de-icing and anti-icing systems. In the de-icing systems ice is allowed to accrete on the surface and the focus is to minimize energy which is needed to detach ice from the surface. Usually ice removed periodically with mechanical or thermal systems for example with heating or flexible blades. On the other hand anti-icing strategy focuses on to completely avoid or reduce the ice nucleation and accretion. [3, 8, 16]

These large scale strategies can also be divided into the methods that utilize specific techniques. Dividing can be made based on the use of external energy on the surface. The systems that exploit external energy from different sources – such as thermal, chemical or pneumatic – in the icing prevention are called active methods. Alternatively systems that does not exploit external energy, but merely rely on icing mitigation properties of the surface, are known as passive methods. [8, 16, 41] The classification of ways to prevent ice adhesion and accretion is presented in Fig. 26.

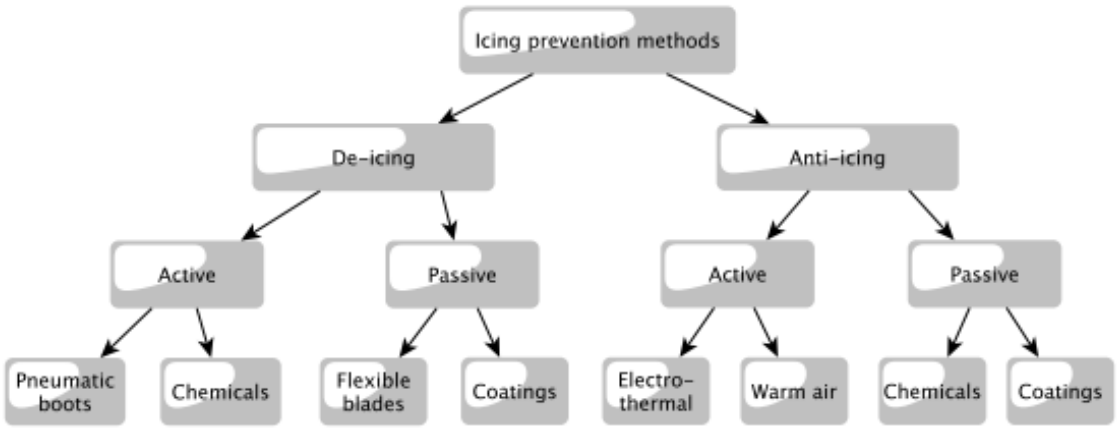

Figure 26. *Collection of strategies and methods for prevention of icing nucleation and accretion.*

Prevention of ice accretion can be achieved by following different approaches. The first way is to minimize ice adhesion between the ice and surface below it. The second approach is diminishing ice nucleation and prevention of supercooled droplets to freeze upon impact. Third approach is to utilize different methods for example both active (heating) and passive (surface treatment) in order to minimize ice nucleation and accretion. [3]

At the moment the research has been focused on the systems that utilize both passive and active methods. The reason behind this phenomenon is that passive anti-icing and de-icing systems can not alone offer sufficient surfaces that would repel ice formation.[8, 16, 41, 83] That is why active systems are used together with passive methods.

In this literature review primary attention is concerned to different coatings and surface treatments, which are used in the anti-icing solutions. However some of the most interesting active anti-icing and de-icing solutions are presented in order to get better understanding of field of icing.

4.1 Methods against icing

Several methods against icing have been applied and studied during the past decades. Due to increased activity in the cold climates, have different industries and other instances searched for methods which could help to overcome problems related to icing. These methods have been classified in literature different ways, but in this thesis the classification has been done according to IEA's, which first classifies the methods into anti-icing and de-icing.[2] Anti-icing means that the method prevents the ice freezing on the surface and de-icing means that ice is allowed to accrete on surface before the ice is removed. Anti-icing methods will protect systems in manner that they can be running during the icing events. Some of de-icing methods require the systems shut down, for example the mechanical removal of ice from wind turbine blade. Second stage classification is based on energy consumed for ice release in each method and the methods have divided into passive and active. Active methods utilize external energy in ice release or prevention and passive methods does not need any extra energy in prevention or releasing of ice.[2] In this chapter the most interesting anti- and de-icing methods are presented. Due to large variety of the methods the emphasis in this thesis has been focused into most interesting methods; which have been utilized in the industry and the passive anti-icing methods.

4.1.1 De-icing methods

As mentioned before, de-icing systems allow ice to accrete on the surface and the ice is removed afterwards [16, p. 26]. De-icing methods can be divided into two different categories, active and passive, as the Fig. 26 illustrates. The passive de-icing methods are presented first and then the active methods.

Because of the ice accretion on the surface, there are not many passive de-icing methods that would release ice loads from surfaces. Nevertheless two different methods have been proposed. First passive de-icing method is based on flexible blades that would shed the accreted ice layer from the blade. Flexible blades have not been widely adapted on the wind turbines and the result of its efficiency in operation has not been published. The reliability of ice release on thin ice layer may not sufficient, and therefore the remaining ice could cause problems on the aerodynamics of blades. [7, 8]

The other passive de-icing system called active pitching has been proposed, but it has limited usability and demonstration on its working. The idea behind the active pitching is that after the ice has accreted on the blades, they are turned against the sun. Solar radiation should melt the ice away, or at least heat the blade in a manner that it will release the ice load. This method is at the best only suitable for light icing conditions, and it has no evidence about its usability in real icing conditions. [8]

Active de-icing methods on the other hand have gained much attention in recent years. These active methods can be divided into two classes, mechanical and thermal techniques, based on the form of removal energy. Flexible pneumatic boots are the most interesting mechanical method and it is widely applied on the airplane wings, where it has been used to remove ice from leading edge of the wing. Pneumatic boots are usually air filled and the ice removal happens when these boots are inflated. The change in the wing's profile after inflation can be observed from the Fig. 27, where wing's profile is presented before and after the inflation.[84, p. 14] After the pressurization the ice is expected the crack and shatter of the surface.[8, 12, 83] Air flow around the wing the removes loosened up ice after the inflation of the boots.[12] However in the glaze ice events, the runback ice can be formed behind the leading edge, where it cannot be removed with pneumatic boots. [8, 83]

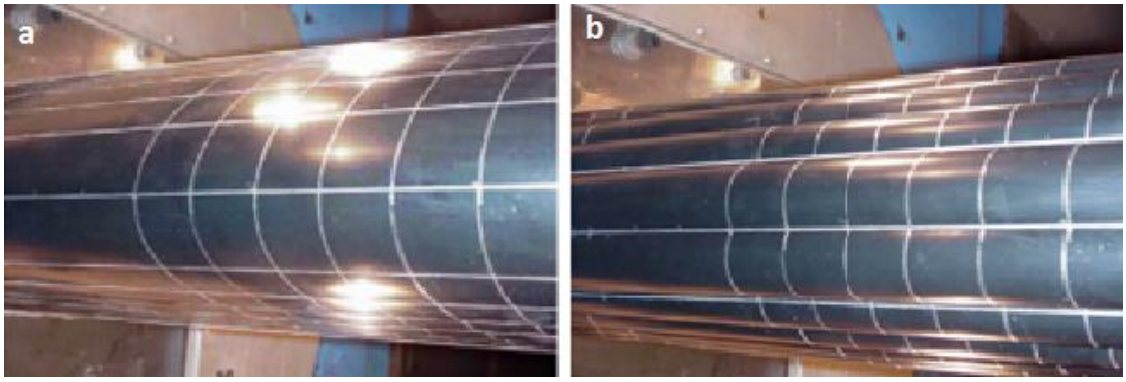

Figure 27. *Pneumatic de-icing boots on the aircraft wing. a) uninflated and b)inflated. [84, p. 14]*

Other mechanical methods based on the physical removal of the ice are utilized, when different systems like wind turbines are stopped. These methods also require the manpower and possibly lifting equipment. [85] The most classic way to get rid of ice is remove it with hand tools. [12] For example the wind turbine owner Tuulisaimaa, utilizes expert climber, who manually remove ice from the blades and other structures, as Fig. 28 points out. [85] This method consumes a lot of time and efforts, which makes removal costs and standstill costs very remarkable. In addition hand removal of the ice can't be conducted if the weather conditions are harsh. The ice is also typically removed manually in sea vessel and offshore platforms. When the ice is removed manually, there is always possibility for injuries due to falling ice. [12]

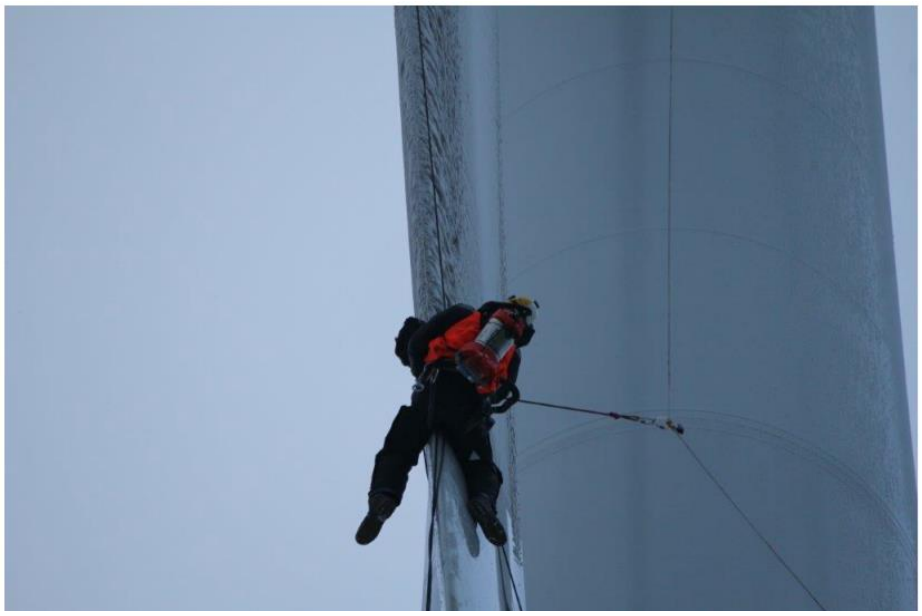

Figure 28. *Manual ice removal from the wind turbine blade. [85]*

The Swedish owned Alpine Helicopter AB offers an alternative solution for mechanical ice removal. The company utilizes helicopter which is spraying hot water to ice on the wind turbine blades. Helicopter is capable to carry 900 liters of water at the time and the water temperature is around 65 °C. The firm has done some promising field test in Canada. The benefit of method is that it can be used for all turbine types. The main disadvantage is that it cannot be utilized if the weather conditions are too harsh. Also its cost-effectiveness cannot compete with the thermal methods. Helicopter spraying hot water to de-ice accreted ice from wind turbine blade is presented in Fig. 29 [86]

Figure 29. *Ice removal with hot water sprayed from the helicopter. [86]*

Other methods that are applied at the standstills are thermal methods, which include methods based on the heating resistance or warm air blower. These methods can be classified into anti-icing methods, if they can be applied during the operation. The heat-

ing resistance is produced by inserting heating element on the blade's leading edge. The warm air blower, consisting of fan and heating element to heat air, are usually located inside the wing or blade. The schematic presentation warm air blower is presented in Fig. 30. These methods are based on the melting of the accreted ice via thermal energy, which should create water film between the surface and ice. External forces, such as centrifugal forces, should be sufficient to detach ice. The melting of the ice into water is energy consuming process, although nowadays the thermal efficiency is close to 100 %. [8, 41]

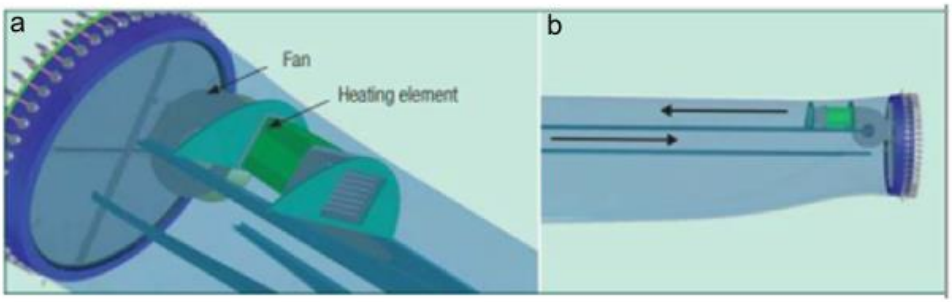

Figure 30. *The electrothermal warm air based de-icing system. a) is showing the placing of the system in the wind turbine blade and b) is demonstrating the circulation of air inside the blade. [72]*

Heating blades offer an alternative for warm air blowers and the heating blades are applied inside the blade's structure in the construction phase. The electrothermal methods have given promising results in rime ice detachment, but in the heavy icing environments this method have failed to produce sufficient heating power [8]. The other disadvantage is that the heating element is only applied in to the most critical areas such as the leading edge, which makes the other areas vulnerable to runback icing or other forms of ice accretion. The accreted ice on the other areas decreases the aerodynamic behavior of the blade or wing and also sets extra loads on the structure. [8, 16]

There are also commercial de-icing systems which are based electrothermal origin. Enercon utilizes the warm air to melt ice of the blade. Its system includes the fan and heating element as described in Fig. 30. The heated air is circulated into the most challenging areas such as the leading edge and back to the fan. [87] The alternative electrothermal de-icing system is based on the heating element and Siemens has applied it on its wind turbines [2, p. 26].

4.1.2 Anti-icing

Anti-icing stand for that normal operations can be conducted and the structures and operative parts remain ice-free. The methods exploiting this strategy can be divided into the passive and active methods with the same criteria than the de-icing methods. The active methods utilize the same techniques than in electrothermal de-icing. On the other hand the passive methods include coatings and chemicals, which are aiming to reduce ice adhesion or prevent the ice accretion.

The active anti-icing methods are aimed to prevent ice accretion on the protected surface. This goal is achieved by heating the surface during the forecasted icing events. In practice this means that the surface needs to be over 0 °C in order to keep water drops in liquid form. The placement of electrothermal heating elements is presented in Fig. 31. As mentioned in the previous chapter, this produces rivulets due aerodynamic forces, which eventually forms runback ice into unprotected area [8, 83]. The runback ice increases the loads that structures should hold. In order to prevent runback ice formation the adhesion between the runback ice and the surface should be on the level that aerodynamic forces would break ice down.[8, 16, 41]

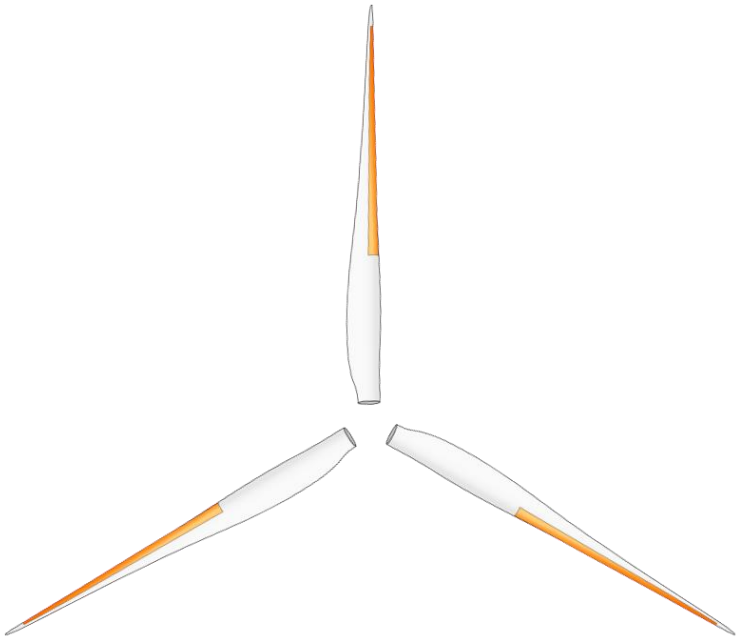

Figure 31. *An example of the placement of the heating elements on the leading edges of the wind turbine blades.* ***[88]***

The properly functioning electrothermal anti-icing system requires working control system, which communicates between the heating element and ice detectors to adjust sufficient energy output on the heater. Because increased runtime of the icing prevention system, the required amount of thermal energy also increases. IEA (2011) [2, pp.25-27] states that the electrothermal anti-icing system consumes < 2 % of annual energy production, which is depending on the severity of icing. [2, pp. 25–27]

The different kind of chemicals has been also used to minimize ice adhesion and also to melt accreted ice for example from airplane wings and highways. These chemicals include different sorts of chloride salts, acetate compounds, glycol based solutions and some other substances. These chemicals are either sprayed or spread on the protected surface. These chemicals will gradual lose their properties, which make them only tem-

porally option. In many cases the can also corrode the protected surface, for example the underlying metallic surface [12, 89].

The most widely used anti-icing chemicals have been chloride salts, where sodium chloride is the most widely applied on the highways. However it is corrosion inhibitor and it has a limited usage on the metallic surfaces. Other chloride salts such as magnesium and calcium chlorides are less corrosive, but will remain slippery surface after the snow or ice accretion, which limits their utilization on the sea vessels and offshore platforms. Acetate based compounds, such as calcium magnesium acetate, potassium acetate and sodium acetate, are less corrosive than chloride salts, but they are expensive. The glycol based compounds are effective against snow and ice, but they are toxic substances.[12] In addition silicone greases and other chemicals contain harmful ingredients, which make the use of chemicals debatably due to their harmful impact on the environment. [17]

The environmentally friendly, energy saving and safety solution to icing could be found from the coatings. The active de-icing and anti-icing methods consume produced energy, which decreases the efficiency. [8, 60, 83] Mechanical methods do not consume excess energy, but the ice fall risks and operations in heights cause major safety risks. If these coatings can guarantee the desired level of operation, they would replace other anti- or de-icing methods due to reasons mentioned above. The coatings or other surface treatments in the anti-icing solution would give a solution, which would respond to nowadays green values.

However, the manufacturing of totally ice repelling coatings is very challenging because of the complexity of icing. The current research of anti-icing coatings has been focused on minimization of ice adhesion of the coatings. The realistic aim in the utilization of anti-icing coating is to exploit them together with other anti-icing systems for example with the electrothermal methods. The benefit of the coatings would be decreased ice adhesion between the surface and ice, which decrease the required heating. The less heating output would mean higher efficiency. [3,pp.264-265, 8]

The different approaching in the coating development has been used and the proposed materials have been varied from polymer coatings into the superhydrophobic polymer composite coatings. The surface roughness combined with the surface free energy has been demonstrated to produce superhydrophobic surfaces. The surfaces that have contact angles above 150 ° and small contact angle hysteresis are defined to be superhydrophobic. [90]

One major research approach has been the studies of superhydrophobic coatings in the prevention icing or minimization of ice adhesion on the surfaces [30, 58, 60, 83, 91, 92]. Although there has been opposite opinions on the effectiveness of superhydrophobicity

[17, 31, 90, 93], it has been proposed that superhydrophobic surfaces would deteriorate during repeated icing/de-icing cycles. The roughness of the superhydrophobic surfaces contains two types of roughnesses; microroughness and nanoroughness. Microroughness and combined micro- and nanoroughnesses are illustrated in Fig.32.

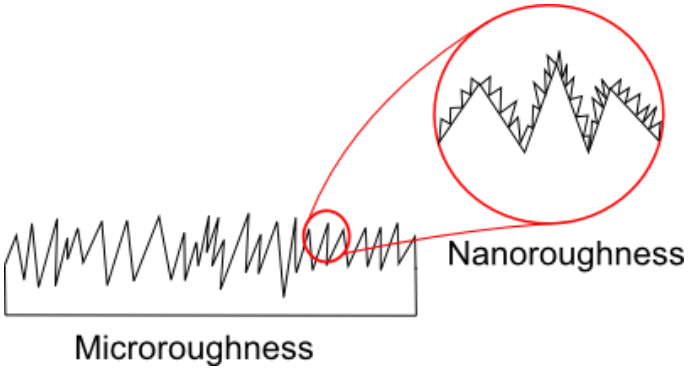

Figure 32. *Schematic presentation of microroughness and nanoroughness on the top the microroughness.*

Microroughness forms the overall topography of the surface and nanoroughness is located on the top of microroughness. The forces that hold this structure together are relatively weak and the mechanical interlocking of the ice can damage the asperities of the surface. The destruction of the surface roughness will diminish the superhydrophobicity of the surface which can increase the ice adhesion considerably. [31, 90, 93]

The best results have been obtained by altering the particle size in the superhydrophobic coatings. Cao et al. (2009) [91] have conducted outdoor icing tests in the freezing rain with the different particle sizes of the superhydrophobic coatings and discovered that the coatings with 50 nm particles actually repealed the accretion of the ice and lowered the adhesion between the ice and the coating. [91]

4.2 Anti-icing coating materials

The lack of interest on coatings in the icing prevention or ice adhesion mitigation, has affected negatively the image of the coatings as passive anti-icing strategy [83]. The coatings can offer significant improvements in anti- and de-icing properties compared to the materials currently utilized in the different industrial sectors. The anti-icing properties of various, versatile materials with different combinations have been discussed widely in the literature. Different polymeric coatings have been applied on the surfaces such as PDMS (poly(dimethylsiloxane)) [9], PSS (sulfonated polystyrene), PAA (aminoterminated polyacrylate) [89] and also more traditional polymeric coatings such as PMMA and PC have been tested. [94]

The different material approaches on the icing mitigation and decreasing the ice adhesion have been proposed by Arinpour et al (2012) [30], Farhadi et al. (2011) [31] and Li et. al (2012) [9], who have used silicone rubber coatings. The other major material group, which has been examined, is the fluoropolymers from which the most common

material has been PTFE (polytetrafluoroethylene) [1, 13, 75, 95, 96]. Also the fluorination or silanization have been performed to decrease the surface energy of the coatings. However, nowadays the focus of the research has been concentrated on the polymer composite coatings. These coatings include different matrix materials such as polymeric, fluoropolymeric or silicone compounds, which are reinforced with ceramic particles to improve the mechanical properties and also to give different surface texture for the coatings. [30] This chapter is divided into several subchapters by the different material approaches presented in the literature.

4.2.1 Polymeric coatings

Polymer coatings exhibit interesting and easily accessible choice for icephobic coating. The different composition of polymeric coatings has been applied widely in the different branches of industries. The conventionally utilized polymers such as PMMA and PU do not offer very interesting options for icephobic coatings, because their ice adhesion has been demonstrated to be similar to aluminum. [17, 83] Aluminum is not ideal icephobic material, because it has a high surface energy value [97]. Also the wettability of the aluminum is hydrophilic, which means that water will wet the surface texture. During the freezing the water will penetrate on the topography of the surface, which increases the ice-surface- contact area that increases the ice adhesion strength. Good icephobic coatings have the proper combination of wettability (hydrophobic or superhydrophobic), suitable surface roughness and low surface free energy.[41, 98, 99] Several explanations have been proposed to explain the high adhesion values for PMMA and PU. Antonini et al. (2011) [83] have stated that due to hydrophilicity of polymer coatings, droplet will wet the texture of the surface, which causes the external forces to be insufficient to remove water before it freezes. [83] Also other types of pure polymeric coatings, like PC, PEMA, PBMA, PSS, PAA and PE-PP-copolymers, have been found to provide only slight improvement on the ice adhesion values compared to bare aluminum. [83, 89, 92, 94, 100]

Greater interest has been focused on the fluoropolymer coatings, which should provide the better surface chemistry compared to traditional polymer coatings. Different authors have studied the icephobic behavior of PTFE coatings with the different particles size, ranging from nanoscale to microscale. [1, 83, 92, 95, 96] Fluorine containing surfaces are low surface-energy materials, which indicate low interaction with water or ice. Low interactions between the surface and water lead to hydrophobicity of the surface. Hydrophobicity has been discussed to lead icephobicity of the surface due to low interactions. [16, 92, 95]

In addition, other fluorine containing coatings than PTFE have been examined due to their low surface energy values. Kulinich (2011) [90] has studied the anti-icing behavior of the FAS-17 (1H,1H,2H,2H-perfluorodecyl-triethoxysilane) and Farhadi (2011) [31] investigated performance of FAS-13 (1H,1H,2H, 2H - perfluoroethoxysilane). These

coatings were produced by first etching the aluminum substrate in 17 % HCl, which changed the surface texture of the aluminum plates. After etching the aluminum plates were first cleaned with deionized water and dried in air for one hour. Finally the aluminum plates were dipcoated in either FAS-17 or FAS-13-solutions. Both of these substances, FAS-13 and FAS-17, contain highly fluorinate hydrocarbon chains as demonstrated in Fig. 33. High fluorine content guarantees low interaction with water. In addition their icephobic performance is great FAS-13 showing 55 kPa and FAS-17 40 kPa ice adhesion shear strength values. Ice adhesion strength for mirror polished aluminum is ~360 kPa in the centrifugal ice adhesion test. [31, 90]

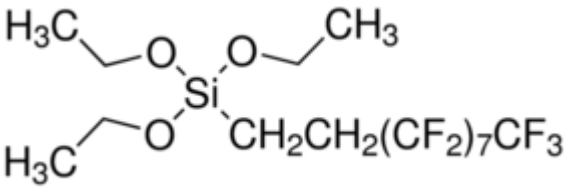

Figure 33*. 1H,1H,2H,2H-perfluorodecyl-triethoxysilane. [101]*

Besides, Zonyl 8470 (perfluoroalkyl methacrylic copolymer, DuPont) has been also studied in the literature. Zonyl 8470 have been used as low surface energy matrix material in the several polymer composite coatings. [31, 90, 102, 103] Also, the fluorinated POSS have been presented as a matrix material for some polymer composite coatings [92]. The complex structure of fluorinated POSS is presented in Fig. 34. Drawback of the fluorine containing coatings is their price and, therefore their amount is wanted to keep as low level as possible.

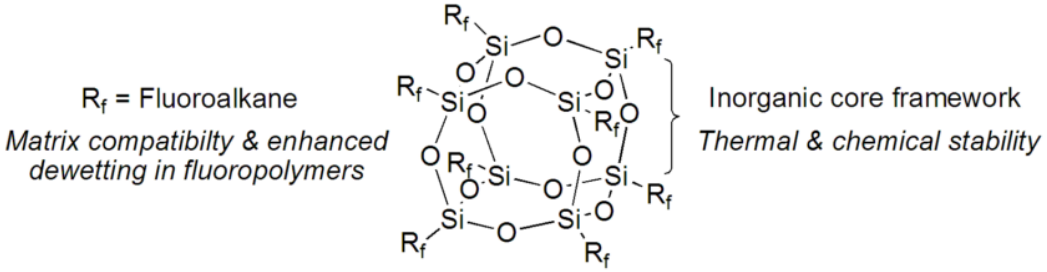

Figure 34. *Typical structure of fluorinated POSS. [104]*

The other alternative approach to offer low surface energy material is silicone based coatings. Different types of silicon rubber coatings have been widely applied on the parts of the power network structures, mainly on the conductors.[3, p. 231, 9] The reason behind application of these coating is related to their self-cleaning and hydrophobic properties, which have been found out to mitigate over voltages. [9] Especially room temperature vulcanized (RTV) silicon rubber coatings have been discovered to produce good icephobic behavior. Bharathidasan et al. (2014) [17] have investigated the ice adhesion strength of two different types of silicone containing compound; R2180 (silicone elastomer, Nusil technology LLC, Carpinteria) and RTV11 (RTV silicone rubber, GE Bayer Silicones). Both of these coating exhibited exceptional icephobic properties

R2180 having the ice adhesion strength 43 kPa and RTV11 25 kPa. The bare aluminum has the 1072 kPa ice adhesion strength, which was measured with zero degree cone test.[17] The hydrophobic low surface energy materials with the suitable surface roughness provide the proper properties that influences also the on the icephobic behavior. [17] The polymeric coatings for ice adhesion minimization are presented in Table 5, where commercial name, chemical name, ice adhesion strength. and ARF-values are shown. ARF means adhesion reduction factor compared to aluminum and higher ARF-value indicates better icephobic properties.

Table 5. *Collection of polymeric coatings presented in the literature. ARF stands for adhesion reduction factor compared to aluminum.*

Commercial name	**Chemical name**	**Ice adh. strength (kPa)**	**ARF**	**Ref.**
PMMA	Poly(methyl methacrylate)	463-1535	<1	[17, 83, 94]
PEMA	Poly(ethyl methacrylate)	510	-	[94]
PBMA	Poly(butyl methacrylate)	384	-	[94]
PC	Polycarbonate	129-400	4,4	[92, 94]
PU	Polyurethane	820	1,4	[17]
PSS	Polystyrenesulfonate	-		[89]
PAA	Aminoterminated polyacrylic acid	-		[89]
PDMS	Polydimethylsiloxane	291	-	[94]
PTFE	Polytetrafluoroethylene	60	20,2	[97]
PTFE	Polytetrafluoroethylene (Superhydrophobic)	-	3,5	[83, 105]
PTFE, UF-8TA	Polytetrafluoroethylene, particle size 0,3 µm	-	-	[95]
PTFE, MP-55	Polytetrafluoroethylene, particle size 4 µm	-	-	[95]
PTFE	Polytetrafluoroethylene , particle size 200 nm	209,6	2,4	[1]
PTFE	Polytetrafluoroethylene, particle size 200 nm	100-150		[13, 75]
F-POSS, FL0590	Trifluoro cyclopentyl polyhedral oligomeric silsesquioxanes	-	-	[92]
FAS-13	1H,1H,2H,2H-perfluoro-octyltriethoxysilane	55	6,6	[31]
FAS-17	1H,1H,2H,2H-perfluorodecyl-triethoxysilane	40	9	[90]
R2180	Silicone elastomer	43	25,2	[17]
RTV11	RTV silicone rubber	25	43,2	[17, 97]
HVIC 1547	Silicone rubber	190	1,9	[30]
F-PU	Fluorinated polyurethane	1000	1,2	[97]
F-RTV SR	Fluorinated RTV silicon rubber	401	3	[97]
F-Clean	EFTE, copolymer of tetrafluorethylene and ethylene	150	-	[23]
	Fluorosilicone+epoxy+ethyl acetate	-	-	[106]

Table 5 points out three main categories exist, when the polymeric icephobic coatings are concerned. First group consist of engineered plastics, and the second category contains fluorine containing polymers, of which the PTFE is the most widely studied icephobic material. Besides some other fluorinated polymers such as triethoxysilanes and fluorinated POSS have been introduced in the literature. The third category includes silicone containing polymers, of which RTV silicones have been widely applied on the power network insulators. As discussed in this chapter, polymeric coatings can offer even very good icephobic properties, but some drawbacks exist. Firstly the price of the fluorine containing coatings is high [107, pp. 3–5], which can limit their applicability on the large surface area applications. In addition, the wear resistance of the purely polymeric coatings is limited, and addition of reinforcing particles may improve wear properties. [27] Therefore enhancement to the icephobic and on other demanded properties have been searched by incorporating hard particles into the polymeric matrix.

4.2.2 Polymer composite coatings

Given insufficient properties of pure polymeric coatings have many enhancement attempts described in the literature. Polymer composite coatings consist of hard phase, which is bind into polymer matrix. Hard phase is typically some oxide ceramic particles like titania [30, 31, 103], silica [17, 57, 91, 106, 108, 109], ceria [30, 31], which size varies from nanometer size to micrometer size. Materials introduced in Chapter 4.2.1 have been typically acted as binder matrix. In addition to these binder materials cheaper polymer materials such as epoxy and polyester have been included in the polymer composites [8]. Cheaper materials, e.g. carbon black, glass and carbon fibers, have been also used to replace more expensive materials like ceria and zirconia [90, 102, 110]. This chapter is divided in to three different sections; fluoropolymer composites, silicone-containing composites and other composites structures.

Different factors, such as surface roughness, wettability and surface energy, have influence on the ice adhesion strength. It has been proposed that the increasing water contact angle should decrease ice adhesion strength. In other words due to high water repellency of the superhydrophobic surfaces should have low ice adhesion values and slower ice accumulation rate. [30, 58, 60, 83, 91, 92] The opposite opinions that superhydrophobicity does not guarantee low ice adhesion strength, have been also widely presented based on the frost formation on the surfaces and mechanical interlocking effect.[17, 31, 90, 93, 111] Chen et al. (2012) [93] tested silicon wafers with the four different wettabilities and the results are presented in the Fig. 35.

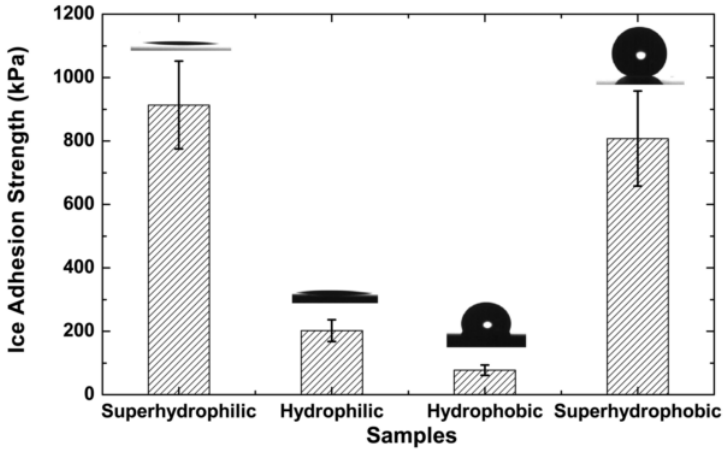

Figure 35. *Ice adhesion strength of four silicon wafers having different wettabilities. [93]*

Figure 35 illustrates that superhydrophobicity itself does guarantee low ice adhesion values. Instead the water contact angle hysteris (CAH) is more significant in determination of correlation between wetting behavior and ice adhesion strength. [75, 83, 94] Dynamic behavior of water actually has more effect on the ice adhesion values than static angles. The droplets' mobility and repellency is increased when contact angle hysteresis is decreased. [75, 94] Meuler et al. (2010) [94] have founded out that ice adhesion strength is depended on receding contact angle. Figure 36 shows the dependency between ice adhesion strength and receding contact angle.[94] Even so some dependency can be observed; the values have high variation from the fitting line. Zou et al. (2011) [98] have studied the influence of both wetting behavior and surface roughness and have discovered that the correlation between water contact angle and ice adhesion strength only exist for surfaces having similar surface roughness [98].

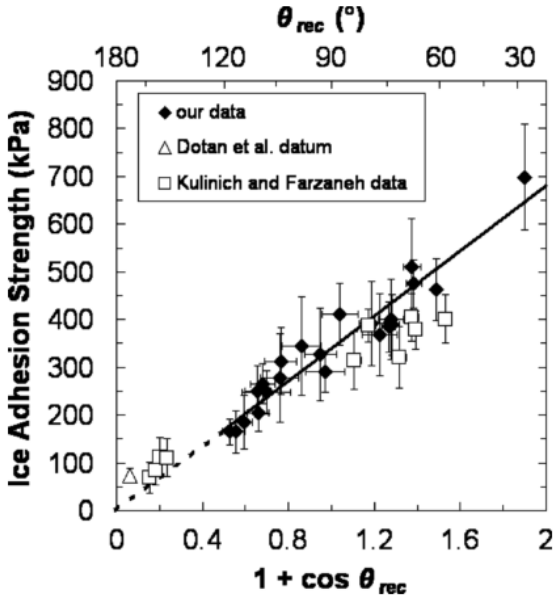

Figure 36. *Dependency between ice adhesion strength and receding contact angle. Meuler et al. (2010) [94] have fitted the data from other studies [110] as shown in the specifications of the symbols.*

Surface roughness has also an effect on ice adhesion values. It has been demonstrated the increasing the surface roughness will increase the ice adhesion values. [97, 112] Yang et al. (2011) [97] have studied PTFE surface with different roughnesses, where the surface roughness was increased by sandblasting the PTFE surface. As a result of sandblasting the ice adhesion strength raised from 60 kPa to 160 kPa in zero degree cone test. In addition, they studied the effect of surface chemistry on the ice adhesion strength by measuring the surface chemical composition and ice adhesion values for PTFE, fluorinated PU and fluorinated RTV silicon rubber. In this study, it was discovered that the higher fluorine content gives lower ice adhesion values. Alternatively higher oxygen content increases hydrogen bonding between ice and the surface increasing also the ice adhesion strength. [97] According to studies of Koivuluoto et al (2015) [113] and Bharathidasan et al. (2014) [17] the coatings that have similar roughnesses can have very different ice adhesion strengths. The results of Koivuluoto et al (2015) study are presented in the Fig. 37. For example Koivuluoto et al (2015) measured ice adhesion strength for polished aluminum and PTFE having similar roughness, and find out that ice adhesion strength were 380 kPa for aluminum and 32 kPa for PTFE. Even so the similar ice adhesion strengths (~40 kPa) were measured for two superhydrophobic surfaces (SH1 and SH2) having different roughnesses. [113] These findings underline that different factors influence significantly on the ice adhesion strength. The ice adhesion strength has been discussed to depend on contact angle hysteresis, surface roughness and surface chemistry. [17, 41, 97, 113]

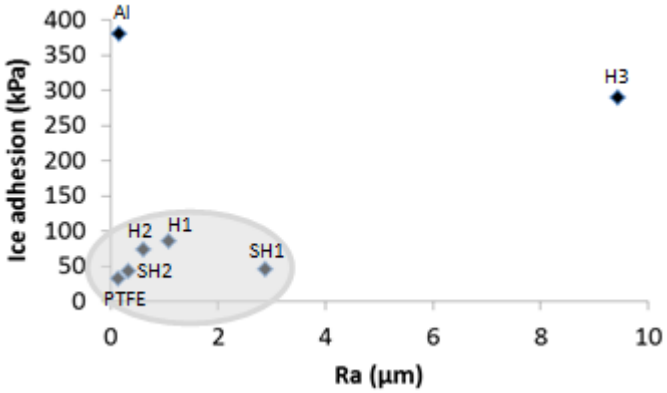

Figure 37. *Ice adhesion strength plotted against mean surface roughness (R_a). [113]*

Fluorine-containing polymer composite coatings have been used to produce superhydrophobic surfaces that have discussed to act also as icephobic coatings [31, 90–92, 106, 110]. The popular choice for the polymer matrix material has been Zonyl 8470 (perfluoroalkyl methacrylic copolymer, DuPont). [31, 90, 102, 103, 110] Different types of ceramic particles, TiO_2, CeO_2 and ZrO_2, have been added to Zonyl 8470 matrix. All of these composite coatings were manufactured by adding oxide ceramic powder in the liquid matrix. This suspension was sonicated 30 min prior the Zonyl 8470 addition, which after the suspension was stirred for 3 h. Finally coatings were either spincoated or sprayed on the aluminum substrates. [31, 90, 102, 103, 110] Besides of the ceramic particles, the noble nano-Ag particles have been added into the polymer matrix, to give

certain morphology for the surface. Nano-Ag suspensions were produced with the same manner than ceramic oxide suspensions and nano-Ag coatings were also sprayed or spincoated. [102]

As discussed previously the superhydrophobicity is produced when rougher micro-roughness peak are covered with the nanoroughness peaks and also low surface free energy is needed. All of these fluoropolymer composite coatings exhibit superhydrophobic behavior, which means static contact angles (CA) over 150 ° and contact angle hysteris (remainder of advancing and receding angles, CAH) under 10 °. [31, 90, 102, 103, 110] However it was observed that spray coating produces high contact angle hysteris over 70 °, whereas spincoating produces surfaces with lower CAH (under 10 °).[102, 103, 110] According to authors the superhydrophobic droplet behavior with the low CAH inflicts Cassie-Baxter wetting state, where droplets rest on the top the surface asperities, which is illustrated in Fig. 38 a). [31, 99, 103] Zonyl 8470 containing fluoropolymer composite coatings showed from 3 to 6 times lower ice adhesion values compared to bare aluminum. The best ice adhesion value of 65 kPa was obtained with Ag-nanoparticles (80-400nm) [102] and for ZrO_2 (20-30nm) [110]. Spincoated ceria (<50 nm) containing coating showed ice adhesion value of 80 kPa [31] and spincoated titania (<50nm) 110 kPa [103]. 3D-surface profile of Zonyl 8470 and titania is presented in Fig. 38 b). It is interesting to notice that ice adhesion strength for spray coated titania and zirconia coatings is significantly higher – at the same level than aluminum. [103, 110]

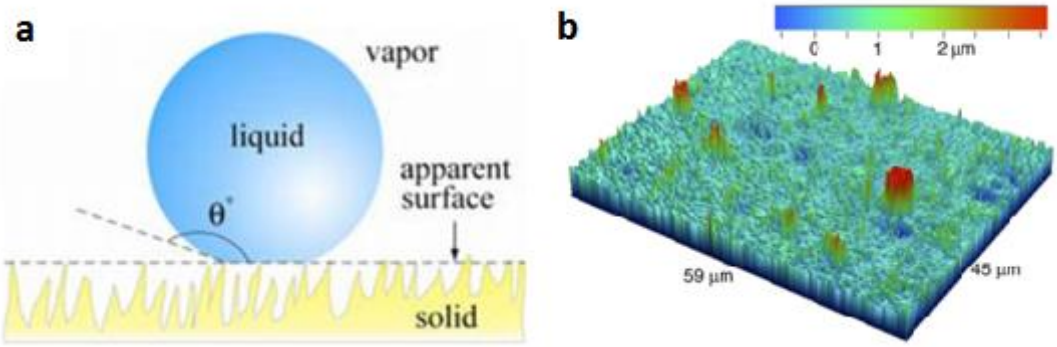

Figure 38. *Illustration of schematic Cassie-Baxter wetting state and its connection to surface roughness. a) Cassie-Baxter wetting state [114] and b) 3D-optical profile of the TiO_2-Zonyl 8470 spincoated surface showing both nano- and microroughness asperities. [103]*

As discussed previously superhydrophobic surfaces have gained some critic of their performance as anti-icing coatings. [31, 90, 115–118] Superhydrophobic surfaces have been reported to lose their wetting properties in high humidity. [94, 115, 118] In high humidity conditions, water can condensate into surface texture of superhydrophobic surface.[118] Furthermore in high humidity subzero temperatures frost formation can occur on the asperities of surfaces. [119] The frost formation on the superhydrophobic surface is illustrated in the Fig. 39. Frost is formed, when supercooled condensate water

starts to nucleate and form ice. As can be seen from the Fig. 39 d) the frost does not choose the site, where it adheres. Frost accumulation creates hydrophilic spots, which increase the ice adhesion strength. [119]

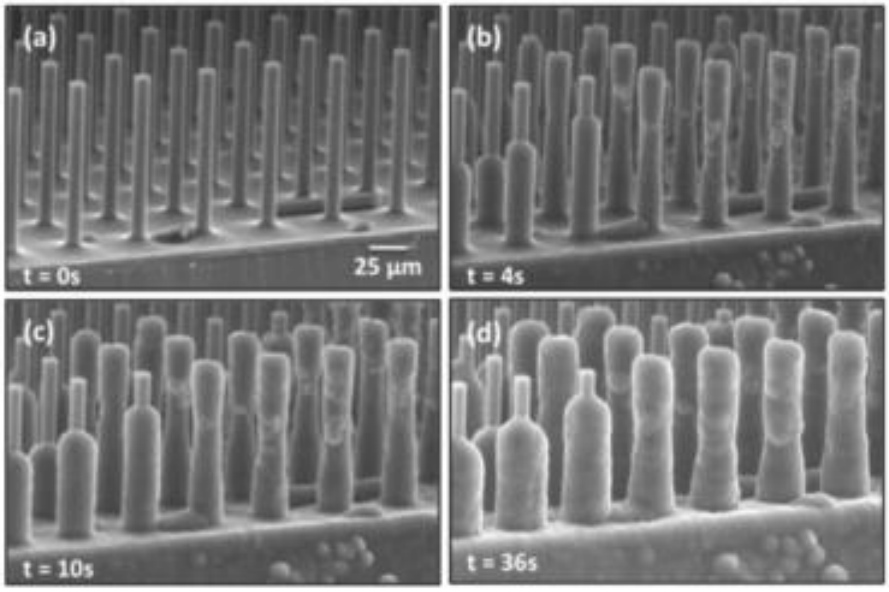

Figure 39. *Environmental scanning electron microscope (ESEM) images of frost formation on a superhydrophobic surface. a) dry surface and b)-d) snapshots of frost accumulation. At beginning of frost exposure, the pressure was 100 Pa and the vapor pressure was constantly increased until the frost nucleation occurred. The temperature was set to -13 °C. [119]*

In addition to the resistance against high humidity conditions the wear resistance of superhydrophobic surfaces is widely discussed in literature. [31, 90, 103, 115, 116] One way to evaluate the wear resistance of superhydrophobic surfaces is cyclic icing tests. Cyclic tests are performed by first accreting ice on the samples and measuring the ice adhesion strength. [31, 90, 103, 115, 116] Number of cycles varies between different studies from six icing/de-icing cycles [103] to 30 cycles [115]. During icing/de-icing cycles superhydrophobic surfaces will gradually lose their wetting performance. The loss of performance is related to gradual destruction of surface texture due to ice release. According to this model, the sharp asperities of the surface would be destroyed. [31, 90, 103, 116] In the Figure 40 schematic model of destruction of asperities is presented.

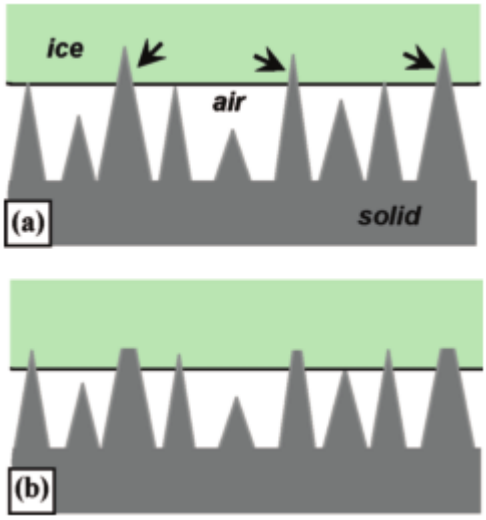

Figure 40. *Schematic presentation of ice on the surface roughness peaks. a) Ice resting on the top of the surface peaks and b) destruction of tips of surface asperities. [90]*

The destruction of surface texture can be evaluated by measuring the wetting behavior or surface roughness between the cycles. [31, 99, 103, 116] Farhadi et al. (2011) [31] have measured both static contact angle and root-mean-square roughness, which both are presented in Fig. 41. From the Figures 41 a) and b) it can be seen that the ice adhesion strength increases gradual with increasing number of icing cycles. This increase is related to decrease of both static contact angle and surface roughness. These decreases indicate the destruction of surface texture of superhydrophobic surface, as shown in Fig. 41 c). [31] Similar results have been obtained by [99, 103] and [116]. Only Dou et al. (2014) [115] have discovered unchanged ice adhesion strengths in cyclic icing test.

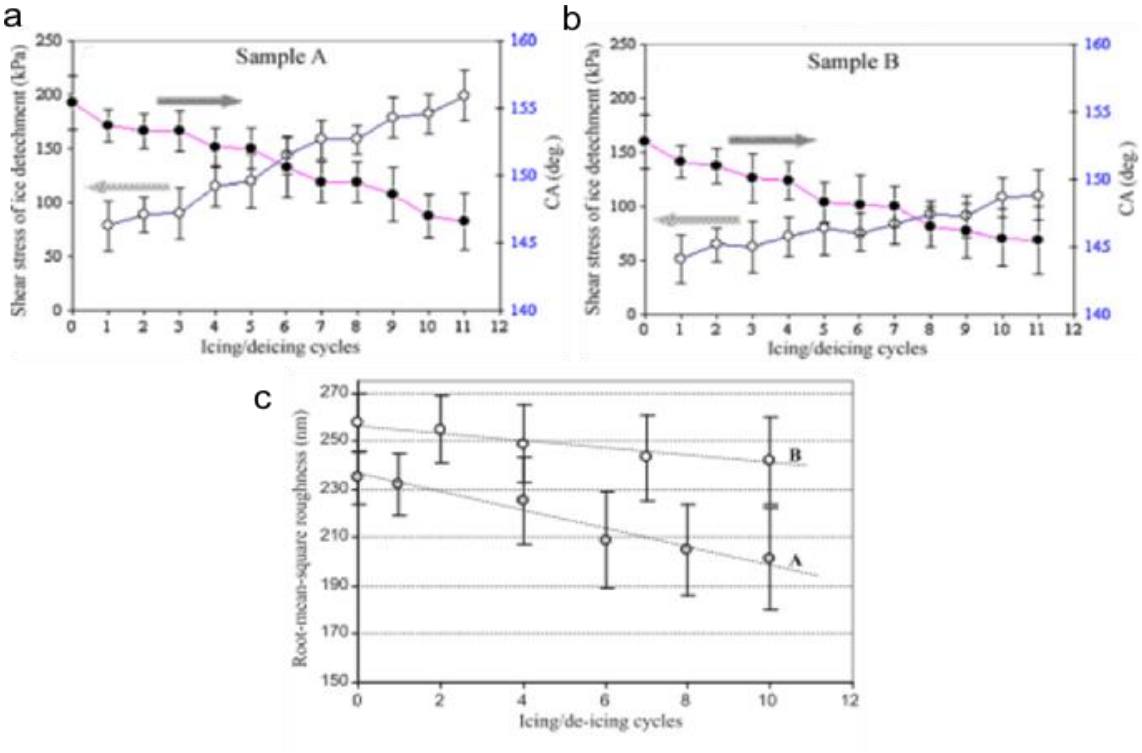

Figure 41. *Cyclic icing results for ceria-Zonyl 8470 (Sample A) and for FAS-13 (Sample B). In a) and b) the ice adhesion strengths are presented with the open dots and static contact angles with filled dots. In c) Root-mean-square roughness is presented for samples A and B. [31]*

Dou et al. (2014) [115] have prepared modified polyurethane (PU) surfaces by incorporating PU anionomer with dimethylolpropionic acid (DMPA) and isophorone diamine (IPDA) into aqueous solutions. As results of this polymerization reaction polyurethane was chain-extended with IPDA. The particles created in this reaction are presented in Fig. 42 a), where the hydrophobic core and hydrophilic corona are illustrated. Curing agent and y-butyrolacone were added to PU, and that mixture was spincoated on various substrate such as aluminum, stainless steel, ceramic and rubber, to demonstrate coating's applicability on different applications. The cyclic ice adhesion test were performed for this coating with the home-made apparatus, where ice was formed by molding and ice adhesion was measured by pushing the ice block and measuring the shear strength with force transducer. The results of cyclic ice adhesion test are presented in Fig.42 b).[115] Dou et al. (2014) [115] have reported that ice adhesion strength remained unchanged, 27 $\pm$6,2 kPa, over 30 icing cycles and they justified the low values with presence of aqueous lubricating layer between the sample's surface and ice. The aqueous lubricating layer is illustrated in Fig. 42 c).

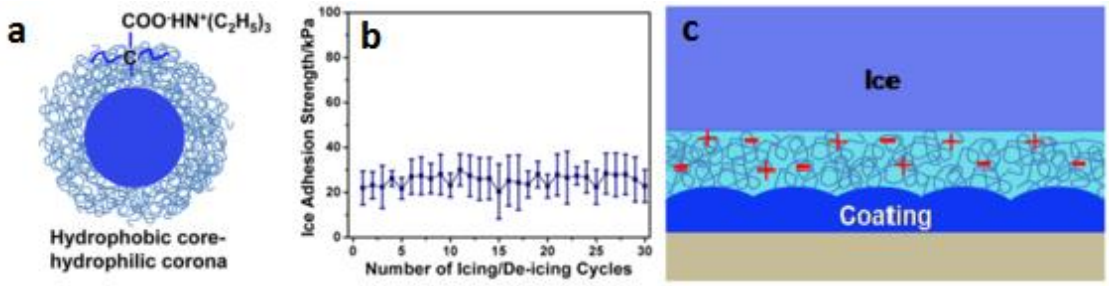

Figure 42. *Theoretical models aqueous lubricating layer and results of cyclic ice adhesion tests. a) Reaction product core-corona particle, b) results of cyclic ice adhesion tests and c) schematic illustration of aqueous lubricating layer.* [115]

Formation of aqueous lubricating layer is related to amide groups on the hydrophilic core of core-corona-particle. The bound water is formed over the amide groups, which means that few molecules thin layer of unfrozen water that lubricates the interface between ice and coating. Few molecules thin layer is enough to cover surface roughness, hence minimizing the effect of surface defects on ice adhesion. Thickness of lubricating layer is controlled by adjusting the amount of DMPA in PU dispersion – the more of DMPA the thicker layer. [115]

Other types of fluorine containing polymer matrix have been applied in the composite structures. Peng et al. (2012) [120] have studied anti-icing properties of modified PVDF (polyvinylidene fluoride). Modification was proceeded by adding ammonium bicarbonate (NH_4HCO_3), which is commonly used as raising or foaming agent to produce porous structure in the industrial applications such as plastics and ceramics manufacturing. In this study the porous, superhydrophobic PVDF surface was created and SEM-image of the porous surface is presented in Fig. 43. [120] Superhydrophocity was achieved with surface roughness and $–CF_2$ groups pointing out of the surface will lower the interactions with water. It was observed in this paper that no ice accumulation was formed on the modified PVDF surface in the laboratory icing tests, which were conducted by spraying supercooled 1mm sized droplets on the surface for 60min and the weight gain was measured. [120] However the situation of accretion could be different in outdoor conditions or in the icing wind tunnel.

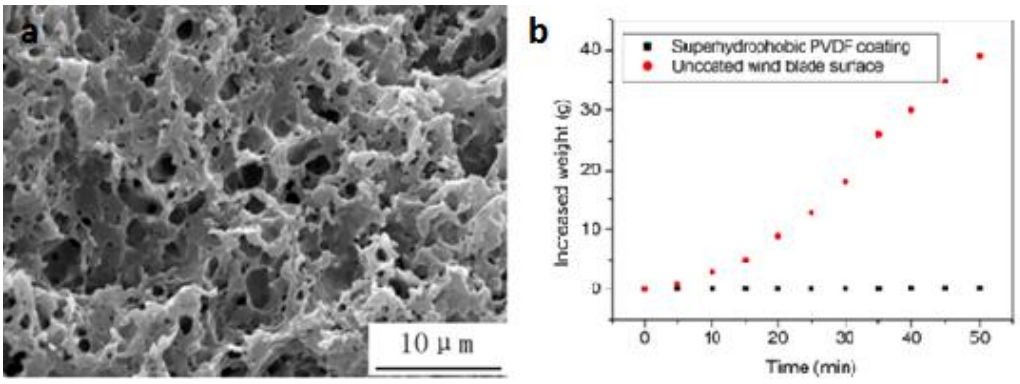

Figure 43. *Structure of porous PVDF surface and ice accretion results. a) SEM-micrographs of porous PVDF surface and b) ice accretion results of PVDF coating vs. uncoated wind turbine blade. [120]*

Also Ozeki et al. [23] have studied the fluoropolymer composite coatings by testing the composition of glass fiber cloth, PTFE and TiO_2 combination. They founded out that this hydrophilic offers lower ice accretion on the sea ice spraying test. [23] Zou et al. (2011) [98] have studied the icephobic performance of multilayer thin films The first layer of the coating, silicon doped hydrocarbon was applied on the aluminum substrate by PIID (plasma immersion ion deposition) and PECVD (plasma enhanced chemical vapor deposition). The role of the first coating layer was to bring thickness and low surface energy characteristics underneath the top coating layer. Fluorinated carbon layer 10nm layer was applied over 200nm thick silicon doped hydrocarbon layer with DRIE (deep reactive ion etching). [109] Zou et al. (2011) [98] founded out that the increasing surface roughness also raised ice adhesion values, which also was discovered by Cao et al (2009) [91].

Besides the fluoropolymer, silicone containing polymers have been used in the polymer composite coatings. PDMS [9, 94, 108, 121], RTV silicone rubber [17, 30, 31] and triethoxysilanes [122] have been popular choices in the literature. The silicone containing polymers offer low surface energy, suitable electrical conductivity and therefore they been applied on the conductors, where self-cleaning, low ice adhesion and weathering-resistance is required. [3, p. 231, 30, 121]

Silicon rubber based polymer composite coatings have been studied in the different papers. [17, 30, 31] Arianpour et al. (2013)[30] have studied the anti-icing performance of silicon rubber coatings with different nanoparticles additives, ceria (<25nm), titania (<100nm) and carbon black (42nm) [30]. These coating were produced by spincoating the aluminum sheets with suspensions. Suspensions were prepared by adding different powder into silicon rubber matrix and mixed magnetic stirrer. Aim of this paper was to study hydro- and icephobic properties of doped silicon rubber coatings. [30] Ceria and titania doped coatings showed ice adhesion values ~50 kPa and carbon black coatings have ice adhesion values of ~75kPa or ~125kPa depending on the concentration of carbon black. [30, 31] The mirror polished aluminum showed ice adhesion strength of 362 kPa.

Hard phase addition does not always improve icephobic properties. Hydrophilic fumed silica nanoparticles (10-15nm) have also been added to RTV silicon rubber, but the ice adhesion values were ten times higher (243 kPa) compared to ice adhesion of pure RTV silicon rubber (25kPa). The surface profiles of these coatings have been presented in Fig. 44. The high ice adhesion values were explained with high surface roughness values (R_a=4,46), which lead to the situation where water can penetrate between the cavities of the surface. This incursion of water causes so called mechanical interlocking effect, which the means that ice can have locking effect between asperities which increases ice adhesion strength substantially. [17] The distance and shape of the asperities i.e. surface roughness have a significant effect on the ice adhesion values. [91]

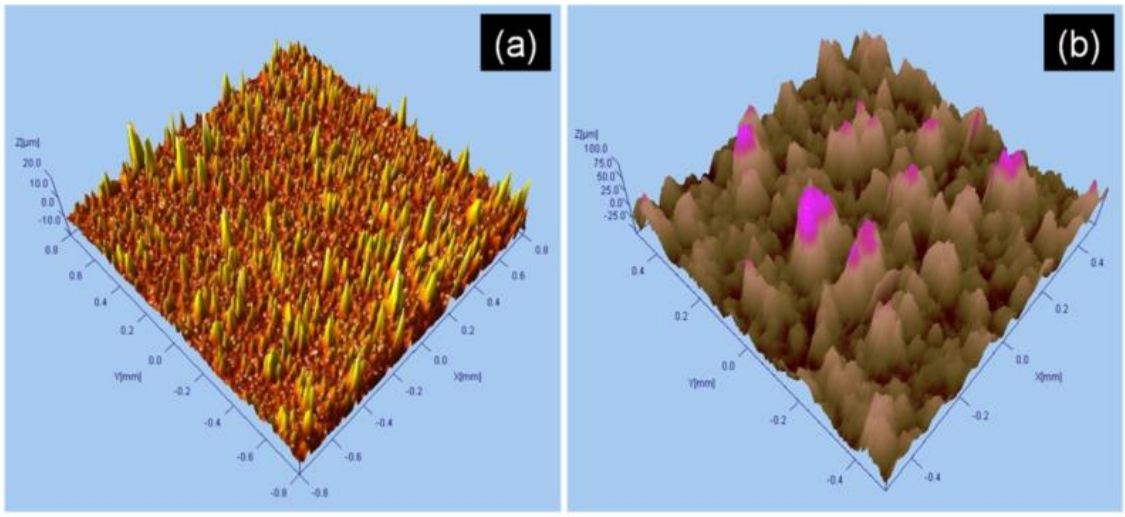

Figure 44. *3D-surface profiles of a) R2180+EH5 and b) RTV11+EH5. R_z-values are 1,62 µm and 4,46 µm, respectfully. [17]*

More complex polymer composite coatings have also been studied. Silica nanoparticles have been modified with the fluorine containing polymers like FAS-17 to improve their hydrophobicity. [9, 109] These modified silica nanoparticles were embedded into PDMS matrix and spray coated on the glass insulators. Modified silica nanoparticles were manufactured with sol-gel method. Silica gel was prepared by mix TEOS with ammonium hydroxide to obtain polymerization reaction. In order to create surface modificated silica particles FAS-17 and γ-aminopropyltriethoxysilane were added into silica gel. Silica gel was heat treated at 120 °C to get rid of the remaining solvents. Finally dried gel was grinded into nanosized silica powder, which mixed PDMS matrix. [9] The schematic illustration of the modified silica nanoparticles in the polymeric binder is presented in Fig. 45. Li et al. (2012) [9] have discovered that ice accretion on coated insulator was decreased compared to RTV silicon rubber coated insulator

Figure 45. *Schematic illustration of PDMS/modified nanosilica coatings. [109]*

Susoff et al. (2013) [122] produced sol-gel coatings from silica and fluorinated triethoxysilicates or PEG (polyethylene glycol). These sol-gel coatings were produced using TEOS (tetraethylorthosilicate) and GPTMS ((3-glycidylpropyl)trimethoxy silane) as precursors. Different additivities were added two types of fluorinated triethoxysilanes or PEG were added to produce polymer matrix. These fluorinated silica sol-gel coatings showed 20 times lower ice adhesion values compared to bare aluminum. Although the addition of fumed silica particles created superhydrophobic surface, it also increased the ice adhesion values over the aluminum ice adhesion strength. [122] Lazauskas et al. (2013) [123] have also created sol-gel surface of silica nanocomposites, but observed

that superhydrophobic surfaces do not guarantee icephobic properties. Due to destruction of nanosurface roughness, superhydrophobic surfaces will lose their wetting properties responsible of water repellency. [123]

Modified silica nanoparticles have also been used in different polymer matrix. Liao et al. (2015) [106] have mixed hydrophobically modified fumed silica nanoparticles (15-25nm) into mixture of different polymer grades.[106] The combination was fluorosilicone, epoxy resin and ethyl acetate, which exhibited hydrophobic surface. The addition of nanosized fumed silica created micro and nanostructures that combined with suitable surface energy inflicted superhydrophobic behavior. In this paper, it was reported that the accreted mass of ice was decreased for the superhydrophobic coating compared to traditional glass insulator. [106]

Cao et al. (2009)[91] have studied the influence of particle size of hard phase on the icing probability [91]. In this research organosilane modified silica nanoparticles with different particle size (20nm, 50nm, 100nm, 10µm, 20µm) were prepared by adding them into acrylic polymer resin, which was synthesized from styrene, butyl methacrylate and glycidyl methacrylate. Surfaces having particle size up to 10 µm showed superhydrophobic behavior and the best icephobic behavior was observed with particle sizes 20nm and 50nm. These results were based on laboratory scale icing testing, where supercooled water was pour on the tilted samples and icing was visually inspected. Outdoor tests were conducted for the 50 nm silica/acrylic resin coating, and the comparison between the untreated aluminum and superhydrophobic coating is presented in Fig. 46. [91]

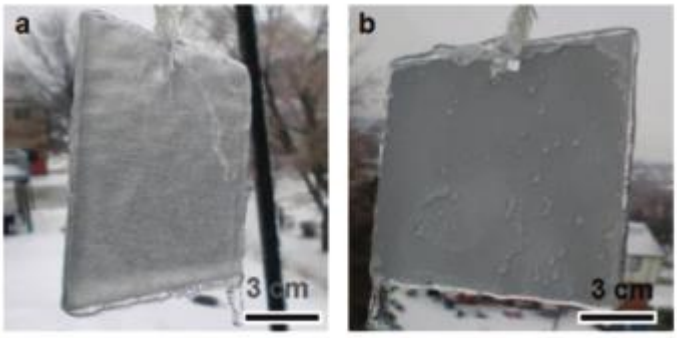

Figure 46. *Outdoor tests in the freezing rain for a) untreated aluminum and b) silica/acrylic resin*. [91]

It can be observed from the Fig. 46 that the aluminum is completely covered in glaze ice and on the contrary silica/acrylic resin- coating has only minor accretion on its surface and the edges of the plate. The plates were placed outside to wait the freezing rain to occur in Pittsburgh, USA in January. [91] Table 6 collects polymer composite coatings presented in the literature.

Table 6. *Collection of polymer composite coatings presented in the literature. WB stands for wetting behavior SH stands for superhydrophobic, HP for hydrophobic and HF hydrophilic. ARF stands for adhesion reduction factor compared to aluminum.*

Polymer matrix	**Hard phase**	**WB**	**Ice adh. (kPa)**	**ARF**	**Ref.**
Zonyl 8470	TiO_2 (<50 nm)	SH	110	3,3	[103]
Zonyl 8470	ZrO_2 (20-30 nm)	SH	65-80	4,5-5,5	[90], [103], [110]
Zonyl 8470	CeO_2 (<50 nm)	SH	80	4,5	[31]
Zonyl 8470	Ag (80-400 nm)	SH		5,7	[102]
Zonyl 8470	Ag (100-600 nm)	SH	85	4-4,2	[31], [102]
PVDF	NH_4HCO_3	SH	-	-	[120]
Glassfibre+PTFE	TiO_2 coating	HF	350	-	[23]
Silicone-hydrocarbon	Fluorinated carbon film	HP	160	2,1	[98]
HVIC 1547 SR	CeO_2 (<25nm)	SH	50	7,2	[30]
HVIC 1547 SR	TiO_2 (<100nm)	SH	50	7,2	[30], [31]
HVIC 1547 SR	carbon black (42nm)	SH	75	4,8	[30]
R2180, silicone elastomer	EH5, hydrophilic fumed silica (10-15nm)	SH	258	4,2	[17]
RTV11, RTV silicone rubber	EH5, hydrophilic fumed silica (10-15nm)	SH	243	4,4	[17]
PDMS	FAS-17 modified nano SiO_2	SH	-	-	[9]
F-POSS	SiO_2	SH	74	18,3	[92]
Fluorolink®S10 α,ω- triethoxysilane terminated polyfluorinated polyether	SiO_2 (solgel)	HP	~80	20	[122]
Fluorotelomer V, halfly triethoxysilane terminated fluorinated polyether	SiO_2 (solgel)	HP	200	8	[122]
Fluorolink®S10 α,ω- triethoxysilane terminated polyfluorinated polyether (PFPE)	Aerosil R805, SiO_2	SH	~1000	1,5	[122]

Table 6 summarizes the trends in the designing of icephobic polymer composite coatings. Similar polymer matrix materials have been utilized in the composites as listed in Table 5. Nanosized silica has been tested in the different matrixes with or without further modifications. In addition the different oxide ceramic have been applied in the composites.

4.2.3 Surface treatments

Different types of surface treatments have been applied to modify surface characteristics such as surface morphology and chemistry. There exist variety of methods that can be

utilized to produce surface modifications and chemical compound additions on the surface. In this chapter, some methods from the literature are described.

Metallic and silicon surfaces have been modified to obtain micron level textures on the surfaces by using laser ablation or lithograph. Charpentier et al. (2013) [89] have exploited laser ablation technique to engrave certain micron size patterns on surface of the 316L stainless steel, illustrated in Fig. 47. These created micropillars were functionalized with PSS (polystyrenesulfonate) and PAA (Aminoterminated polyacrylic acid). Authors have concluded that textured surfaces with the chemical dopants show that freezing temperature can be reduced compared to undoped textured surface. This can be explained due to higher contact angle, which means that there is less contact area with liquid and substrate. Ultimately this leads to situation, where less nucleating agents are available at the interface. Trapped air could also work as an insulating layer between solid substrate interfaces. In this study it was also discovered that these coatings decrease freezing temperature by 7 degrees compared to stainless steel. With surface modifications water contact angle can be decreased, which also decreases the contact area between liquid and surface. The decreased area means less nucleating sites on the surface, which slows down the freezing rate. [89]

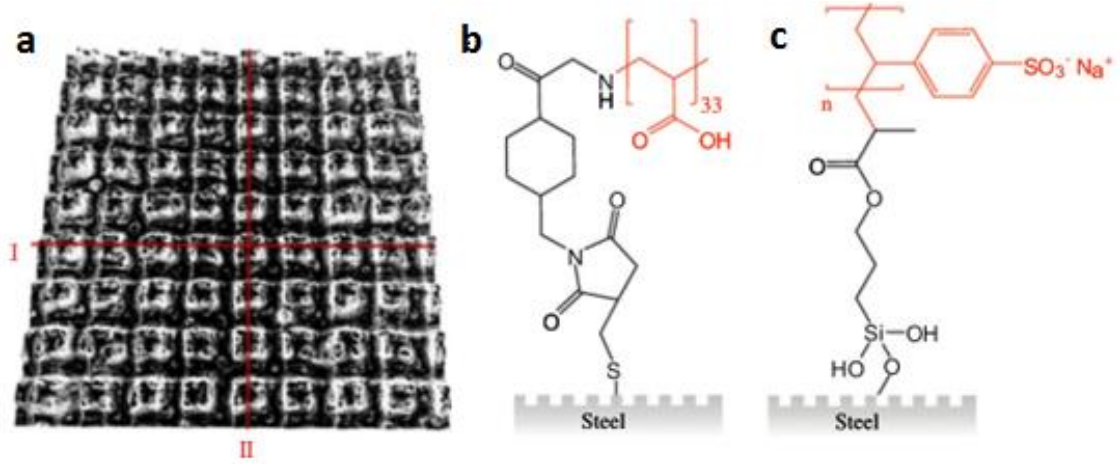

Figure 47. *Laser ablation and surface modifications. a) Micropillars on the 316L stainless steel's surface manufactured with laser ablation. Functionalization of the textured surface by b) PAA and c) PSS. [89]*

Second approach to craft textured surfaces was presented by He et al. (2014) [124], whom utilized the lithography technique. They have studied the effect of geometrics of the micropillars and also the influence of nanoroughness on the top of the micropillar, as illustrated in Fig. 48. Ice accretion was performed by placing 10 µl droplet on the surface, which was led to freeze in -15 °C. The ice adhesion strength was measured by pushing the droplet with small probe with force transducer. They discovered that the application of nanoroughness decreased the ice adhesion (420kPa) compared microtextured surface (1350kPa). It was also concluded that geometry has only little effect on the ice adhesion behavior. [124]

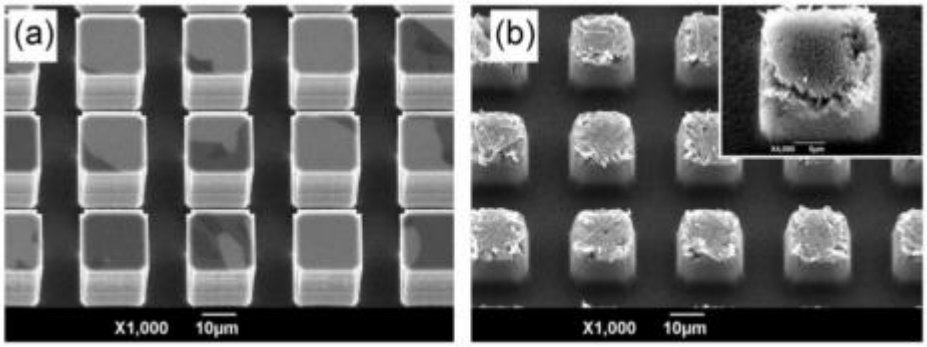

Figure 48. *Lithography crafted a) micropillars and b) nanoroughness on the top of the micropillars [124]*

Ruan et al. (2013) [125] have created superhydrophobic surfaces with electrochemical anodic oxidation and chemical etching. Electromical anodic oxidation was performed with the different sets of chemicals; first including sulphuric acid (H_2SO_4), oxalic acid ($C_2H_2O_4$) and glycerol ($C_3H_8O_3$) and the second was performed with phosphoric acid (H_3PO_4). The chemical etching was with iron (III) chloride ($FeCl_3$) and hydrochloric acid (HCl) by changing etching times. In this study, it was found out that the freezing time was increased for the superhydrophobic surfaces compared to uncoated aluminum samples. [125]

4.3 Summary of the materials and results from literature

As this Chapter 4 points out, multiple methods have been applied on the different structures to lower ice adhesion strength. Nowadays many of the methods are classified as active techniques, which utilize external energy in the removal of ice or prevention of icing. As described previously, heating elements have gained the wide popularity and in addition the pneumatic boots are applied in the airplanes. Still in the many cases the ice removal is performed manually with hammers and bats. Also some structures do not have any ice removal strategy, which is the case with many tall structures and also power network structures.

As was the case with anti and de-icing methods, also multiple coating materials have been proposed in the literature. The most common materials have been fluoropolymers like PTFE and silicone based compounds e.g. RTV silicone rubbers. The ice adhesion values of these fluoropolymer and silicon rubber coatings have been low, but the drawback of these coatings is their mechanical durability. Therefore different ceramic particles have been added to improve mechanical durability or change the topography of the surface. The involvement of nanorough texture combined with low surface energy material produces superhydrophobic surfaces. Icephobic behavior of the superhydrophobic surfaces is based on high droplet mobility on the surface, which leads to droplets to bounce off the surface. Alternatively it is stated that the droplets do not penetrate in the valleys of the asperities, but stay on top of the surface. This should in theory lead into

the situation, where the contact area between the droplets and surface is lowered, which reduces the ice adhesion values. As Tables 7 and 8 point out superhydrophobic coatings as the icephobic coatings have been widely studied.

Table 7. *Collection of anti-icing coatings and surface, which are tested with centrifugal ice adhesion test. WB stands for wetting behavior, SH stands for superhydrophobic, HP for hydrophobic and HF hydrophilic. AFR stands for adhesion reduction factor compared to aluminum.*

Coating	**WB**	**Ice formation**	**Ice adh. measurement**	**Ice adh. (kPa)**	**ARF**	**Ref.**
FAS-17	SH	spray icing	centrifugal	40	9	[90]
HVIC1547+ CeO_2 (<25nm)	SH	spray icing	centrifugal	50	7,2	[30]
HVIC1547+ TiO_2(<100 nm)	SH	spray icing	centrifugal	50	7,2	[30]
FAS-13	SH	spray icing	centrifugal	55	6,6	[31]
Zonyl 8470+Ag(80-400nm)	SH	spray icing	centrifugal	60	5,7	[102]
Zonyl 8470+ ZrO_2 (20-30nm)	SH	spray icing	centrifugal	65	5,5	[102]
F-POSS+silica	SH	spray icing	centrifugal	74	18,3	[92]
HVIC1547+ carbon black (42nm)	HP	spray icing	centrifugal	75	4,8	[30]
Zonyl 8470+CeO2 (<50nm)	SH	spray icing	centrifugal	80	4,5	[31]
Zonyl 8470 + ZrO2 (20-30nm)	SH	spray icing	centrifugal	80	4,5	[90]
Zonyl 8470 + Ag (100-600nm)	SH	spray icing	centrifugal	85	4,2	[31]
PTFE	HP	spray icing	centrifugal	-	3,5	[105]
Zonyl 8470 + TiO_2 (<50nm)	SH	spray icing	centrifugal	110	3,3	[103]
PC	HP	spray icing	centrifugal	129	4,4	[92]
HVIC1547	HP	spray icing	centrifugal	190	1,9	[30]
PTFE	HP	spray icing	centrifugal	210	2,4	[1]
Mirror-polished aluminum	HF	spray icing	centrifugal	~360	1	[30, 31, 90, 103, 110]
Al6061	HF	spray icing	centrifugal	505	1	[1]

Table 8. *Collection of coatings and surfaces presented in the literature, which ice adhesion is measured with zero cone degree test or other self-made apparatus. WB stands for wetting behavior, SH stands for superhydrophobic, HP for hydrophobic and HF hydrophilic. AFR stands for adhesion reduction factor compared to aluminum.*

Coating	**WB**	**Ice formation**	**Ice adhesion measurement**	**Ice adhesion value (kPa)**	**ARF**	**Reference**
RTV11	HP	molding	zero	25	43,2	[17]
R2180	HP	molding	zero	43	25,2	[17]
Fluorolink S10 +SiO_2	HP	molding	zero	~80	20	[122]
Fluorotelomer V+silica	HP	molding	zero	~200	8	[122]
RTV11+EH5 (fumed silica)	SH	molding	zero	243	4,4	[17]
R2180+EH5 (fumed silica)	SH	molding	zero	258	4,16	[17]
PU	HF	molding	zero	820	1,4	[17]
Fluorolink S10+Aerosil R805+silica	SH	molding	zero	~1000	1,5	[122]
F-PU	HP	molding	zero	1000	1,2	[97]
PMMA	HF	molding	zero	1535	<1	[17]
Bare Al	HF	molding	zero	1072	1	[17]
Bare Al	HF	molding	zero	1600	1	[122]
PDMS	HP	molding	peltier	291	-	[94]
PBMA	HP	molding	peltire	384	-	[94]
PC	HP	molding	peltire	400	-	[94]
PMMA	HF	molding	peltire	463	-	[94]
PEMA	HF	molding	peltire	510	-	[94]
Bare steel	HF	molding	peltier	698	-	[94]
F-Clean	HF	molding	push	150	-	[23]
Glassfiber+PTFE	HF	molding	push	380	-	[23]
Silicon doped hydrocarbon +fluorinated carbon film	HF	freezed droplet	push	160	2,1	[98]

As Tables 7 and 8 show, high fluorine and silicone containing coatings have occupied the tops of these tables. Low ice adhesion values have been found in the literature and

the best adhesion reduction factor over 43 (compared to aluminum) has been measured for RTV11 (RTV silicon rubber coating). The best ARF factor for fluorine containing coating has been measured for silica embedded in Fluorolink S10 matrix. In addition, R2180 (silicone elastomer) show ARF value of 25,2, which is exceptionally high. Tables 7 and 8 display that the performance of the superhydrophobic coatings do not reach the level of the best polymer coatings. However the ice adhesion reduction factors stay between 3,3 and 7,2. Significantly higher values have been obtained for engineering plastics such as PMMA, PC and PU, which ice adhesion strength is close to bare metals' ice adhesion. The ice adhesion strength is depended of the measuring method of ice adhesion, which is why it varies between different measuring techniques. For aluminum the measured ice adhesion strengths vary between ~360 kPa and 1600 kPa.

However, Tables 7 and 8 indicate the great difference in ARF values between different ice adhesion measurement techniques. Molding has been used to create on for surfaces on Table 8 and on the contrary icing wind tunnel spray icing have been used to accrete ice on the coatings in Table 7. Naturally, icings performed in the icing wind tunnel simulate more accurately real icing event, which were described in Chapter 3. Also the ice adhesion measurement techniques in Table 8 involve methods, where ice piece is either pushed or pull e.g. the ice block on the surface faces forces from external objects. On the other hand in the centrifugal ice adhesion test no external objects are in contact with ice block over the surface. Due to similar measurement techniques of ice adhesion and ice accretion, Table 7 can be used to compare directly the values measured in this thesis.

Properly functioning icephobic coatings would have great benefits compared to currently utilized anti- and de-icing applications. Icephobic coating would operate without external energy, offer environmentally friendly option and could be modified to multiple applications. The present icephobic coatings still have issues with their durability. The cyclic ice adhesion tests have showed that at least superhydrophobic surfaces will lose their icephobic behavior during the multiple cycles. [75, 90, 99, 103, 115] In order to function properly, the icephobic coating should release ice under the influence of external forces i.e. wind and gravity. In practice this would mean that ice adhesion strengths should be close to zero. This level is not yet been achieved, as Table 7 and 8 point out.

5 RESEARCH METHODS AND MATERIALS

The main goal of this thesis was to figure out how different icing conditions affect icing. By characterization of the surfaces and coatings connections between the icing condition and ice adhesion strengths were studied. The secondary objective was to discover limitations of test equipment i.e. how ice accretion of different ice types could be performed in different temperatures. Focus was also to assess the reliability of test equipment, when different ice types were accreted. Ice accretions were performed for all tested samples in nine different conditions and ice adhesion was measured in every condition. The surfaces were characterized by measuring the wetting behavior i.e. static and dynamic contact angles with the water. Also the effect of surface roughness was evaluated with optical profilometer.

5.1 Contact angle measurements

Contact angles with the water and wettability measurements were performed with KSV CAM2000 equipment (KSV Intruments Oy, Finland). The measurements were conducted in a conditioned room, where ambient conditions are 23 °C and 50 % relative humidity. In order to analyze the wettability of the samples both static and dynamic angles were evaluated. Static contact angles were measured at least from five droplets, which were let to settle for 5 seconds. Due to high variety of wettability in the test series, two different droplets sizes were used; 5 µl for hydrophobic and 10 µl for superhydrophobic surfaces. Larger droplet size for superhydrophobic surfaces was necessary in order to prevent droplets to fall off from the sample. Dynamic contact angles were measured in a way that droplets were filled up to 30 µl and unfilled back to capillary. Pump rate was set to 1 µl per second and the images were taken every second during the measurement. Advancing and receding droplets are presented in Fig 49.

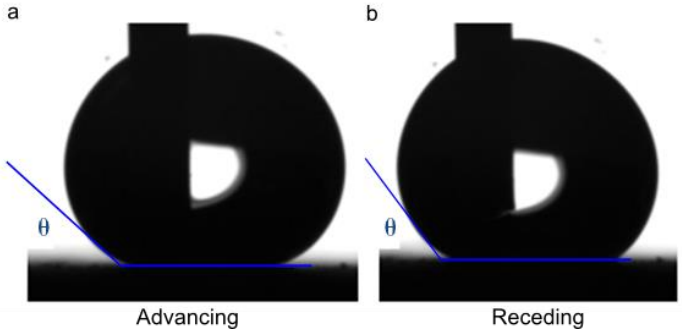

Figure 49. *Example of droplets on superhydrophobic surface in dynamic contact angle measurement. a) advancing and b) receding contact angle. [49]*

5.2 Surface roughness

Surface properties (surface profile, Ra, Sa values) were analyzed by Alicona Infinite Focus G5 optical profilometer (Alicona Imaging GmbH, Germany) with the 20x objective magnification, resulting in a measurement field size of 0.81 mm x 0.81 mm on the xy-plane. Vertical resolution achieved with this magnification is 50 nm. Ra- and Sa-values were measured from areas as large as possible.

5.3 Ice accretion

The ice accretion was performed with small scale icing wind tunnel, which was designed and constructed by Riku Ruohomaa at Tampere University of Technology (TUT). [49] Icing wind tunnel is placed in the climatic room, which temperature could be controlled, respectively, down to -40 °C. All the in-cloud ice types – rime, glaze and precipitation ice – are possible to be produced with equipment that has been discussed in the chapter 3. The icing wind tunnel is presented in the Fig. 50 and it is consistent of the following parts; 1,1 kW centrifugal fan (Suomen imurikeskus), stabilizing metal web, contraction component and nozzle system (Spray Systems ¼ J+SU12) to spray distilled water. The equipment is a U-shape and it is placed upside down in order to save floor base.

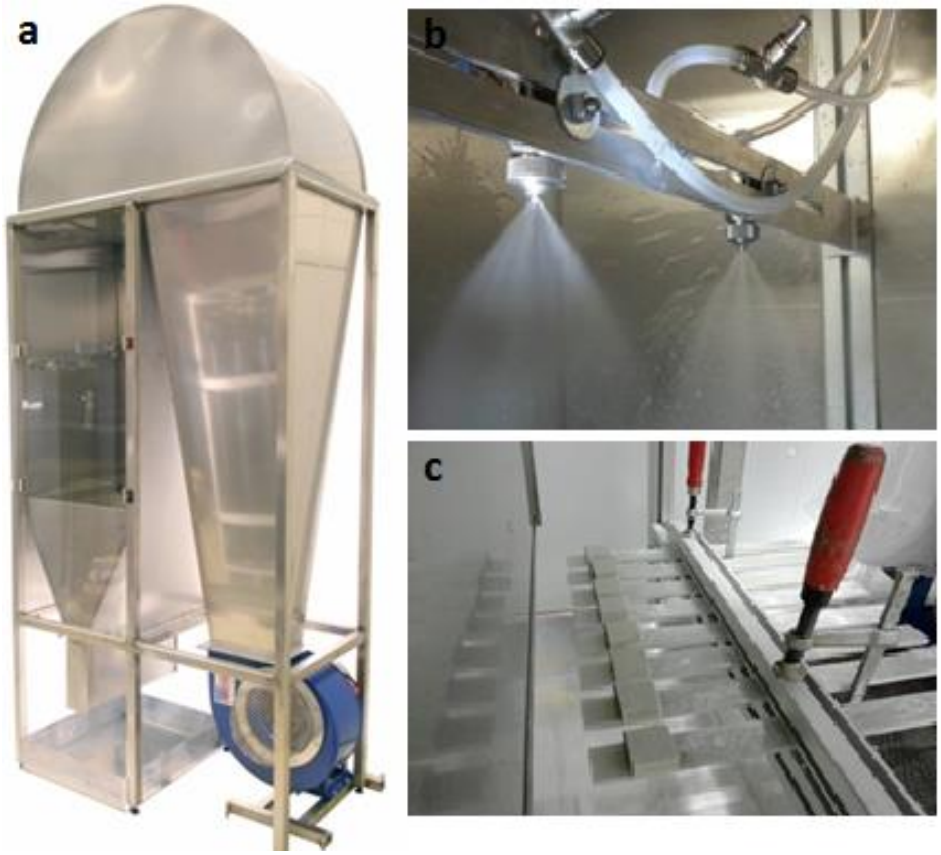

Figure 50. a) *Icing wind tunnel, b) nozzle system inside the wind tunnel and c) typical set of samples with masks at TUT.*

The basic idea of wind tunnel is to blow air in to U-turn where the flow is turned downwards into to contraction component, which increases the wind speed significantly up to 25 m/s. Before the contraction component, there are two nozzles where the distilled water is led with the separate hoses. Nozzles use compressed air to atomize water into to droplets, which volume median radius could be altered between 25-1000 µm. This spray jet accelerates due to wind and hits to exposed sample under the contraction component. Ice is usually accreted on the 30 mm x 30 mm area defined with masking. Masking block dimension are 30 mm x 30 mm x 10mm. The aimed ice height is 10 mm and it is inspected visually utilizing the height of masking. In Fig. 50 c) there is presented the typical set of masked samples.

The three different ice types, which were created in this thesis, were rime ice, mixed ice and glaze ice. Mixed ice is ice type having density as close as possible to glaze ice's density, but mixed ice does not have any icicles formed, which would change area of accreted ice. Mixed ice has been commonly used as standard ice in TUT's icing laboratory. The purpose of accretion of different ice types was discovering the limitation of the conditions where all three ice types could be formed. In Figure 51 the three ice types are presented.

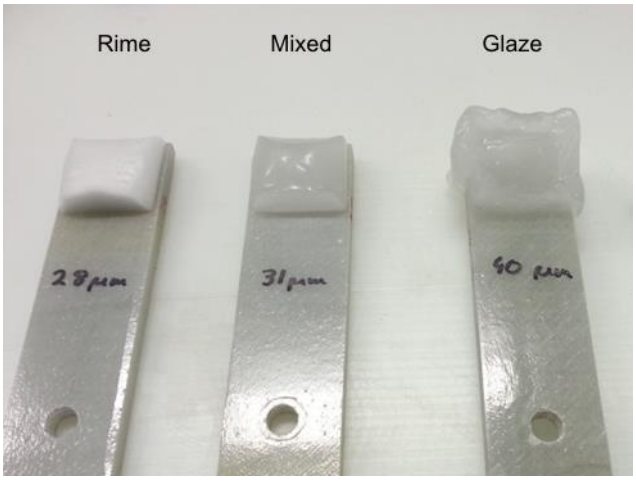

Figure 51. *Three different ice types from the previous icing trials The numbers presented in the each blade are the volume median particle sizes for sprayed water droplets.*

The icing tests were conducted by following the test matrix presented in Table 9, which also includes the remarks for each ice type at each temperature. The purpose of the tests was to be able to form three ice types presented in Fig. 51 at three different temperatures -5 °C, -10 °C and -15 °C. Typically ice accretion at the TUT has been conducted at -10 °C and the ice type accreted is mixed test ice, which is illustrated in the middle blade in Fig. 51.

In totally this thesis contained ice accretions in nine different conditions, as described in Table 9. The ice adhesion strength was measured also in all of these conditions. Results are presented in Chapter 6.4

Table 9. *Test matrix for condition testing.*

Ice type	**Temperature**		
	-5 °C	*-10 °C*	*-15 °C*
Rime	x	X	x
Mixed	x	X	x
Glaze	x	X	x

5.4 Ice adhesion

In a centrifugal ice adhesion test, the ice-accreted samples (presented in Fig. 52 a) are rotated with the constant acceleration until the ice block detaches. The detachment is observed with acceleration sensor, which is attached into the protective dome around blade. The samples are attached into the blades with screws and the blades are balanced to minimize vibration and stress for the servo motor and its axis. The equipment (presented in Fig. 52 b) is designed and built by Riku Ruohomaa [49] and it is based on equipment described by Laforte and Beisswenger [126].

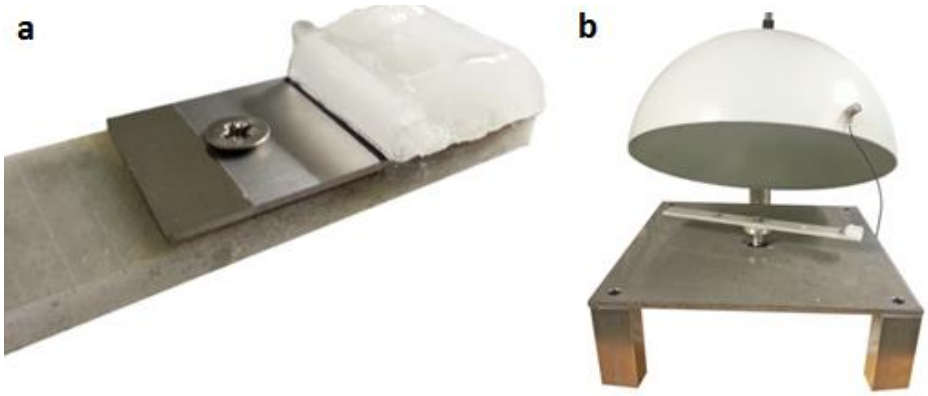

Figure 52. *a) Example of the sample with ice block accreted in the icing wind tunnel and b) centrifugal ice adhesion test device.*

When adhesion area is measured and the speed of rotation at the moment of detachment is known, the maximum adhesive shear strength can be calculated. The centrifugal force F can be written as shown in Equation 7:

$$F = mr\omega^2 \tag{7}$$

Where m is the mass, r is the radius of rotation and ω is angular velocity. By measuring RPM value at the moment of ice release, angular velocity can be calculated. The mass of ice block is measured by weighting the sample before and after ice detachment. The radius of the rotation is 17 cm, which constant in every test. The shear stress τ can calculated with the Equation 8:

$$\tau = \frac{F}{A} \quad (8)$$

where F is centrifugal force and A are of detached ice. After the ice detachment area of accreted ice block can be measured. By dividing the centrifugal force with the area of detached ice, the ice adhesion shear strength can be calculated. Ice adhesion strength for each sample is calculated as an average of five.

5.5 Materials

Different type of surfaces and coatings were selected as samples for this thesis. This group included samples with different wettabilities, different material groups (polymeric, metallic, polymer composite) and different surface roughnesses. The reason why this group of samples was selected is that they should cover as various ice adhesion values as possible. The samples used in this test are listed in to Table 10.

Table 10. *Samples with descriptions for condition testing.*

Sample code	Description
Al	Polished aluminum
PP	Polypropylene tape
PU-paint	Commercial two component polyurethane paint
SH1	F-containing superhydrophobic hybrid coating, Millidyne
SH2	Superhydrophobic coating, Ultra-Ever Dry®
PTFE	Teflon tape, Polytetrafluoroethylene tape (3M™ 5490)

Aluminum was selected as a reference material, because it is widely used in the literature.[1, 17, 30, 31, 90, 97, 99, 102, 103, 105, 116] The behavior of polymer surface was also researched, which is why PP and PTFE surfaces were selected. Different types of paint coatings are used in wind turbine blades, ships, trains and construction materials, therefore polyurethane based paint was chosen. SH1 and SH2 represent superhydrophobic coatings, which have been widely tested in the literature.[17, 30, 31, 90, 92, 93] PTFE stands for PTFE-tape, which signifies the fluorine containing polymer. Tape form was selected, because it is easy to apply new untouched surface for each test.

Tested samples had five parallel samples; except the aluminum had 3 parallel samples and PU-paint had four parallel samples. The ice accretions were done previous afternoon and ice adhesion test were performed next morning. Accreted ice blocks had about 16 hours to freeze properly.

6 RESULTS AND DISCUSSION

In this chapter the results obtained from this thesis are presented and analyzed. First in Chapter 6.1 the wettability results are presented and compared with the literature. Surface roughness measurements with 3D- roughness profiles are illustrated in Chapter 6.2. Ice accretion in nine different icing conditions are described in Chapter 6.3. In Chapter 6.4 ice adhesion test results from nine different icing conditions are evaluated.

6.1 Wettability

Wetting behavior of samples was analyzed by measuring static and dynamic water contact angles. Surfaces can be divided into the different categories depending on their water contact angle values. Hydrophilic surfaces possess water contact angles below 90°, which means that the water will wet surface. This indicates that the water penetrates into surface texture, and this state is called Wenzel state. When the water contact angle is over 90°, the surface is called hydrophobic. The maximum water contact angle value for flat hydrophobic is 120°. [114] In the cases, where the water contact angles are above 150 ° and the contact angle hysteresis is below 10°, the surface is called superhydrophobic.[31, 90, 92, 100, 120] The corresponding wetting state for superhydrophobic surface is named as Cassie-Baxter-state. Wenzel and Cassie-Baxter states are presented in Fig. 53.

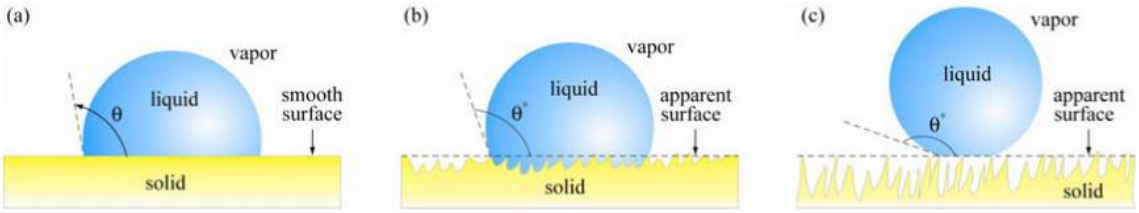

Figure 53. *Schematic presentation of different wetting states. a) water droplet on smooth hydrophobic surface, b) water droplet in the Wenzel-state and c) water droplet in the Cassie-Baxter-state. [114]*

Samples tested in this thesis were preselected to bear different wettabilities. Mirror-polished aluminum and PU-paint have clearly hydrophilic characteristics having static contact angles of 66° and 79°. Contact angle hysteresis describes the droplet mobility on the surface and the lower hysteresis the better movement of droplet. Droplet movement on the hydrophilic surface is non-existent. In addition PP falls into hydrophilic category having static contact angle of 89°. Only hydrophobic sample was PTFE, having 100° of water contact angle and hysteresis of 16°. Two hydrophobic samples (SH1 and SH2)

had static contact angles over 150° and hysteresis below 10°. SH1 had higher hysteresis of 10° compared to SH2, which had extremely low hysteresis of 2°. Water repellency and droplet movement on the SH2 was great. The contact angle values with hysteresis are presented in the Table 11.

Table 11. *Static, advancing, receding and contact angle hysteresis (CAH) of samples.*

Sample	**Static (°)**	**Advancing (°)**	**Receding (°)**	**CAH (°)**
Al	66	80	20	60
PU-paint	79	79	20	59
PP	89	91	52	39
PTFE	100	108	92	16
SH1	159	161	151	10
SH2	165	166	164	2

Measured water contact angles are in line with values presented in the literature. Static contact angles measured for aluminum varies between 57° and 83°. [17, 98, 102] Bharathidasan et al. (2014) [17] has measured 67° for static contact angle of aluminum, which is consistent with 66° measured in this thesis. [17] High CAH values are characteristic for aluminum [102], which means that the droplet movement on the surface is poor .Static contact angle for two component PU-paint has been measured as 73° and sliding angle over 90°. [17] Static contact angle for PP has been reported 96° and 104° for PTFE. [92] These values correspond well the values in Table 12.

Table 12. *Comparison of hydrophilic and hydrophobic samples on the values presented in literature. Static contact angles, CAHs and surface energies are presented. Wetting results obtained in this thesis are bolded and italic.*

Sample	**Static (°)**	**CAH (°)**	**Surface energy (mN/m)**	**Ref.**
Al	***66***	***60***	**-**	
Bare Al	67	-	101,80	[17]
Mirror-polished Al	57	50	-	[102]
PU-paint	**79**	**59**	-	
PU-paint	77	-	86,67	[17]
PP	**89**	**39**	**-**	
Polypropylene	96	-	30,1	[92, 127]
PTFE	**100**	**16**	**-**	
PTFE	104	-	20	[92,127]

Two superhydrophobic coatings with different wetting properties were selected in this thesis. Droplet movement on SH2 is better compared to SH1, which CAH is higher. Surfaces having wetting properties similar to SH1 have been presented in the literature.

[30], [102] Arianpour et al. (2013) [30] have measured static contact angle of 150° and CAH of 9° for silicon rubber+titania (100nm) coating. Kulinich et al. (2009) [102]have studied polymer composite coatings with different hard phase additions. Superhydrophobic polymer composite coatings of Zonyl 8470 and Ag-nanoparticles or zirconia (20-30nm) have showed static contact angles of 151° and 152°. Ag-nanoparticle coating had hysteresis of 9,5° and zirconia composite coating of 7,8°. [102]

Surfaces having wetting properties in line with SH2 have been also studied in the literature. CAH of 2° indicates very high water repellency. [91, 128] Cao et al. (2009) have manufactured coatings with CAH <2° by incorporating different sizes organosilane modified silica-nanoparticles in acrylic resin, and found out that 50nm and 100nm silica nanoparticles create highly superhydrophobic coatings. [91] Bharathidasan et al. (2014) [17] have utilized even smaller silica powder (EH-5, 10-15nm), which was mixed into silicone elastomer (R2180) and RTV silicon rubber (RTV11) matrices. Corresponding static contact angles and sliding angles for R2180+EH5 and RTV11+EH5 are listed in to the Table 13, where SH1's and SH2's wetting properties are compared to values in the literature.

Table 13. *Comparison of the superhydrophobic coatings of SH1 and SH2 with values presented in the literature. Static contact angles, CAHs and surface energies are presented. Wetting results obtained in this thesis are bolded and italic.*

Sample	**Static (°)**	**CAH (°)**	**Surface energy (mN/m)**	**Ref.**
SH1	***159***	***10***	-	
Zonyl 8470+ Ag (100-600nm)	151	9,5	-	[102]
Zonyl 8470+ Ag (80-400nm)	153	8,1	-	[102]
Zonyl8470+ ZrO_2 (20-30nm)	152	7,8	-	[102]
SR+TiO_2 (100nm)	150	9	-	[30]
Zonyl 8470+ TiO_2 (<50nm)	152	6	-	[103]
SH2	***165***	***2***	-	
Acrylic+organosilane modified silica (50nm,100nm)	~158	2	-	[91]
R2180+EH5	155	2	6,86	[17]
RTV11+EH5	158	2	5,33	[17]

Interaction between water and surface plays an important role in wetting behavior. Water molecule has unique characteristic to form hydrogen bonds with polar molecules on

the surface. The hydrogen bonding has the greatest impact on the adhesion of water or ice on the surface. [42] More polar surface the higher the intensity of interactions is. Furthermore higher interaction between the water molecules and surface are the higher sticking between the water and surface is observed. In other words polar surfaces form hydrogen bonds with water, which increases surface energy.[17] Higher the surface free energy is the lower the contact angles are. Superhydrophobicity is achieved for surface having low surface energy i.e. low interactions with water and naturally certain level of surface roughness. It has been stated that lower surface energy i.e. water repellency should indicate lower ice adhesion values [42, 92, 106].

6.2 Surface roughness

Surface roughness has great impact on the wetting characteristics. [17, 122] Different degrees of surface roughnesses can be achieved with different methods, for example utilizing etching, sand blasting or different coating methods. Spin- and spray-coating techniques have been utilized in the literature, and clear difference in wetting behavior has been discovered. [102, 103, 110] Spincoated coatings produce superhydrophobic surface with low CAH due to microscale rougher surface compared spraycoated ones. On the contrary static contact angles of spraycoated surfaces are over 150°, but CAH values are over 50°. [102, 103] Effect of difference between roughnesses of spin- and spraycoated surfaces is presented in the Fig. 54. Asperities of spraycoated surface are much finer compared to spincoated one, which leads into different wetting states. Superhydrophobic surfaces with low CAH will have similar surface roughness that is presented Fig. 54 a). On these surfaces the wetting state is Cassie-Baxter, which indicates air is entrapped between the surface and droplet. On the contrary on surface that have high static contact angles, but high CAH, will be in the mixed Cassie-Baxter and Wenzel- wetting state. In the mixed wetting state the droplets will rest deeper in the surface texture, which decreases drastically the droplet movements. [103]

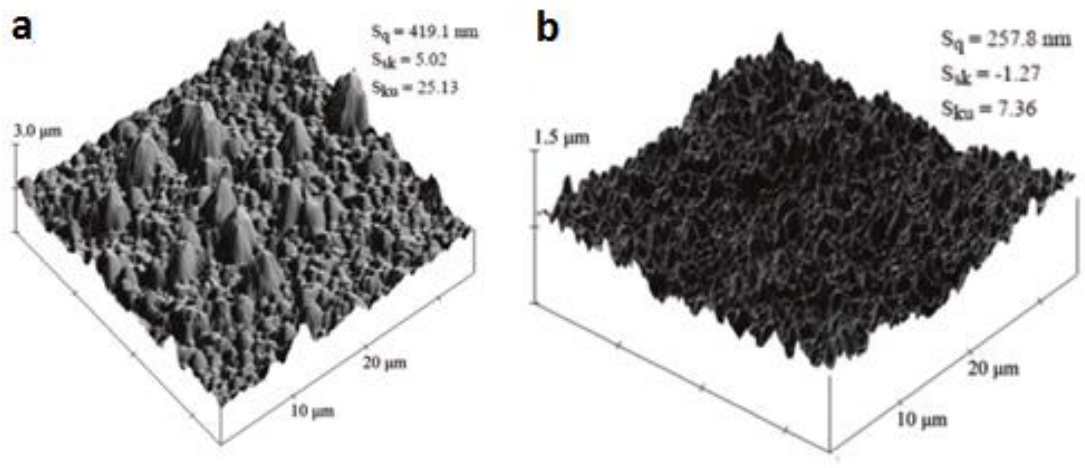

Figure 54. *AFM images of surface roughness profiles of Zonyl 8470+ZrO_2 polymer composite coatings produced by a) spincoating and b) spraycoating. [110]*

Surface roughnesses were measured in this thesis with the optical profilometer. Only the homogeneous samples PP and PTFE, where left out from this characterization. PP and PTFE are in form of tape, which is why surface is smooth and pristine for every icing test. Different surface roughness values are presented in Table 14. R-values are measured from 2D-line and S-values are measured from 3D-area.

Table 14. *Surface roughness values measured by optical profilometer. R_a is average roughness, R_z is mean peak to valley height of roughness profile, S_a is average height of surface area and S_z is maximum height.*

Sample	**R_a (nm)**	**R_z (µm)**	**S_a (nm)**	**S_z (µm)**
Al	169	1,15	225,24	19,93
PU-paint	867	5,65	2240	32,49
SH1	2890	18,62	6840	84,97
SH2	336	2,78	698	38,75

Based on Table 14, Aluminum has roughness values typical for smooth surface. PU-paint has rougher surface compared to aluminum. Superhydrophobic surfaces have certain level of microroughness and additionally nanoroughness over the microroughness peaks. Table 14 points out the clear difference between the SH1 and SH2. R_z values of these surface display the difference in the kurtosis of surfaces, SH2 having larger distance from valleys to peaks.

The 3D-surface profiles were also measured. Figure 55 shows the comparison of hydrophilic surfaces aluminum and PU-paint 3D profile of aluminum surface shows smooth surface with only a few microscale scratches. On the other hand, PU-paint is showing more uneven surface. When the larger area of PU-paint is explored, it can be seen that large areas that are either elevated or shallow. In addition there are circular peaks, which are probably agglomerates of PU. PU-paint is only coating that has been applied with foam brush when other coatings have been produced by spraycoating. It is clearly visible that the surface quality of PU-paint is irregular, which partly explains poor droplet movement on the surface.

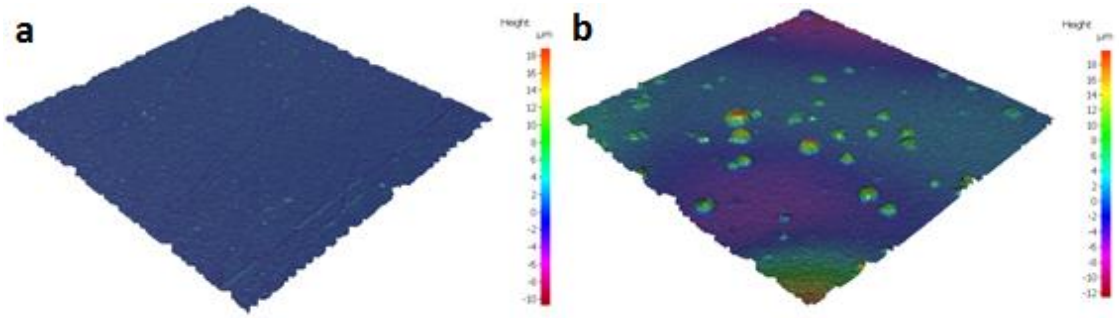

Figure 55*. 3D-surface profiles of hydrophilic samples; a) aluminum and b) PU-paint.*

Figure 56 illustrates surface profiles of superhydrophobic coatings SH1 and SH2. Better droplet movement was observed with superhydrophobic surfaces. However there were great difference in the CAH values of SH1 (CAH 2°) and SH2 (CAH10°), which can be explained with presence of different textures on the surfaces. SH1 has much rougher topography, whereas SH2 has smoother surface texture. 3D-profile of SH1 shows that the elevated areas are surrounded with deep valleys. The poorer droplet movement on the SH1 can be explained with the valleys, where water droplets will impinge. The valleys and elevated areas also explain the high R_z and S_z values of SH1. On the other hand SH2 has a finer roughness on its surface, having only some peaks formed by the agglomerates. These agglomerates do not affect the droplet movement on the SH2.

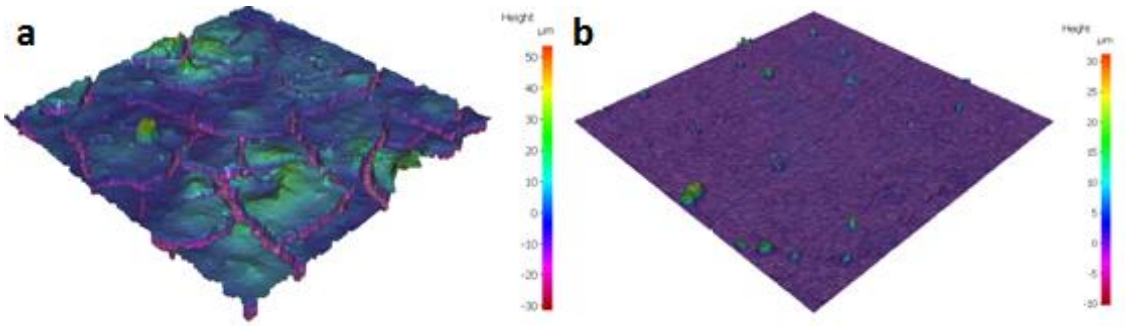

Figure 56. *3D-surface profiles of superhydrophobic samples; a) SH1 and b) SH2.*

Surface roughness has been measured for similar materials, which are tested. Roughness of bare aluminum has been measured in different publications and values of average roughnesses have varied between 0,25-0,3 µm.[17, 122] R_a value of 0,39 µm has been also measured for PU-paint. 3D roughness profile of the PU paint is presented in the Fig. 57, which is compared to PU-paint measured in this thesis. [17] Similar elevated and shallower areas are visible in the Fig. 57 a).

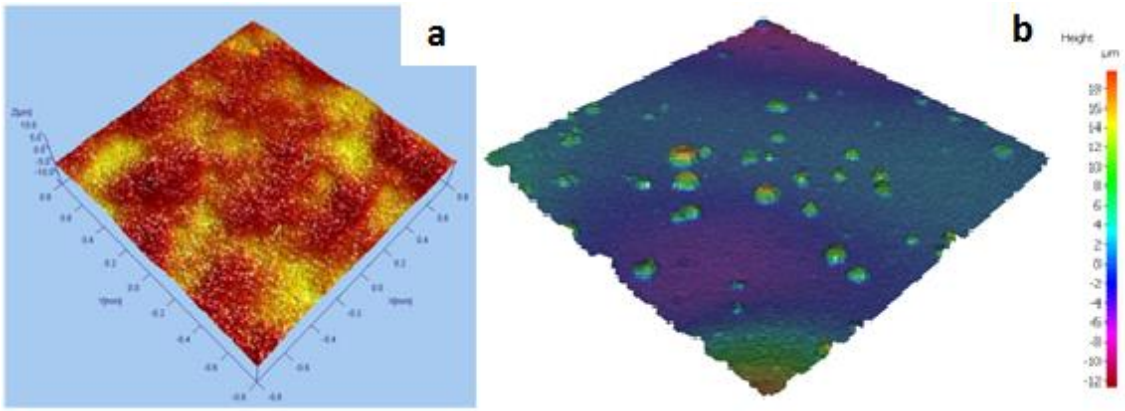

Figure 57. *Comparison of 3D-roughness profiles of PU-paints. a)PU-paint used in Bharathidasan et al. (2014) [17] and b) PU-paint used in this thesis.*

Kulinich et al. (2011) [103] have measured 3D-roughness profile of similar surface to SH2, which are illustrated in Fig. 58. [103] In the both 3D-profiles there is fine micro-roughness and some higher asperities rising from the surface. Both of these surfaces exhibit superhydrophobic characteristics.

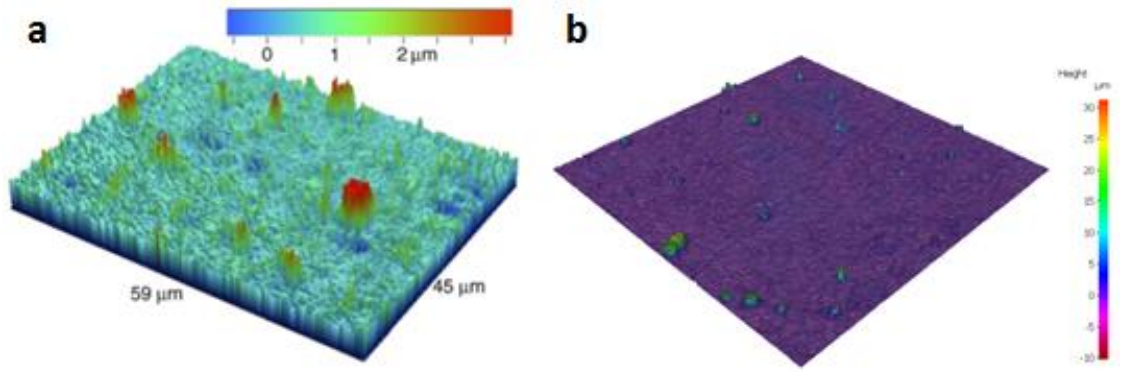

Figure 58. *Comparison of 3D-roughness profiles of a) TiO_2 (<50nm) + Zonyl 8470 [103] and b) SH2.*

The role of surface roughness on wettability and ice adhesion strength has been studied in the literature. The general finding, that ice adhesion strength increases as the surface roughness increases. [56, 97, 98, 122] This effect was demonstrated by roughening aluminum samples into different levels of coarseness, of which the ice adhesion strength was measured. Also the effect of surface energy combined with surface roughness was evaluated. Surface with different coarseness were coated with lower surface energy materials i.e. fluorine or silicone containing compounds. [98, 122] Susoff et al (2013) [122] have exploited fluorine containing sol-gel coatings, which was applied on the surface having different degrees of roughness. In Fig. 59, influence of fluorine coating into the ice adhesion strength is presented. [122]

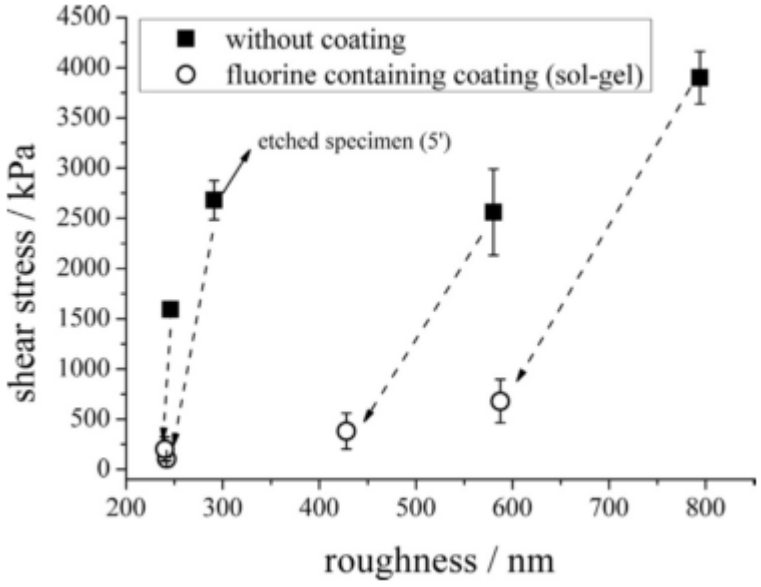

Figure 59. *Influence of fluorine containing to ice adhesion strength for different samples having different roughness.[122]*

Ice adhesion strength clearly decreases when the 1 µm thick fluorine containing coating is applied on the surfaces. It should be noted that the roughness itself also decreases when the thin layer of coating is applied. [122] Even so Zou et al. (2011) [98] have discovered that the lowering the surface energy lowers ice adhesion strength.

6.3 Accretion of different ice types at different temperatures

Formation of the different ice types is affected by several factors such as droplet size in the water spray, temperature and wind speed. The greatest factor that decides the ice type is droplet size. Larger droplets typically form glaze ice and smaller droplets can create rime ice. [3, p. 8, 40, 51, 52, pp. 21–22, 128] Furthermore the degree of supercooling of the droplets is important in the creation of different ice types. When the degree of supercooling is high, rime ice formed due to instant freezing of water droplets. On the contrary glaze ice formed in the lower degrees of supercooling, and the droplets will form splats when contacting the surface. [3, p. 8, 40, 52, pp. 21–22] Three different ice types, rime, mixed and glaze ice, were formed in three different temperatures (-5 °C, -10 °C and -15°C). Schematic illustrations of the ice types are presented in Fig. 60.

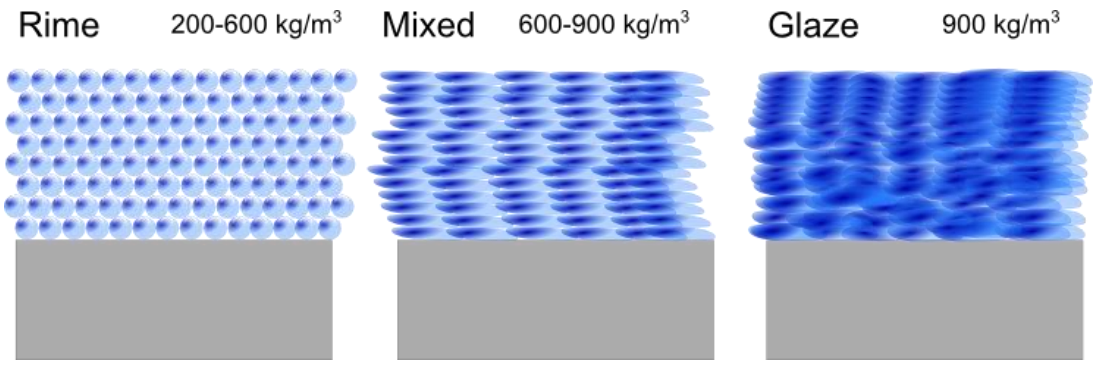

Figure 60. *Schematic illustration of ice types accreted in this thesis. The densities of the ice types are presented. [63]*

Droplets having median volume diameter close to 25 µm usually form rime ice either soft or hard (IEA2, s17). In this test series the aim was create hard rime, which characteristic features are hard surface, opaque and white appearance. Figure 61 show that this goal was reached. Rime ice accretion happens usually when the clouds and fogs containing super cooled droplets will contact some physical obstacles. Rime ice is typically formed in the temperatures below -10°C. [42, 56]When the rime is formed, water drops are supercooled and will freeze instantly when contacting the surface. Due to this kind of behavior, water droplets will freeze in spherical form over the surface, which will cause relatively porous ice. The porosity in rime ice causes it to lose its transparency making it opaque. [2, p. 12, 63]

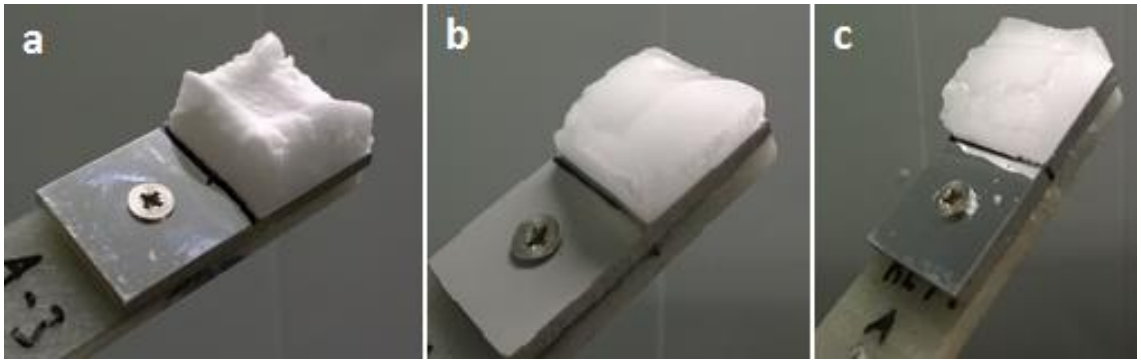

Figure 61. *Examples of different accreted ice types in the icing condition testing. The ice types are a) rime, b) mixed ice and c) glaze ice. The edges of the glaze ice block have been carved with the knife.*

On the other hand, glaze ice formation happens, when the larger drops (around 40 µm) will accrete on the surfaces forming dense, clear and tightly adhered ice blocks. The glaze ice has also some characteristics features like runback ice and heavy icicle formation due to heavy draining of water streams. The typical features of glaze ice are illustrated in Fig. 62 a). The other ice types accreted on the aerodynamic profile are presented in Fig. 62. In theory, the ice adhesion of glaze ice should be the highest compared the other ice types. Also its density is around 0.9 kg/m^3, hard rime's 0.6-0.9 kg/m^3 and soft rime's 0.2-0.6 kg/m^3.[63] The mixed ice is something between of the glaze ice and rime ice having some features of both classes.

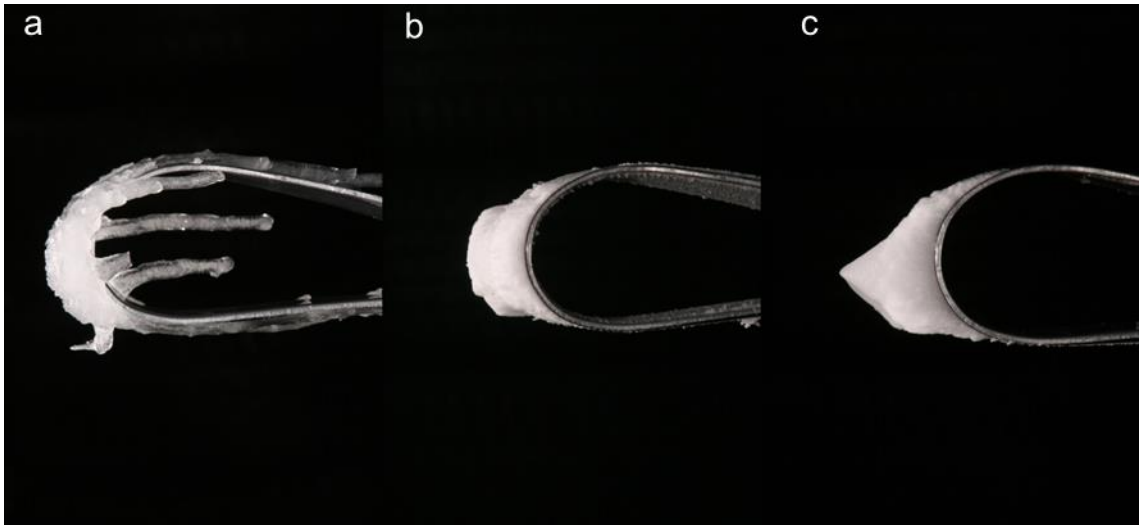

Figure 62. *Image of three different ice types accreted on the aerodynamic profile. a) glaze ice, b) rime ice and c) mixed ice.*

Due to the nature of ice adhesion test, ice accretion has some demands that will help the test process; minimum amount of runback ice, no icicle formation and composition as close to glaze ice as possible. The minimization of runback ice and icicle is done to minimize the amount of treatments to accreted ice blocks. For example carving of the icicles on the edges of ice block, can cause some tension which can inflict cracks on the ice block. Carving is a necessary step, because otherwise the area of ice block could not be determined. The reason why the mixed ice has been chosen to be as close to glaze ice as possible, is that in theory the glaze ice has the highest ice adhesion value due to dense structure [41]. Also the significant factor is type of failure mode. Failure occurs adhesively until the cohesive force of the ice is reached. Typically the tested surfaces and coatings are expected to possess low ice adhesion values, which is why the failure mode can be anticipated to be adhesive in the most of the cases.

Formation of different ice types in different temperatures is illustrated in the table 15, where easiness of accretion and adjustments are presented. The easiness of accretion is displayed with different colors; green means easy accretion, blue manageable and red unsuccessful accretion. Different adjustment were mandatory, in order to achieve characteristic conditions for formation of different ice types. As discussed previously different degrees of supercooling and droplet sizes are needed to create either rime, mixed or glaze ice. Generally the supercooling was increased by extending the distance between the nozzles and samples or by decreasing the droplet size.

Table 15. *Test matrix with the annotations. Green color stands for easiness of accretion; red is the limitation for the equipment and blue means that the successful accretion can be achieved by adjusting icing wind tunnel parameters.*

Temperature / Ice type	Rime	Mixed	Glaze
-5 °C (Additional 1.2m water pipe)	Difficult and slow -Droplets do not supercool fast enough	Adjustable -Height of nozzles -Pressure	Easy and fast -Droplets stay easily in liquid form
-10 °C	Adjustable and slow -Increasing pressure	Normal test ice -Standard procedure	Adjustable -Pressure adjustment
-15 °C (Full insulation and heating)	Easy -Droplets supercool easily before hitting the surface	Adjustable -Height of nozzles - increasing water flow	Adjustable -Height adjustment -Pressure min

As stated in Table 15, there have been a lot of differences in ice accretions at different temperatures and ice types. The colors for each cell indicate the easiness of the accretion and it can clearly be seen that a lot of adjustments are needed when spraying parameters are concerned. The most undemanding ice type which can be made with this icing equipment is mixed test. This can be explained due to fact that research team has been gathered a lot of data related spraying and quality of this ice type. Rime ice accretions are the most challenging due to slow accretion rate, but at -15 °C rime ice accretions were relatively easy due to high degree of supercooling of droplets. Contrary, glaze ice is relatively easy to produce, but the edges of ice blocks need to be smoothened with the knife, because heavy icicle formation during the accretion. However, some modifications were needed, when the temperature was changed from -10 °C either to -5 °C or -15 °C. These adjustments had to be made in order to prevent nozzles from freezing.

At temperature -5 °C, sprayed droplets are much warmer than at -10 °C, if adjustments are not made. It was observed that temperature of the water flow should be around 3 °C, which was the lowest temperature where the nozzles did not freeze. Cooling of the water flow the nozzles was done in a simple manner; the water pipes to the nozzles were extended. After the testing of different pipe extensions, the 1.2 m extension performed the best way. Ice accretion at the -5 °C were the most challenging ones, because close at the zero temperature the icing tends to be more pronounced to variations of the accretion parameters. For example the water temperature in the nozzles is only 3 °C, and the

smallest variations in the water flow affects a lot of composition accreted ice or can even cause nozzle freezing.

The accretion of the different ice types at the -5 °C temperature showed clearly the limitations of the equipment. The glaze was easy to accrete, because the sprayed droplets should stay in liquid form when hitting the samples. Due to lower cooling rate, which the droplets experience during air flight, droplets will be in liquid form when contacting sample surface. Although the lower cooling rate in air flight, makes it harder to produce the other ice types, where fast supercooling in the air flight is needed.

The only limitation for the equipment founded in this thesis was the rime ice accretion at -5 °C. The ice accretion was performed using the maximum spraying height, air pressure and minimum water temperature to guarantee the maximum cooling for the sprayed water droplets. The reason behind this limitation can be found from the cooling rate of the droplets. The air flight time is insufficient for the supercooling of the droplets, which is why the droplets will hit the target surface and form splats instead of instant freezing remaining spherical form. This kind of behavior produces mixed ice instead of rime ice, because in order to create rime ice droplets should freeze immediately in contact with the surface. Instantly freezing spherical droplets will create porosity in the structure of ice. This result is in the consistent with literature, because rime is typically formed in the temperatures below -10 °C. [42, 56]

The ice accretions at the -10 °C were the easiest ones to perform due to previous icing experiences at these conditions. Extra adjustments were not needed to make for the water pipes. At the -10 °C water temperature in the nozzles is aimed to be around 5-6 °C, which is relatively easy to achieve by controlling the pressure of water and the water flow. When the targeted water temperature is reached, the different ice types can be created by altering the compressed air pressure. The higher compressed air pressure atomizes water drops into the smaller droplets, which create porous ice called rime ice. On the other hand, lower compressed air pressure does not shatter the water flow so much, which keeps the water drop size greater. These larger water droplets form splats when hitting the surface and responsible for the creation of the glaze ice.

As the ice accretions at the -5 °C, were the icings at the -15 °C challenging because lack of experience at these conditions. Expectations were that nozzles would be very sensitive to freeze over and that the formation of glaze ice would be difficult due to higher cooling rate during air flight of the droplets. The freezing problem of the nozzles was resolved by applying the full length insulation for the water pipe leading to the nozzles and also putting on heating resistor inside the insulation. Cooling rate at these conditions is more rapid than at other test temperatures, and therefore the formation of rime ice is easy. The accretion of mixed test and glaze ice is harder to implement, because the droplets tend to freeze before hitting the samples' surfaces. Due to increased cooling

rate, the air flight of the droplets was decreased and also the water flow and compressed air pressure was adjusted on the optimum level.

However, adjustments did not guarantee the completely expected behavior, especially the glaze ice blocks were removed quite easily, when the icicles on the edges of the samples were carved with knife. The example of the carved edges of the sample can be seen from Fig. 61 c).

The critical factor affecting on the quality and the type of ice are the spraying parameters. The most important spraying parameters are the temperature of water at the nozzles (T_{water}) and pressure of compressed air (P_{air}). The other parameters that have impact on the spraying process and accreted ice are flow rate of water (F_{water}), pressure of water (P_{water}) and spraying height (h_{nozzle}) i.e. the distance between the nozzles and exposed samples. The parameters used in this test series are listed in Table 16.

Table 16*. Ice accretion parameters used in this study.*

		Temperature (°C)		
Ice type	**Parameter**	***-5***	***-10***	***-15***
RIME	T_{water} (°C)	3.2-3.8	5.6-5.9	9.5-10.5
	F_{water} (L/min)	0.125	0.125	0.15
	P_{water} (bar)	4.1	3.9	3.6
	P_{air} (bar)	6.0	5.5	3.5
	h_{nozzle} (m)	1.75	1.50	1.45
MIXED	T_{water} (°C)	3.4-4.1	5.9	9.3-10.7
	F_{water} (L/min)	0.125	0.125	0.16
	P_{water} (bar)	3.1	2.8	3.4
	P_{air} (bar)	3.7	3.9	2.5
	h_{nozzle} (m)	1.50	1.50	1.40
GLAZE	T_{water} (°C)	2.2-2.7	5.1-5.4	12.1-12.9
	F_{water} (L/min)	0.125	0.125	0.14
	P_{water} (bar)	3.0	3.9	3.5
	P_{air} (bar)	2.7r	2.3	2
	h_{nozzle} (m)	1.50	1.50	1.35

The water temperature at different room temperatures varies from 2.2 °C to 12.9 °C which is significant difference. The water temperature can be adjusted by altering the flow rate of water and also the pressure of pressurized vessel. The water temperature at the nozzles was adjusted on the level, which kept the nozzles open in other words prevented the freezing of the nozzles. The water temperatures for different ice types are

consistent at the temperatures of -5 °C and -10 °C, but the temperature of glaze ice accretion at -15 °C was higher than the other accretion temperatures at -15 °C. There were some difficulties to prevent freezing of the nozzles, which is why the water temperature was increased. The need for increase can be explained by looking at the other parameters at this accretion; the height of the nozzles was set to 1,35m, which is the lowest height where the nozzles can be placed. Also the pressure of compressed air is relatively low. These adjustment were mandatory, because otherwise the droplets hitting the samples were not wet enough which could create normal test ice. As mentioned in the requirements for the formation of glaze ice, droplets should be complete in liquid state that these droplets could form splats in the collisions. By using these adjustments, glaze ice accretion was done successfully and externally the ice blocks had the characteristics of the typical glaze ice – runback ice and icicles. Although the results of this accretion will show lower adhesion values compared the other glaze ice values at -5°C and -10 °C, which could be partly result of these spraying parameters. The lower compressed air pressure creates larger droplet size and higher temperature delays freezing time.

As mentioned before, the rime ice accretions were very challenging, because accretion took 3-6 times longer than the accretion of the other ice types. High compressed air pressures, 6.0 bar and 5.5 bar, were needed to create small droplet size (25µm) and to guarantee high cooling rate for droplets in the air flight. Although at the -15 °C, compressed air pressure was 3,5 bar, because the cooling at this temperature is significantly higher. If the high compressed air pressures have been used at -15 °C, the result would be snow or soft rime instead of rime ice. As can been seen from Table 15, the rime ice accretion at -5 °C was not successful and the mixed ice was obtained instead of rime ice. Too low or too high cooling rate causes problems in the accretion, which need to be overcome by altering the parameters, utilizing extra pipe length or introducing heating and insulation in the system. The parameters in Table 16 give the background information for the future test and the starting point for further parameter optimization.

6.4 Results of the ice adhesion tests

The aim of ice accretion and ice adhesion tests was to analyze the effect of temperature and ice type on the ice adhesion values. The ice adhesion tests were done in total for nine different sets of samples. The ice adhesions were measured as descripted in Chapter 5.4. At first the results in the different temperatures (in order -10 °C, -5 °C and -15°C) are presented and the effect of ice type on the ice adhesion strength is discussed. Additionally ice adhesion strengths for each ice types are presented. Furthermore the correlation between the ice adhesion strength and wettability and surface roughness is evaluated. Finally ice adhesion results of this thesis are compared the results presented in the literature. Only the results in the literature that utilize similar ice accretion and ice adhesion strength measuring techniques are taken into account, because there is huge variation between the values of different measuring techniques. Even so some compari-

son could be done by proportioning ice adhesion strength values to aluminum i.e. utilization of ARF-values.

Ice adhesion strength is normally measured at TUT in -10°C with mixed ice. The for selection of -10 °C can be found from literature, where several authors have also measured ice adhesion strength at -10 °C. [30, 31, 75, 90, 94, 97, 99, 102, 103, 110, 116] At -10 °C the supercooling rate is high enough in order to guarantee proper supercooling of the droplets, which is required in simulation of atmospheric icing conditions. The results at -10 °C are presented in the Table 17 and Fig. 63, where ice adhesion strengths for samples are presented.

Table 17. *Ice adhesion strengths for samples at -10 °C. Values for different ice types are presented. Avg means average of ice adhesion measurements and Std stands for standard deviation.*

Quantity	**Sample**					
	Al	**PP**	**PU-paint**	**PTFE**	**SH1**	**SH2**
Rime (Avg)	333	294	248	100	101	66
Rime (Std)	18	98	74	19	21	37
Mixed (Avg)	380	38	82	32	46	43
Mixed (Std)	70	17	7	4	13	-
Glaze (Avg)	289	108	149	60	68	39
Glaze (Std)	86	40	27	16	17	26

The order of ice adhesion strength values at -10 °C was as anticipated. Aluminum had the highest ice adhesion value with each ice type, which ice adhesion for mixed ice was 380 kPa. Centrifugal ice adhesion strength has been measured also for mirror-polished aluminum in the literature, which has been ~360 kPa. The second highest value was measured for PU-paint and third highest for PP, which represent polymeric surfaces. It was observed that ice type did affect the ice adhesion strength of PU-paint and PP, which had the lowest ice adhesion strength with mixed ice. PP had high variation in its values rime ice adhesion was as high as 294 kPa and mixed ice adhesion was only 38 kPa. PP has untypically low ice adhesion values with mixed ice and further analysis is needed in order to understand this behavior. PTFE showed low ice adhesion values for all ice types, ranging from 32 kPa to 100 kPa. SH1 had ice adhesion strength between 46 kPa and 101 kPa. The lowest values were discovered with SH2, which had its highest value of 66 kPa in the rime ice test and the lowest value in glaze ice test 39 kPa. Overall the ice adhesion tests at -10 °C were successful and same consistence between the values of different ice types was discovered.

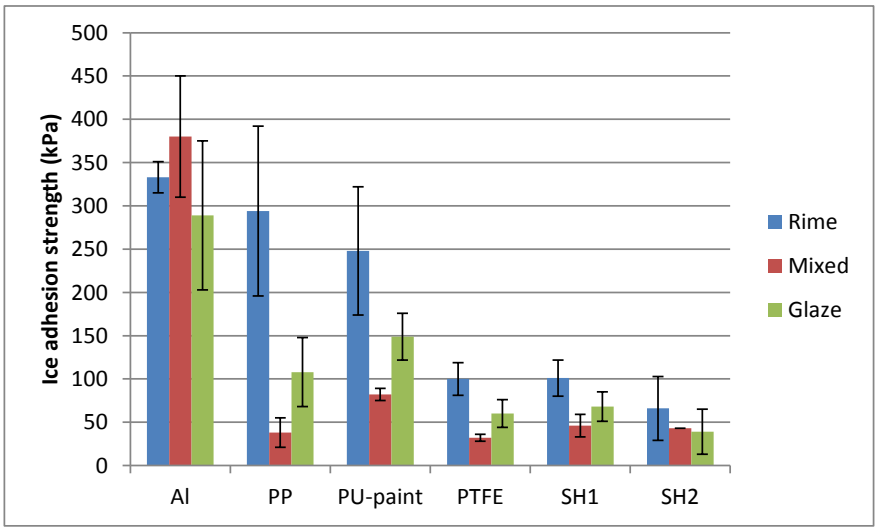

Figure 63. *Ice adhesion strength for samples at -10 °C. Different ice types are presented with different colors; blue stands for rime ice, red for mixed ice and green for glaze ice.*

Superhydrophobic samples (SH1 and SH2) and PTFE showed low ice adhesion values with each ice type, which indicates great icephobic behavior of these surfaces. These surfaces have the lowest value with mixed and the highest with rime ice. Rime ice adheres tightly on the surfaces and breaks cohesively due to high porosity. High level of porosity decreases the bonding area of frozen droplets, which decreases the cohesive strength of ice. Due to tendency for cohesive failures rime ice was difficult to remove from the surface. [42] Example of cohesively failure is presented in Fig. 64.

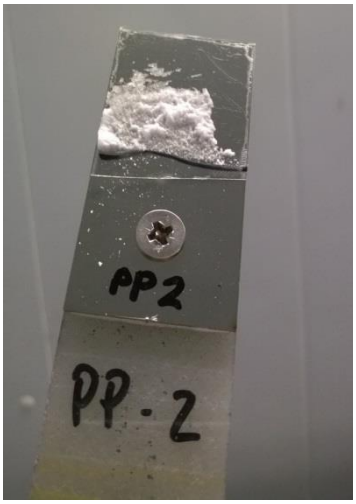

Figure 64. *Cohesive failure of the rime ice sample at -10°C.*

Cohesive release for rime ice could be caused by mass difference of rime ice and glaze ice blocks. Mass difference was arisen due to due to testing arrangement, where the dimensions (height and area) of the accreted ice block were kept constant. The same sized rime ice block weights half of the glaze ice blocks weight, which changes forces affecting the ice block during the spinning. Because of the lighter rime ice blocks, there is a significant difference between the RPM (measured speed at the moment of ice release) values; rime ice has nearly two times higher values than the other ice types (normal test,

glaze). Rime ice is expected to have lower cohesive forces in the ice than glaze, which is why the fracture happened inside the ice block rather than at the interface between ice and substrate. [42]

All but the SH2 did break cohesively in the rime ice adhesion measurements. SH2 have a Cassie-Baxter wetting mode, which allows air to be entrapped between ice and surface texture, which decreases the ice adhesion strength. In other words, instantly freezing droplet will froze on the top of the surface roughness peaks leaving air pockets on the ice-surface- interface. This might explain the adhesive failure of SH2 with rime ice and also the best icephobic behavior.

Ice adhesion results at the -15 °C are presented in Table 18 and Fig. 65. Rime and mixed ice results were in consistence with results at -10 °C, but untypically low values of glaze ice adhesion are discussed later. Mixed ice results showed that order of the samples was similar to mixed ice results at -10°C. Aluminum had high ice adhesion value of 450 kPa and the second the highest value of 98 kPa was measured for PU-paint. Surprisingly SH1 had the third highest ice adhesion strength of 56 kPa. PP and PTFE displayed ice adhesion strengths of 48 kPa and 46 kPa. The lowest value was again for SH2, 35 kPa.

Table 18. *Ice adhesion strengths for samples at -15 °C. Values for different ice types are presented. Avg means average of ice adhesion measurements and Std stands for standard deviation.*

Quantity	**Sample**					
	Al	**PP**	**PU-paint**	**PTFE**	**SH1**	**SH2**
Rime (Avg)	371	230	188	163	124	N.A.
Rime (Std)	98	26	55	18	12	-
Mixed (Avg)	450	48	98	46	56	35
Mixed (Std)	92	3	9	8	30	17
Glaze (Avg)	43	39	73	28	56	50
Glaze (Std)	16	2	11	-	9	-

The order of the rime ice results deviated from the mixed ice results. Order of the ice adhesion values starting from the highest values was following; Al, PP, PU-paint, PTFE, SH1 and SH2. Overall the values are relative high due to characteristic cohesive failure of rime ice. According to Tarquini et al. (2014) [56] rime is the hardest to re-move Failure mode for rime at -15 °C was cohesive over 90% of the samples. Peculiar observation was found with SH2 sample, which exhibited extremely low ice adhesion strength behavior. In removing of the masking piece the ice was more tightly adhered on the PTFE taped surface of masking than on the SH2's surface, which inflicted the removal of the ice from samples surface. Even though the ice adhesion was not able to be measured for SH2, its ice adhesion strength is on the low level. As discussed previ-

ously this might result from the proper level roughness that produces Cassie-Baxter wetting state and high water repellency.

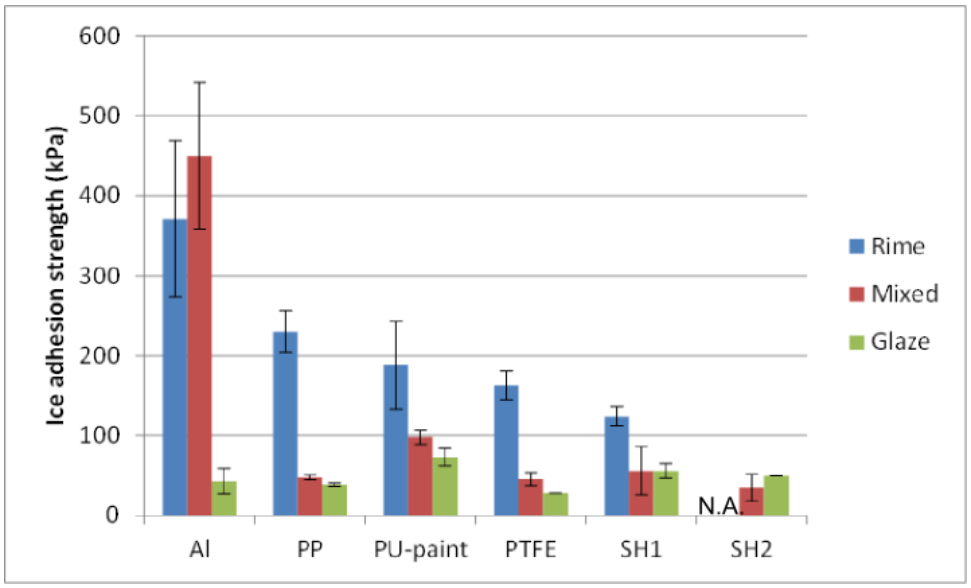

Figure 65. *Ice adhesion strength for samples at -15 °C. Different ice types are presented with different colors; blue stands for rime ice, red for mixed ice and green for glaze ice.*

At -15 °C the supercooling rate was the highest in these conditions testing. Due to increased supercooling it was difficult to prevent excessive supercooling of the droplets. In the formation process of glaze ice it is vital to guarantee supercooling of the droplets and also remaining of the droplets liquid state during the impact with surface. Values of glaze ice adhesion strength are too low compared to values at -10 °C, which results from unsuitable supercooling of droplets. The glaze is not typically formed at low temperatures like – 15 °C, rather in temperatures between 0 °C and -10 °C.[63] Even so the at -15 °C characteristics of glaze ice were achieved, but the temperature at the start of supercooling was overly high ranging from 12,1-12,9 °C. Due to insufficient supercooling, internal stresses might have been formed in the ice's structure. These internal stresses may inflict microcracks and cracks, which will decrease the ice adhesion strength of glaze ice. It should be noted that edges of the glaze ice blocks were carved in order to get rid of icicles. This procedure was not optimal, because it can also inflict extra stresses inside the ice block. Even so the carving was necessary procedure, because otherwise the area of the ice block would have been impossible to determine.

As explained in Chapter 6.3, the rime ice accretion was unsuccessful and mixed was produced instead of rime. The results of ice adhesion test results at -5°Care presented in Table 19 and Fig. 66. The glaze ice accretions were the most successful except the aluminum. Overall aluminum has low ice adhesion values at -5 °C compared to for example the adhesion values at -10 °C. This kind of behavior could be originated from the cleaning procedure and reuse of the samples. The aluminum samples were the only ones, which gone through the whole 9 step test series. After each adhesion test the sam-

ples were cleaned with ethanol and distilled water before the next ice accretion. The aluminum samples' polishing wear out a little bit and a few scratches was formed on the surface. Furthermore it is possible that some contamination could have been formed over the aluminum samples. Other samples were pristine and were tested only once. This has to be taken into consideration, when future test are performed.

Table 19. *Ice adhesion strengths for samples at -5 °C. Values for different ice types are presented. Avg means average of ice adhesion measurements and Std stands for standard deviation.*

Quantity	**Sample**					
	Al	**PP**	**PU-paint**	**PTFE**	**SH1**	**SH2**
Rime (Avg)	101	140	119	17	55	47
Rime (Std)	88	38	33	2	11	31
Mixed (Avg)	33	36	98	29	41	20
Mixed (Std)	10	7	16	3	11	5
Glaze (Avg)	153	82	138	63	94	69
Glaze (Std)	118	45	27	24	38	13

If the aluminum and the rime ice results are left out from consideration, there is some pattern in the results. If the role of effect of different ice type is concerned, it can be observed from Fig. 66 that glaze ice has higher ice adhesion values compared to mixed ice results. Momen et al. (2015) [116] have stated that increasing droplet size should decrease ice adhesion reduction factor (ARF) proportion to aluminum. Superhydrophobic surfaces were compared to aluminum. This is in line with the theory, which states that the glaze ice has the highest ice adhesion strength.[41, 42] Arrangement of the mixed ice adhesion results is following; PU-paint, SH1, PP, PTFE and SH2. Only the difference in the arrangement of glaze ice adhesion results was that PTFE (63 kPa) had slightly lower value than SH2 (69 kPa).

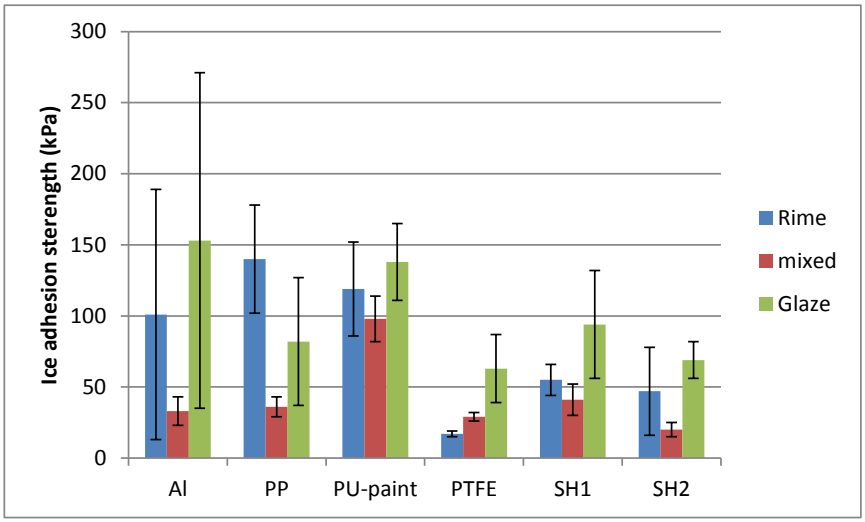

Figure 66. *Ice adhesion strength for samples at -5 °C. Different ice types are presented with different colors; blue stands for rime ice, red for mixed ice and green for glaze ice.*

Overall ice adhesion results at -5 ° displayed high variations in the values of different ice types. For example SH1 had ice adhesion strength 41 kPa for mixed ice and 94 kPa for glaze ice. Similar result were found also for SH2, which had ice adhesion strength 20 kPa for mixed ice and 69 kPa for glaze ice. These variations of superhydrophobic surfaces could originate of droplet impingent on the surface. At -5 °C freezing of the supercooled droplets is slower compared to colder temperatures, which is why the droplets will stay longer in the liquid state. Due to momentum of droplets impacting on the surface, they will fill the surface texture of superhydrophobic surfaces because of delayed freezing. [116] If the droplets will fill the surface roughness and freeze, it will increase the ice adhesion strength, because ice will anchor on the between the surface roughness peaks. This phenomenon is named as mechanical interlocking effect and it is widely accepted in the literature. [3, p. 259, 34, pp. 126–127, 75, 93, 95, 98, 115, 130, 131, p. 20]

The effect of temperature and ice type is illustrated in Figs. 67, 68 and 69. Based on these test results different ice types have certain characteristics that have an effect on the ice adhesion strength. Figure 67 illustrates mixed ice results and it should be noted that aluminum has untypically low value at -5 °C, which probably results from contamination and wearing of sample. Otherwise there is no clear effect of temperature on the ice adhesion values, because values are in line regardless of temperature. Furthermore standard deviations of mixed ice are reasonable compared to other ice types, which have considerably higher standard deviations. The key benefit for mixed ice is that its failure is adhesive in 95% of the tested samples and only aluminum samples detached cohesively because of high ice adhesion strength. Rime ice showed high amount of the cohesive failures and glaze ice had also some tendency to fail cohesively.

Coating/surfaces that have ice adhesion values around 50 kPa can be considered as good icephobic coatings. SH1, SH2 and PTFE were clearly in this category as was anticipated based on Table 7, where superhydrophobic and fluorine combined coatings have low ice adhesion values. Surprisingly PP had also low ice adhesion values, although its rime ice adhesion strength was nearly as high as aluminum’s and glaze ice adhesion slightly less than PU-paint’s. The reason behind this behavior would require further characterization such as surface energy measurements and cyclic ice adhesion tests.

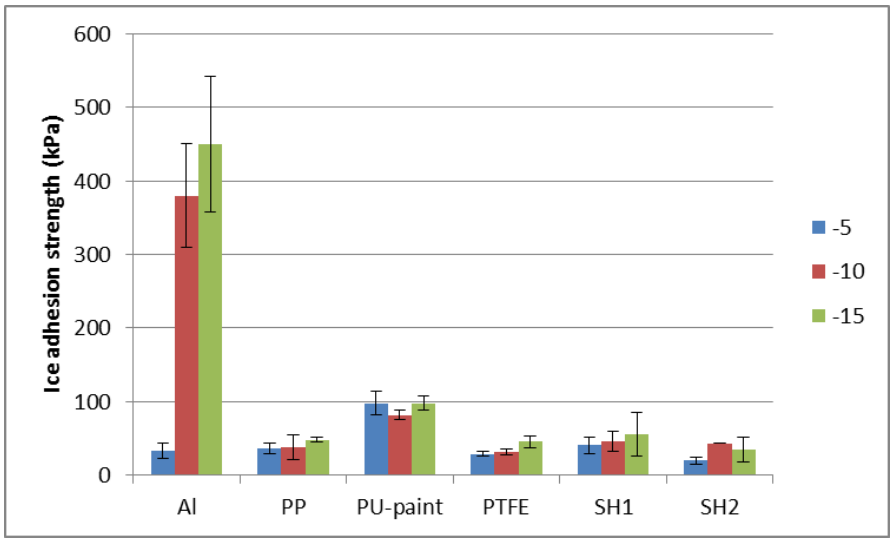

Figure 67. *Ice adhesion strengths for mixed ice in the different temperatures. Blue color stands for -5 °C, red -10 °C and green -15 °C.*

Figure 68 shows ice adhesion strengths for all samples in the different temperature. It should be recognized that rime ice results at -5 °C are incomparable to results from other temperatures, because mixed ice was formed instead of rime ice. Otherwise there is consistence between the values of different samples, because ice adhesion values seem to correlate quite well with wettability and surface roughness values. Hydrophobic (PTFE) and superhydrophobic (SH1 and SH2) have higher water repellency compared to other samples, which results lower values. On the contrary increasing hydrophilicity increases rime ice adhesion strength. Based on Fig. 68 surface energy has also influence on the rime ice adhesion strength. Lower the surface energy is the lower the ice adhesion is. This behavior can be observed, when smooth surface Al, PP and PTFE are compared. Increasing fluorine or silicon content on surface will decrease the surface energy, because less hydrogen bonding is taking place between water/ice with the surface. [131,p.88, 132] PTFE is low surface energy material (20 mN/m) [131, p.26] and it has the lowest ice adhesion strength and aluminum has the highest surface energy (101,8 mN/m) [17] having also the highest ice adhesion strength. PP has the surface energy (30,1 mN/m) between PTFE and aluminum.

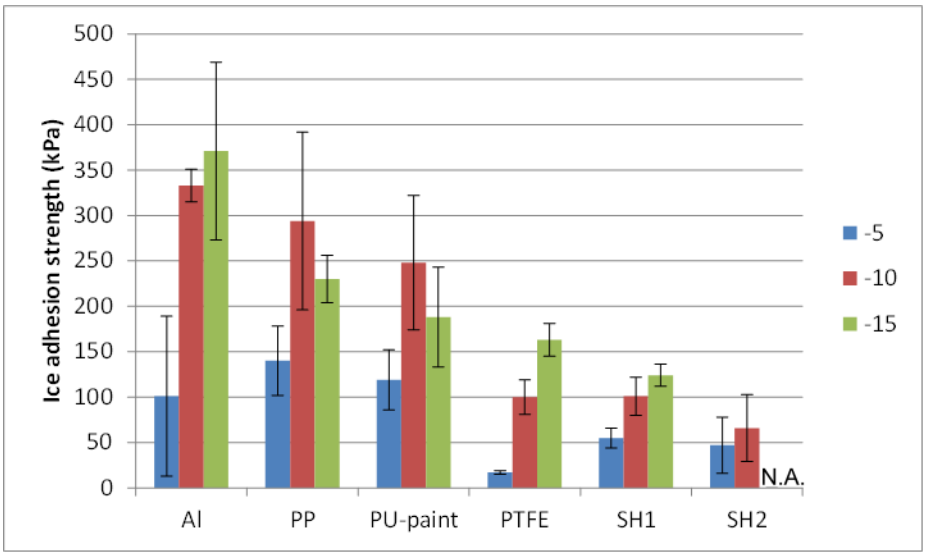

Figure 68. *Ice adhesion strengths for rime ice in the different temperatures. Blue color stands for -5 °C, red -10 °C and green -15 °C.*

Ice adhesion strengths for glaze in different temperatures are presented in Fig. 69. Glaze accretion at -15 °C were challenging, which lead to low ice adhesion values due to high wet content during in freezing of ice. When the freezing ice has more water in it, this might lead to development of cracks inside ice's structure. The best icephobic behavior with glaze ice was discovered with PTFE and SH2 that showed ice adhesion values ~50 kPa. SH1 and PP had slightly increased ice adhesion values compared to mixed ice results. Increased value of SH1 can be explained with characteristic icing conditions for glaze ice. Glaze ice is typically formed in the high humidity conditions, where frost formation on the surfaces can decrease droplet movements on the surface. [94, 115, 116, 118] When the superhydrophocity is lost, the ice adhesion strength also increases.[31, 90] Furthermore the higher momentum of the droplets causes deeper penetration into surface texture and mechanical interlocking effect. [116] Glaze ice should had the highest ice adhesion strength and ice adhesion strength should increase with increasing temperature. [42, 56] Glaze ice has indeed higher ice adhesion strength for some of the samples (PP and PU-paint), but rime ice had the highest values due partly cohesive failure of ice.

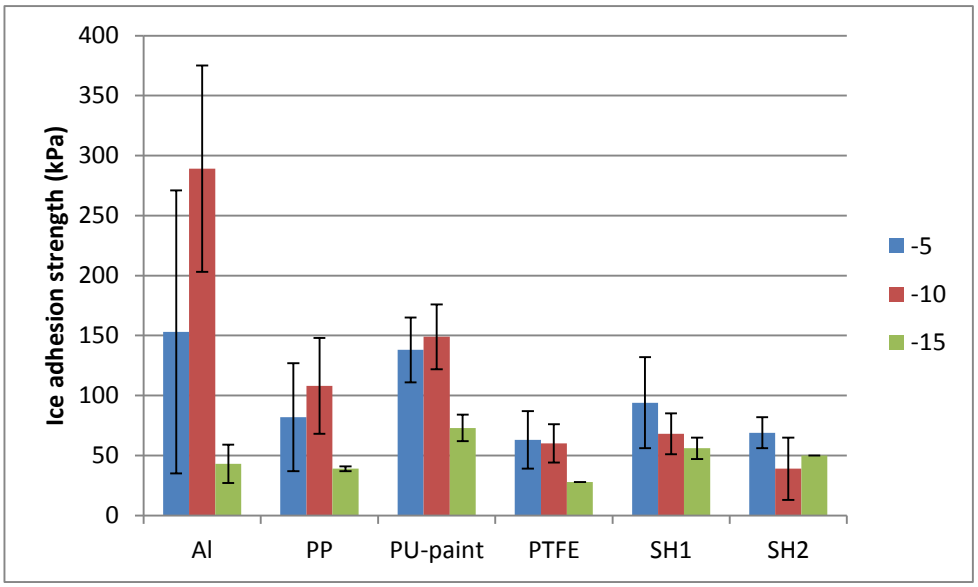

Figure 69. *Ice adhesion strengths for glaze ice in the different temperatures. Blue color stands for -5 °C, red -10 °C and green -15 °C.*

Ice adhesion test results measured in this thesis are comparable with some of the results presented in the literature. In Table 7 there are listed ice adhesion values, which are obtained with centrifugal ice adhesion test. In addition the ice accretions have been done in the same manner by spraying microdroplets in icing wind tunnel. Typically glaze ice has been tested in the centrifugal ice adhesion measurements. [30, 31, 75, 90, 102, 116, 133] In Figure 70 the ice adhesion values at – 10 °C are presented as ice adhesion reduction factor (ARF), which means that the ice adhesion strength are proportioned to aluminum. Values presented in Table 7 can be compared with values presented in Fig. 70 due to similar test procedures, which includes similar ice accretion process, same ice type (glaze) and same adhesion measurement technique.

The glaze ice ARF values have been presented with green color in Fig. 70. ARF-values for PU-paint and PP are 1,9 and 2,7, which can be categorized as low values. SH1 has ice adhesion reduction factor of 4,3, which is typical value for superhydrophobic coating having good droplet movement i.e. CAH values lower than 10 °. Zonyl 8470 based polymer composite coatings with different hard phases, CeO2 (<50nm) (ARF 4,5) [31], ZrO2 (20-30nm) (ARF 4,5) [90] and Ag (100-600nm) (ARF 4,2) [31] have shown similar ARF-values than SH1. PTFE has ARF-value of 4,7 in this study and slight lower value of 3,5 have been presented in the literature. [105] The best ARF-value in this thesis is measured for SH2 being 7,4, which represent very good icephobic behavior. Only ARF-value of 9 has been measured for polymeric FAS-17-coating. [90] ARF-value of 7,2 have been discovered for silicon rubber based polymer composite coatings with the different hard phase additions, CeO2 (<25nm) and TiO2 (<100nm). [30]

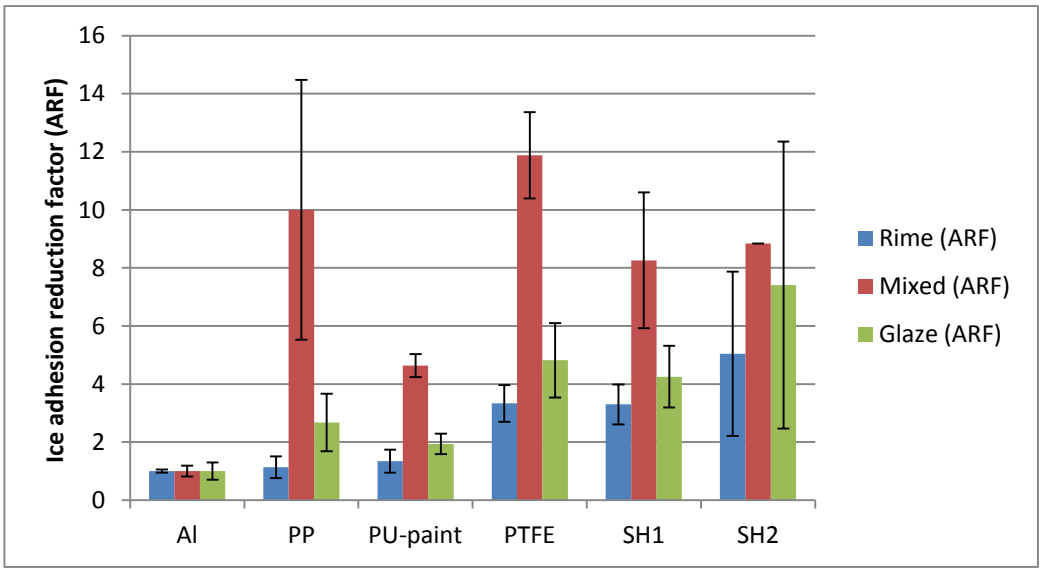

Figure 70. *Ice adhesion results presented with ice adhesion reduction factors proportion to aluminum. Blue color indicates rime ice ARF-results, red mixed ice ARF-results and green glaze ice ARF-results.*

If the ARF values of different ice types are evaluated, it is found that mixed ice had the greatest ARF values and rime ice has the lowest reduction factor. ARF values of glaze ice are between the rime and mixed ice values. It can be seen that there is quite large variation in the reduction factors for different ice types. Samples PP, PTFE and SH1 had high reduction factors with mixed ice, which are dramatically dropped with glaze and rime ice. Momen et al. (2015) [116] have studied the effect MVD on the glaze ice adhesion strength and discovered that increased droplet size reduces ice adhesion strength. Droplet sizes were varying between 40-80 µm. [116] In this thesis droplet size used were; 25 µm for rime ice, 31 µm for mixed ice and 40 µm for glaze ice. Effect of droplet size cannot be directly evaluated, because three different ice types were created and all of them have specific ice formation mechanism. Tarquini et al. (2014) [56] has also studied the effect of droplet size on ice adhesion strength and found out that higher droplet size decreases ice adhesion strength, which are contravened with results of Momen et al. (2015) [116]. Droplet sizes studied were 20µm, 30 µm and 40 µm. [56] These droplet sizes correspond the sizes utilized in this thesis, but no correlation with MVD and ice adhesion strength was found. This indicates the clear need for research of ice formation mechanism for different ice types and their relation to ice adhesion strength.

The influence of the wetting properties and surface roughness values on ice adhesion strength is discussed next. Table 20 presents ice adhesion strengths at -10 °C, wetting properties and surface roughness values. Different factors influences on the ice adhesion strength. Surface roughness has an important role in water repellency, because superhydrophobic surfaces require combined micro- and nanotexture. Furthermore it was found out in this thesis that there exist high variations in the surface textures as was the case with samples SH1 and SH2. Both superhydrophobic surfaces also show relatively low ice adhesion strengths, which underlines the importance droplet movement on the sur-

face. Even so it should be noted that superhydrophobic surfaces offer only limited icephobic solution, because their performance decreases in different icing conditions. [56]

Table 20. *Ice adhesion strengths, wetting properties and surface roughness values for samples at -10 °C. Values for different ice types are presented. Avg means average of ice adhesion measurements and Std stands for standard deviation. CA stands for contact angle of water. R_a is average roughness, R_z is mean peak to valley height of roughness profile, S_a is average height of surface area and S_z is maximum height.*

Quantity	**Sample**					
	Al	**PP**	**PU-paint**	**PTFE**	**SH1**	**SH2**
Rime, avg (kPa)	333	294	248	100	101	66
Rime, std (kPa)	18	98	74	19	21	37
Mixed, avg (kPa)	380	38	82	32	46	43
Mixed, std (kPa)	70	17	7	4	13	0
Glaze, avg (kPa)	289	108	149	60	68	39
Glaze, std (kPa)	86	40	27	16	17	26
Static CA (°)	66	89	79	100	159	165
Advancing CA (°)	80	91	79	108	161	166
Receding CA (°)	20	52	20	92	149	164
CA hysteresis (°)	60	39	59	16	10	2
R_a (nm)	169,4	-	867,3	-	2890	336,2
R_z (µm)	1,15	-	5,65	-	18,62	2,78
S_a (nm)	255,2	-	2240	-	6840	689,1
S_z (µm)	19,93	-	32,49	-	84,97	38,75

The relationship between ice adhesion strength and CAH is presented in Figs. 71,72 and 73 for different types of ice. Correlation between CAH and mixed ice adhesion is concerned, it is clear no distinct correlation exist. All the coatings except aluminum have ice adhesion strength below 100 kPa, but the CAH values vary a lot. For example PP has CAH of 39 ° and ice adhesion comparable to PTFE, which CAH is 16 °. Furthermore aluminum has high ice adhesion strength 380 kPa, but similar CAH values with PU-paint, which ice adhesion is 82 kPa. This difference can be partly explained with difference in the surface energy values, aluminum having higher surface energy hence higher ice adhesion strength.

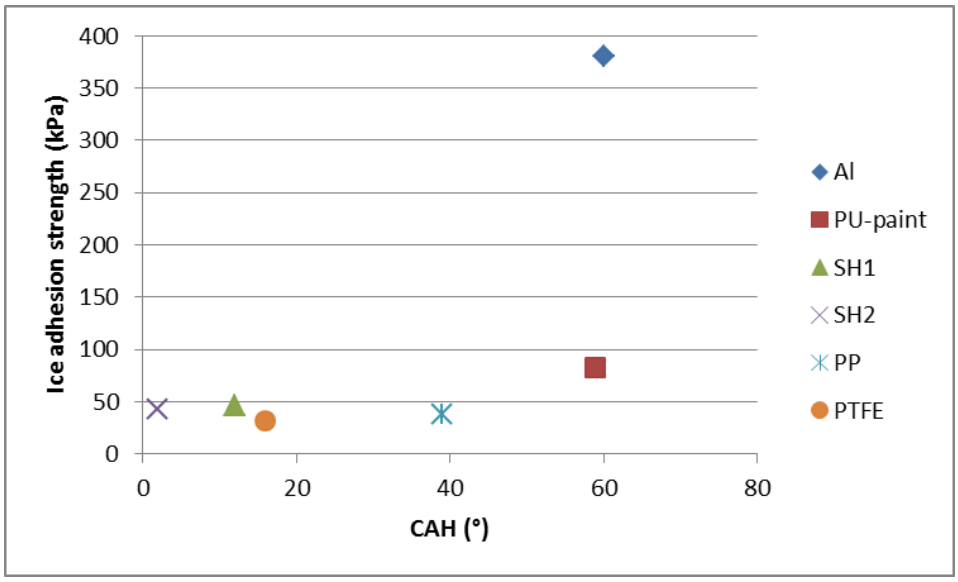

***Figure 71**. Mixed ice adhesion strength versus CAH.*

Surprisingly rime and glaze ice values against CAH show some correlations, as Figs. 72 and 73 point out. Group of samples, SH1, SH2 and PTFE, having low CAH i.e. good droplet movement on the surface, has also lower ice adhesion values compared to samples, Al, PP and PU-paint, having higher CAH. If the rime and glaze ice strengths of high CAH samples are compared, it seen that rime ice adhesion strengths are significantly higher than glaze ice adhesions. Higher values for glaze ice can be explained with partly cohesive failure mode. PP has CAH of 39 °, which indicates poor droplet mobility on the surface. Due to this low CAH values, relatively high difference between glaze and rime ice adhesion values is observed. Rime ice adhesion for PP is nearly 300 kPa and for glaze just over 100 kPa.

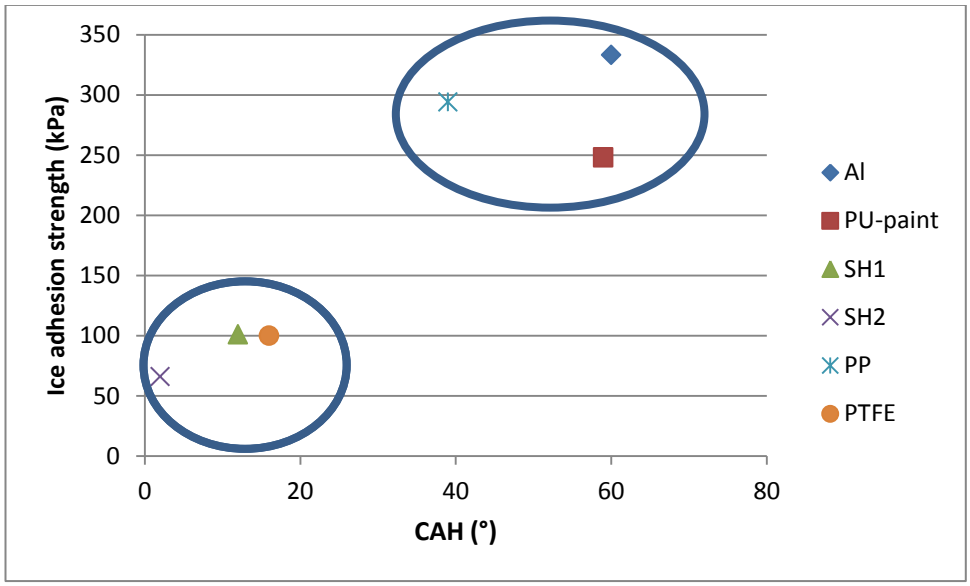

***Figure 72**. Rime ice adhesion strength versus CAH.*

Group samples having low CAH values, exhibits also low ice adhesion strength with both ice types at -10 °C. Arrangement of the samples stays same regardless of accreted ice type. The best behavior is observed with the SH2, which also has the lowest CAH (2°). SH2 is the only sample, which ice adhesion strength stays ~50 kPa regardless of the temperature or the ice type. On the contrary SH1 nearly doubles its ice adhesion strength, when glaze ice values are compared to rime ice adhesion values due to higher CAH values (10°).

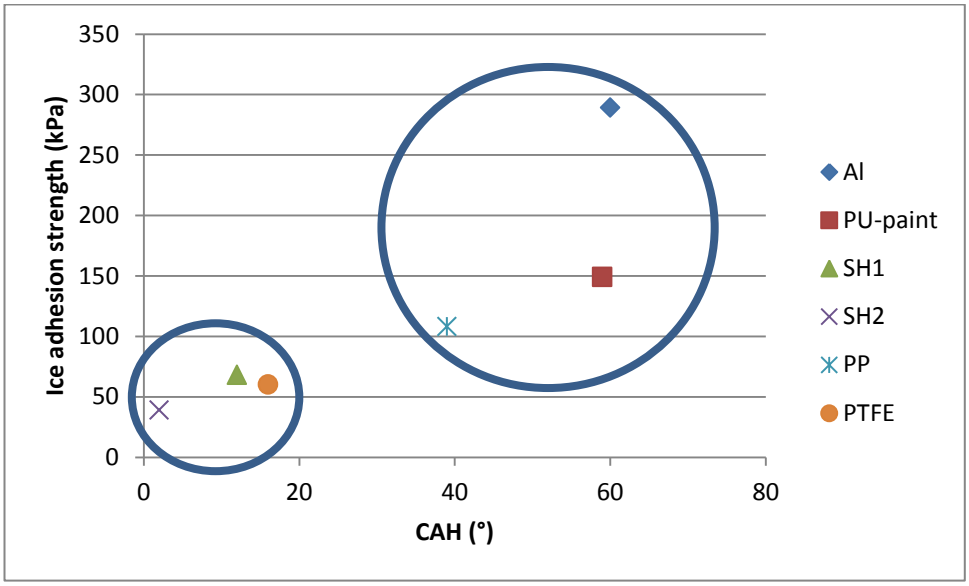

***Figure 73**. Glaze ice adhesion strength versus CAH.*

Mixed ice adhesion results at -10°C are compared with surface roughness quantity of S_a, which illustrates the average roughness on the selected area. Surface roughness of PP and PTFE haven't been evaluated, because it is assumed that there are smooth samples and applied surface is pristine in every condition test. No pattern between the roughness values and ice adhesion strength exist, which was the case with wettabilities. Superhydrophobic samples SH1 and SH2 show that the similar ice adhesion strengths can be reach, with the varying roughness values. SH1 has relatively high roughness value, because there are deep canyons, which surround the elevated areas. Deep cavities cause droplets to stick, which increase the CAH. However the increased CAH and roughness do not have impact on the ice adhesion strength, in the case of SH1. Roughness alone does not influence on the ice adhesion strength, because SH2 and Al have both roughness in the nanoscale but their ice adhesion strengths vary a lot, because of different surface chemistries. Increased roughness has been demonstrated the increase ice adhesion with similar materials [97,122]. It can be concluded that increasing roughness increases ice adhesion strength, but also the wetting behavior and surface chemistry has to be considered.

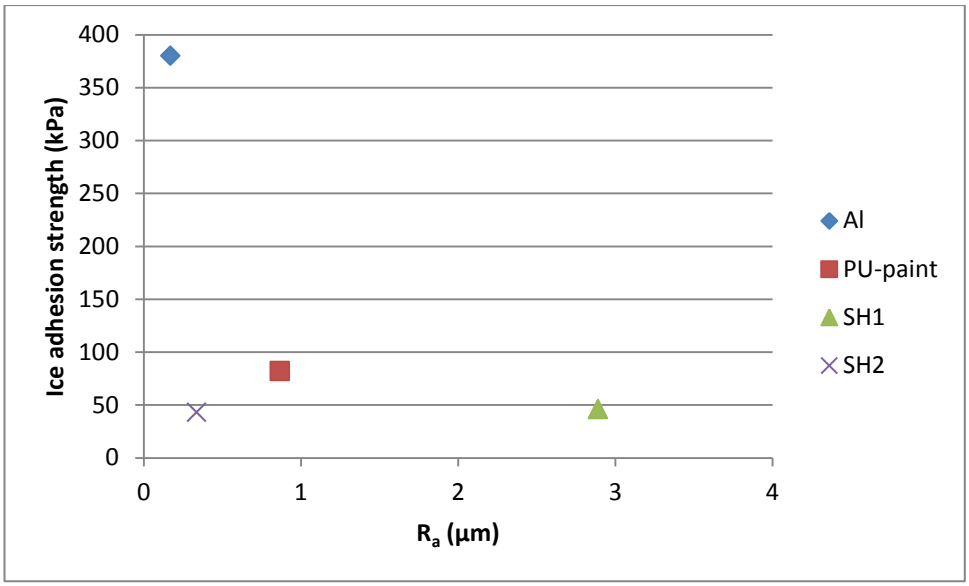

Figure 74. *Mixed ice adhesion strength versus R_a, which stands for average surface roughness.*

Some conclusions can be drawn based on these results, but one factor alone cannot explain why ice adhesion values are on the certain level. It can be concluded based on discussion presented previously that the ice adhesion strength correlates with following listed parameters;

- Wetting behavior
- Surface roughness
- Surface chemistry
- Icing conditions
- Ice type

Droplet movement and water repellency on the surface decreases ice adhesion strength in some icing conditions. However in wet icing events with high wind speeds and high droplet sizes, water will wet the texture and form mechanical interlocking effect, which increases ice adhesion strength. Surface texture enables the presence of different wetting states, such as Wenzel or Cassie-Baxter wetting state. Droplets resting on the top surface asperities will decrease ice adhesion strength in dry icing events, but these surfaces will vulnerable to frost formation in high humidity conditions. Decreasing surface energy will lower the ice adhesion strength, but ice adhesion strength is also strongly related to surface roughness. Icing conditions have indeed effect on the ice adhesion strength. Superhydrophobic surfaces function well in the dry icing events i.e. rime ice accretions showing low ice adhesion strengths (for example SH2), but the values are increased in the wet ice formation i.e. glaze ice events due to water penetration and freezing between the surface roughness peaks. [116] Ice type has also an effect on ice adhesion values. Rime is the most difficult to remove complete from the surface due to cohesive failure mode. [42, 56] On the other hand glaze ice has the highest ice adhesion strength and its

failure mode is typically adhesive. [134] Effect of listed factors should be further studied in order understand icing formation process and critical factors affecting on ice adhesion strength.

7 CONCLUSION

Icing causes substantial problems for different field of industries, by decreasing efficiency, safety and usability of operations. Therefore variety of methods has been presented to deal with issues that icing possesses. Active anti-icing methods are typically based on electrothermal heating element, which melts the interface between ice and substrate, causing ice to be removed due to external forces i.e. gravity and wind. Aviation industry relies heavily on the de-icing methods, which includes the utilization of de-icing chemicals and pneumatic boots. All of these methods are not environmentally friendly options, because the energy is consumed to heat protected surface or contain harmful chemicals. Therefore, passive icephobic coatings would offer improvement, because no external energy is needed and coatings can be tailored to contain environmentally friendly compounds.

Different coating strategies have been utilized. Fluorine and silicone containing polymer coatings have been demonstrated to offer good icephobic properties. However superhydrophobic coatings have been widely tested due to their unique water repellency properties and good icephobic coatings have been found out. Even so the wear resistance and frost formation will cause these surfaces to lose their icephobic performance. Icephobic behavior of different type of surfaces was evaluated in this thesis. Ice was accreted on the samples in the icing wind tunnel, in nine different icing conditions. Ice adhesion strength of the coatings was measured with centrifugal ice adhesion test. Aim of this thesis was to study effect of different icing conditions on ice adhesion strength of variety of the coatings.

Based on the results obtained in this thesis, icing conditions and ice type have an effect on the ice adhesion strength. Rime ice has the highest ice adhesion values and it is the hardest to remove from the surface due to cohesive failure of ice. Mixed ice has the lowest ice adhesion strength compared to other ice types. On the contrary glaze ice has higher ice adhesion strength compared to mixed ice, because in the glaze ice formation process droplets have higher inertia and will wet the surface texture. This increases ice-surface contact area, which further increases ice adhesion strength. Ice adhesion strength of different ice types has not been widely studied in the literature, and thorough investigations are required.

Ice adhesion strengths were measured for three different ice types (rime, mixed and glaze) in three different temperatures (-5°C, -10°C and -15°C). The overall order of the samples remained same in every temperature and the order is following starting from

the highest value; Al, PU-paint, PP, SH1, PTFE and SH2. Ice type has an effect on ice adhesion strengths and order of the samples for rime is changed into; Al, PP, PU-paint, SH1, PTFE and SH2. For glaze ice the order is following; Al, PU-paint, PP, SH1,PTFE and SH2. It was also noticed that CAH correlates quite well with the ice adhesion strengths, because samples with high CAH showed also high ice adhesion values and contrary low CAH samples exhibited low ice adhesion strengths. No correlation between the temperature and ice adhesion strengths was obtained.

Surfaces with good droplet movement on the surface have also lower ice adhesion strength. On the contrary poor droplet movement inflicted high ice adhesion values. Highly water repelling superhydrophobic coating SH2 showed the best icephobic behavior in every icing condition. Other surfaces exhibited variations in ice adhesion strengths between the different ice types, and especially glaze ice was the hardest to detach from the surface. Surfaces having higher surface energies (Al, PU-paint) also showed higher ice adhesion values.

Icing is complex phenomenon, which is influence by many factors such as droplet size, temperature and wind speed. There is no clear cognizance about influencing factors on the ice adhesion strength. Based on the results from this thesis it can be concluded that several properties have influence on the ice adhesion strength. At least water wettability, surface roughness, surface chemistry, icing conditions and ice type have an impact on the icing and ice adhesion strength.

REFERENCES

[1] R. Menini & M. Farzaneh, Elaboration of Al2O3/PTFE icephobic coatings for protecting aluminum surfaces, Surface and Coatings Technology, Vol. 203, No. 14, 2009 pp. 1941–1946.

[2] I. Baring-Gould, R. Cattin, M. Dustewitz, M. Hulkkonen, A. Krenn, T. Laakso, A. Lacroix, E. Peltola, G. Rönsten, L. Tallhaug, T. Wallenius, Wind Energy Projects in Cold Climates, IEA Wind 13.task, 2012 43 p. Available: https://www.ieawind.org/index_page_postings/June%207%20posts/task%2019%20cold_climate_%20rp_approved05.12.pdf.

[3] M. Farzaneh, Atmospheric icing of power networks. Springer, London, United Kingdom, 2008, 381 p.

[4] Continental Airlines, Inc., Flight 1713 McDonnell Douglas DC-9-14, N626TX, National Transportation Safety Board, webpage, Available (Accessed: 8.9.2015): http://www.ntsb.gov/investigations/AccidentReports/Pages/AAR8809.aspx.

[5] In-flight Icing Encounter and Loss of Control Simmons Airlines, American Eagle Flight 4184 Avions de Transport Regional (ATR) Model 72-212, N401AM," National Transportation Safety Board, webpage, Available(Accessed: 08.9.2015): http://www.ntsb.gov/investigations/AccidentReports/Pages/AAR9601.aspx.

[6] Y. Cao, Z. Wu, Y. Su, Z. Xu, Aircraft flight characteristics in icing conditions, Progress in Aerospace Sciences, Vol. 74, 2015, pp. 62–80.

[7] N. Dalili, A. Edrisy, R. Carriveau, A review of surface engineering issues critical to wind turbine performance, Renewable and Sustainable Energy Reviews, vol. 13, no. 2, 2009, pp. 428–438.

[8] O. Parent & A. Ilinca, Anti-icing and de-icing techniques for wind turbines: Critical review," Cold Regions Science and Technology, Vol. 65, No. 1, 2011, pp. 88–96.

[9] J. Li, Y. Zhao, J. Hu, L. Shu, X. Shi, Anti-icing Performance of a Superhydrophobic PDMS / Modified Nano-silica Hybrid Coating for Insulators, Journal of Adhesion Science and Technology, Vol. 26 , No. 4-5, 2012 pp. 665–679.

[10] L. Makkonen, P. Lehtonen, M. Hirviniemi, Determining ice loads for tower structure design, Engineering Structures, vol. 74, 2014 pp. 229–232,.

[11] T. L. E. Broström & L. Söder, Ice Storm Impact on Power System Reliability, in IWAIS XII, Yokohama, Japan, 2007.

[12] C. C. Ryerson, Ice protection of offshore platforms, Cold Regions Science and Technology, Vol. 65, No. 1, 2011. pp. 97–110.

[13] R. Menini, Z. Ghalmi, M. Farzaneh, Highly resistant icephobic coatings on aluminum alloys, Cold Regions Science and Technology, Vol. 65, No. 1, 2011, pp. 65–69.

[14] C. C. Ryerson, Superstructure spray and ice accretion on a large U.S. Coast Guard cutter, Atmospheric Research, Vol. 36, No. 3-4, 1995, pp. 321–337.

[15] R. Carriveau, A. Edrisy, P. Cadieux, and R. Mailloux, "Ice Adhesion Issues in Renewable Energy Infrastructure," vol. 26, 2012 pp. 447–461.

[16] C. Antonini, Superhydrophobicity as a strategy against icing: Analysis of the water/surface dynamic interaction for icing mitigation. Università degli studi di Bergamo, 2011, 238 p. Available:https://aisberg.unibg.it/bitstream/10446/881/1/phd_thesis_Antonini.pdf

[17] T. Bharathidasan, S. V. Kumar, M. S. Bobji, R. P. S. Chakradhar, B. J. Basu, Effect of wettability and surface roughness on ice-adhesion strength of hydrophilic, hydrophobic and superhydrophobic surfaces, Applied Surface Science, vol. 314, 2014, pp. 241–250.

[18] Aviation safety: New computer tool forecasting icing hazards, National Center for Atmospheric Research, webpage, Available (Accessed 8.9.2015): https://www2.ucar.edu/atmosnews/news/4296/aviation-safety-new-computer-tool-forecasts-icing-hazards.

[19] Continental 1713 Crashes in Denver, De-icing innovations. webpage, Available (Accessed 9.9.2015): http://deicinginnovations.com/?p=3552.

[20] 31 October 1994 - Eagle Flight 4184, Cockpit Voice Recorder Database, webpage, Available (Accessed 9.9.2015): http://www.tailstrike.com/311094.htm.

[21] De-icing, english4aviation, webpage. Available (Accessed 9.9.2015): http://english4aviation.pbworks.com/w/page/24012191/Bad weather.

[22] G. W. K. Moore, A climatology of vessel icing for the subpolar North Atlantic Ocean, International Journal of Climatology, vol. 33, 2013, pp. 2495–2507.

[23] T. Ozeki, R. Yamamoto, K. Izumiyama, T. Sakamoto, Ice Adhesion Tests on Pliable Polymer Sheets for Protection Against Sea-Water Spray Icing, Journal of Adhesion Science and Technology, vol. 26, 2012, pp. 651–663.

[24] NSR traffic in 2014, Northern Sea Route Information Office, webpage. Available (Accessed 9.9.2015): http://www.arctic-lio.com/node/229.

[25] A heavily iced ship after a severe storm, Roberto Barros Yacht Design, webpage. Available (Accessed): http://www.yachtdesign.com.br/ingles/artigos.php.

[26] N. Lehming, Performance analysis of an anti-icing system, Optimizing wind farms in cold climates, presentation, Helsinki, Finland, 2014.

[27] H. M. Slot, E. R. M. Gelinck, C. Rentrop, E. Van Der Heide, Leading edge erosion of coated wind turbine blades : Review of coating life models, Renewable Energy, vol. 80, 2015, pp. 837–848.

[28] A. G. Kraj & E. L. Bibeau, Phases of icing on wind turbine blades characterized by ice accumulation, Renewable Energy, vol. 35, no. 5, 2010, pp. 966–972.

[29] B. Martinez, Implementing H & S strategies to mitigate ice throw risk, Optimizing wind farms in cold climates, presentation, Helsinki, Finland, 2014.

[30] F. Arianpour, M. Farzaneh, S. A. Kulinich, Hydrophobic and ice-retarding properties of doped silicone rubber coatings, Applied Surface Science, vol. 265, 2013, pp. 546–552.

[31] S. Farhadi, M. Farzaneh, S. A. Kulinich, Anti-icing performance of superhydrophobic surfaces, Applied Surface Science, vol. 257, no. 14, 2011, pp. 6264–6269.

[32] Photos of iced up objects, IWAIS 2015, webpage. Available (Accessed 9.9.2015): http://iwais.org/photos-of-iced-up-objects/.

[33] X. Jiang, Z. Xiang, Z. Zhang, J. Hu, Q. Hu, L. Shu, Comparison on ac icing flashover performance of porcelain, glass, and composite insulators, Cold Regions Science and Technology, vol. 100, 2014, pp. 1–7.

[34] A. Safaee, Nanostructured metal surfaces and their passivation for superhydrophoic and anti-icing applications, Université du Québec, 2008, 182 p. Available: http://constellation.uqac.ca/169/1/030112159.pdf

[35] M. Farzaneh, Coatings for protecting overhead power network equipment in winter conditions, *IWAIS 2015*, presentation, Uppsala, Sweden, 2015.

[36] Insulator Performance Under Wintry Conditions Topic of New book, INMR, webpage. Available (Accessed 9.9.2015): http://www.inmr.com/insulator-performance-wintry-conditions-topic-new-book/#!prettyPhoto.

[37] N. Mulherin, Atmospheric icing and communication tower failure in the United States, Cold Regions Science and Technology, vol. 27, no. 2, 1998, pp. 91–104.

[38] L. Makkonen & M. M. Oleskiw, Small-scale experiments on rime icing, Cold Regions Science and Technology, vol. 25, no. 3, 1997, pp. 173–182.

[39] G. Ronsten, Lessons learned from ‘Large scale, cost effective deployment of wind energy in icing climates,’ *IWAIS 2015*, presentation, Uppsala, Sweden, 2015.

[40] S. M. Fikke, J. E. Kristjánsson, B. E. Kringlebotn Nygaard, Modern meteorology and atmospheric icing, Atmospheric Icing of Power Networks, IWAIS XI, Montreal, Canada, 2005, pp. 1–29.

[41] L. Makkonen, Ice Adhesion — Theory , Measurements and Countermeasures, Journal of Adhesion Science and Technology, vol. 26, 2012, pp. 413–445.

[42] G. Fortin & J. Perron, Ice Adhesion Models to Predict Shear Stress at Shedding, Journal of Adhesion Science and Technology, vol. 26, no. 4–5, 2012, pp. 523–553.

[43] T. Raatikainen, A. Nenes, J. H. Seinfeld, R. Morales, R. H. Moore, Worldwide data sets constrain the water vapor uptake coef fi cient in cloud formation, Proceeding of the National Academy of Sciences of the United States of America, Vol. 110, No. 10, 2013 pp.3760-3764.

[44] J. M. Thériault, R. E. Stewart, J. Milbrandt, M. K. Yau, On the simulation of winter precipitation types, Journal of Geophysical Research: Atmospheres, vol. 111, no. 18, 2006, pp. 1–11.

[45] J. Thériault, R. Stewart, W. Henson, On the Formation of Winter Precipitation Types Favorable for Icing on Structures, IWAIS XII, Yokohama, Japan , 2007.

[46] Water cycle diagram, ConceptDraw. Available (Accessed 9.9.2015): http://www.conceptdraw.com/examples/cycle-diagram-software.

[47] H. Wang, G. He, Q. Tian, Effects of nano-fluorocarbon coating on icing, Applied Surface Science, Vol. 258, No. 18, 2012, pp. 7219–7224.

[48] K. Fumoto & T. Kawanami, Study on Freezing Characteristics of Supercooled Water Droplets Impacting on Solid Surfaces, Journal of Adhesion Science and Technology, vol. 26, no. 4–5, 2012, pp. 463–472.

[49] R. Ruohomaa, Icephobic surfaces – development of icing test equipment and superhydrophobic coating prepared with solution precursor flame spray, Tampere University of Technology, unpublished thesis. 2014.

[50] H. Banitalebi Dehkordi, M. Farzaneh, P. Van Dyke, L. E. Kollar, The effect of droplet size and liquid water content on ice accretion and aerodynamic coefficients of tower legs, Atmospheric Research, vol. 132–133, 2013, pp. 362–374.

[51] H. Banitalebi Dehkordi, M. Farzaneh, L. E. Kollar, and P. Van Dyke, Experimental Study of Spray Characteristics and its Uniformity under Different Icing Conditions, IWAIS XIV, Chongqing, China, 2011.

[52] S. Fikke, P.-E. Persson, B. Wareing, J. Chum, L. Makkonen, G. Ronsten, A. Heimo, S. Kunz, M. Ostrozlik, J. Sabata, B. Wichura, T. Laakso, K. Säntti, COST 727: Atmospheric Icing on Structures Measurements and data collection on icing: State of the Art, MeteoSwiss, 75, 2007, 110 p.

[53] H. R. Pruppacher & J. D. Klett, Nucleation in Condensed Matter — Applications in Materials and Biology, 1st ed. Elsevier Oxford, UK, Pergamon, 2010 756 p.

[54] A. J. Bermúdez di Lorenzo, M. A. Carignano, R. G. Pereyra, A statistical study of heterogeneous nucleation of ice by molecular dynamics, Chemical Physics Letters, vol. 635, 2015, pp. 45–49.

[55] P. Wilson, A. Heneghan, A. Haymet, Ice nucleation in nature: supercooling point (SCP) measurements and the role of heterogeneous nucleation, Cryobiology, vol. 46, no. 1, 2003, pp. 88–98.

[56] S. Tarquini, C. Antonini, A. Amirfazli, M. Marengo, J. Palacios, Investigation of ice shedding properties of superhydrophobic coatings on helicopter blades, Cold Regions Science and Technology, vol. 100, 2014, pp. 50–58.

[57] J. Hu, K. Xu, Y. Wu, B. Lan, X. Jiang, L. Shu, The freezing process of continuously sprayed water droplets on the superhydrophobic silicone acrylate resin coating surface, Applied Surface Science, vol. 317, 2014, pp. 534–544.

[58] V. Bahadur, L. Mishchenko, B. Hatton, J. A. Taylor, J. Aizenberg, T. Krupenkin, Predictive model for ice formation on superhydrophobic surfaces., Langmuir : the ACS journal of surfaces and colloids, vol. 27, no. 23, 2011, pp. 14143–50.

[59] Y. Huang, M. Hu, S. Yi, X. Liu, H. Li, C. Huang, Y. Luo, Y. Li, Preparation and characterization of silica/fluorinated acrylate copolymers hybrid films and the investigation of their icephobicity, Thin Solid Films, vol. 520, no. 17, 2012, pp. 5644–5651.

[60] L. B. Boinovich & A. M. Emelyanenko, Anti-icing potential of superhydrophobic coatings, Mendeleev Communications, Vol. 23, 2013, pp. 3–10.

[61] H. Hu & Z. Jin, An icing physics study by using lifetime-based molecular tagging thermometry technique, International Journal of Multiphase Flow, vol. 36, no. 8, 2010, pp. 672–681.

[62] E. P. Lozowski & L. Makkonen, Fifty Years of Progress in Modelling the Accumulation of Atmospheric Ice on Power Network Equipment, IWAIS XI, Montréal, Canda, 2005.

[63] ISO-12494, Atmospheric icing of structures, 2001, 56 p.

[64] R. Blackmore & E. Lozowski, A theoretical spongy spray icing model with surficial structure, Atmospheric Research, vol. 49, no. 4, 1998, pp. 267–288.

[65] L. Makkonen, A model of hoarfrost formation on a cable, *Cold Regions Science and Technology*, vol. 85, 2013, pp. 256–260.

[66] L. Makkonen, Modeling power line icing in freezing precipitation, Atmospheric Research, vol. 46, no. 1–2, 1998, pp. 131–142.

[67] L. Makkonen, Modelling of Ice Accretion on Wires, Journal of Applied Meteorology and Climatology, vol. 23, no. 6, 1984, pp. 929–939.

[68] E. P. Lozowski, K. Szilder, L. Makkonen, Computer simulation of marine ice accretion, Philosophical Transactions of the Royal Society A: Mathematical, Physical and Engineering Sciences, vol. 358, no. 1776, 2000, pp. 2811–2845.

[69] W. B. Wright, Users manual for the improved NASA Lewis ice accretion code (LEWICE), NASA, NASA Contractor Report 185129,1995, 231 p.

[70] Y. Han, J. Palacios, S. Schmitz, Scaled ice accretion experiments on a rotating wind turbine blade, Journal of Wind Engineering and Industrial Aerodynamics, vol. 109, 2012, pp. 55–67, Oct. 2012.

[71] L. E. Kollár, O. Olqma, M. Farzaneh, Natural wet-snow shedding from overhead cables, Cold Regions Science and Technology, vol. 60, no. 1, 2010, pp. 40–50.

[72] V. Lehtomäki & E. Peltola, Blade Protection Systems and Their Performance Under Cold Climate Conditions, Optimizing Wind Farms in Cold Climates, presentation, Helsinki, Finland, 2014.

[73] E. A. Podolskiy, B. E. K. Nygaard, K. Nishimura, L. Makkonen, E. P. Lozowski, Study of unusual atmospheric icing at Mount Zao, Japan, using the Weather Research and Forecasting model, Journal of Geophysical Research: Atmospheres, vol. 117, no. 12, 2012 pp.1-24.

[74] F. Lamraoui, G. Fortin, R. Benoit, J. Perron, C. Masson, Atmospheric icing impact on wind turbine production, Cold Regions Science and Technology, vol. 100, 2014, pp. 36–49.

[75] Z. Ghalmi & M. Farzaneh, Experimental investigation to evaluate the effect of PTFE nanostructured roughness on ice adhesion strength, Cold Regions Science and Technology, vol. 115, 2015, pp. 42–47.

[76] R. J. Kind, M. G. Potapczuk, A. Feo, C. Golia, D. Shah, Experimental and computational simulation of in-flight icing phenomena, Progress in Aerospace Sciences, vol. 34, no. 5–6, 1998, pp. 257–345.

[77] K. Knausgård, Superhydrophobic Anti-Ice Nanocoatings, Norwegian University of Science and Technology, dissertation, 2012.

[78] David Sim, Europe weather: Ice storm downs power lines and freezes trees in Austria, Germany and Czech Repulic, International Business Times, 2014. Available (Accessedd 9.9.2015): http://www.ibtimes.co.uk/europe-weather-ice-storm-downs-power-lines-freezes-trees-austria-germany-czech-republic-1477726.

[79] Freezing Rain, Wikipedia, 2015. webpage. Available(Accessed 9.9.2015): http://en.wikipedia.org/wiki/Freezing_rain.

[80] L. Makkonen & B. Wichura, Simulating wet snow loads on power line cables by a simple model, Cold Regions Science and Technology, vol. 61, no. 2–3, 2010, pp. 73–81.

[81] M. Tomaszewski & B. Ruszczak, Analysis of frequency of occurrence of weather conditions favouring wet snow adhesion and accretion on overhead power lines in Poland, Cold Regions Science and Technology, vol. 85, 2013, pp. 102–108, .

[82] Mt. Washington Summit Stock Photos, Ultimate Chase, webpage. Available (Accessed 9.9.2015):http://www.ultimatechase.com/chase_accounts/mount_ washington_summit.htm..

[83] C. Antonini, M. Innocenti, T. Horn, M. Marengo, A. Amirfazli, Understanding the effect of superhydrophobic coatings on energy reduction in anti-icing systems, Cold Regions Science and Technology, vol. 67, no. 1–2, 2011, pp. 58–67.

[84] E.Hill, M. Rios, G, Botura, J.T. Riley, C.J. Dumont, D. Pullin, S. Uppuluri, A. Broeren, M.S. Selig, D.A. Anderson. Investigations of Performance of Pneumatic Deicing Boots , Surface Ice Detectors , and Scaling of Intercycle Ice, U.S. Deparment of Transportation, Federal Aviation Administration, DOT/FAA/AR-06/48, Springfield, Virginia, 2006, 158 p. Available: http://lessonslearned.faa.gov/Comair3272/ar06-48.pdf

[85] P. Laaksonen, Using De-Icing and Anti-Icing Systems to tackle production loss, Optimizing wind farms in cold climates, presentation, Helsinki, Finland, 2014.

[86] H. Gedda, De-icing of wind turbine blades by means of an helicopter opens new opportunities, Winterwind- International Wind Energy Conference, presentation, 2014.

[87] L. Kokkala & A. M. Nodeland, Icing Studies and ENERCON Rotor Blade Heating System (RBHS), Optimizing wind farms in cold climates, presentation, Helsinki, Finland, 2014.

[88] Wicetec Ice Prevention System, Wicetec, webpage. Available(Accessed 9.9.2015) : http://wicetec.com/product-2-2/.

[89] T. V. J. Charpentier, A. Neville, P. Millner, R. W. Hewson, A. Morina, Development of anti-icing materials by chemical tailoring of hydrophobic textured metallic surfaces, Journal of colloid and interface science, Vol. 394 2013, pp. 539–44.

[90] S. a Kulinich, S. Farhadi, K. Nose, X. W. Du, Superhydrophobic surfaces: are they really ice-repellent?, Langmuir : the ACS journal of surfaces and colloids, Vol. 27, No. 1, 2011, pp. 25–29.

[91] L. Cao, A. K. Jones, V. K. Sikka, J. Wu, D. Gao, Anti-icing superhydrophobic coatings, Langmuir : the ACS journal of surfaces and colloids, Vol. 25, No. 21, 2009, pp. 12444–8

[92] H. Dodiuk, S. Kenig, A. Dotan, Do Self-cleaning Surfaces Repel Ice ?, Journal of Adhesion Science and Technology, Vol. 26, No. 4–5, 2012, pp. 701–714.

[93] J. Chen, J. Liu, M. He, K. Li, D. Cui, Q. Zhang, X. Zeng, Y. Zhang, J. Wang, Y. Song, Superhydrophobic surfaces cannot reduce ice adhesion, Applied Physics Letters, Vol. 101, No. 11, 2012, p. 111603-1-11603-3.

[94] A. J. Meuler, J. D. Smith, K. K. Varanasi, J. M. Mabry, G. H. McKinley, R. E. Cohen, Relationships between water wettability and ice adhesion., ACS applied materials & interfaces, Vol. 2, No. 11, 2010, pp. 3100–10.

[95] R. J. Cano, T. M. Smith, C. G. Stevenson, E. C. Martinez, Minimization of Ice Adhesion to Space Shuttle, Journal of Adhesion Science and Technology, Vol. 26, No. 4-5, 2012, pp. 473–503.

[96] R. J. Cano, E. S. Weiser, T. M. Smith, S. Trigwell, L. A. Curtis,D. Drewry, Characterization of an Ice Adhesion Reduction Coating for the Space Shuttle Liquid Hydrogen and Liquid Oxygen Umbilical Systems, Journal of Adhesion Science and Technology, Vol. 26, No. 4-5, 2012, pp. 621–649.

[97] S. Yang, Q. Xia, L. Zhu, J. Xue, Q. Wang, Q. Chen, Research on the icephobic properties of fluoropolymer-based materials, Applied Surface Science, Vol. 257, No. 11, 2011, pp. 4956–4962.

[98] M. Zou, S. Beckford, R. Wei, C. Ellis, G. Hatton, M. A. Miller, Effects of surface roughness and energy on ice adhesion strength, Applied Surface Science, Vol. 257, No. 8, 2011, pp. 3786–3792.

[99] S. Farhadi, M. Farzaneh, S. Simard, On Stability and Ice-Releasing Performance of Nanostructured Fluoro-Alkylsilane-Based Superhydrophobic Al alloy2024 Surfaces, International Journal of Theoretical and Applied Nanotechnology, Vol. 1, No. 1, 2012, pp.38-45.

[100] V. Hejazi, K. Sobolev, and M. Nosonovsky, From superhydrophobicity to icephobicity: forces and interaction analysis, Scientific reports, vol. 3, 2013, p. 2194.

[101] 1H,1H,2H,2H-Perfluorodecyltriethoxysilane, Sigma-Aldrich, webpage. Available (Accessed 10.9.2015): http://www.sigmaaldrich.com/catalog/product/aldrich/658758?lang=fi&region=FI.

[102] S. A. Kulinich & M. Farzaneh, Ice adhesion on super-hydrophobic surfaces, Applied Surface Science, Vol. 255, No. 18, 2009, pp. 8153–8157.

[103] S. a. Kulinich & M. Farzaneh, On ice-releasing properties of rough hydrophobic coatings, Cold Regions Science and Technology, Vol. 65, No. 1, 2011, pp. 60–64,.

[104] S. Iacono, A. Vij, G. Yandek, D. Smith, J. Mabry,A. Peloquin, Fluorinated Polyhedral Oligomeric Silsesquioxanes (F-POSS), Air Force Research Laboratory (AFMC), AFRL-RZ-ED-TP-2010-070, Seattle, USA, 2010, 16p.

[105] R. Jafari and M. Farzaneh, Stable icephobic Teflon-like coatings deposited on an anodized aluminium surface, IWAIS XIV, Chongqing, China, vol. 257, no. 2010, 2011, pp. 1540–1543.

[106] R. Liao, Z. Zuo, C. Guo, A. Zhuang, Y. Yuan, X. Zhao, Y. Zhang, Ice accretion on superhydrophobic insulators under freezing condition, Cold Regions Science and Technology, Vol. 112, 2015, pp. 87–94.

[107] J. G. Drobny, Technology of Fluoropolymers, 2nd ed. CRC Press, BocaRaton, 2009, 227p.

[108] L. Zhu, J. Xue, Y. Wang, Q. Chen, J. Ding, and Q. Wang, Ice-phobic Coatings Based on Silicon-Oil-Infused Polydimethylsiloxane, Applied Materials & Interfaces, Vol. 5, No. 10, 2013.

[109] H. Zhou, H. Wang, H. Niu, A. Gestos, X. Wang, T. Lin, Fluoroalkyl silane modified silicone rubber/nanoparticle composite: a super durable, robust superhydrophobic fabric coating., Advanced materials, vol. 24, no. 18, 2012, pp. 2409–12.

[110] S. a Kulinich & M. Farzaneh, How wetting hysteresis influences ice adhesion strength on superhydrophobic surfaces, Langmuir : the ACS journal of surfaces and colloids, Vol. 25, No. 16, 2009, pp. 8854–8856.

[111] M. Nosonovsky & V. Hejazi, Why Superhydrophobic Surfaces Are Not Always Icephobic, ACS Nano, Vol.6, No. 10, 2012, pp. 8488–8491.

[112] M. F. Hassan, The variation of ice adhesion strength with substrate surface roughness, Measurement Science and Technology, vol. 21, 2010, pp. 1-9.

[113] H. Koivuluoto, C. Stenroos, R. Ruohomaa, G. Bolelli, L. Lusvarghi, and P. Vuoristo, Research on icing behavior and ice adhesion testing of icephobic surfaces, IWAIS 2015, Uppsala, Sweden, 2015.

[114] Q. Zheng & C. Lü, Size Effects of Surface Roughness to Superhydrophobicity, Procedia IUTAM, vol. 10, 2014, pp. 462–475.

[115] R. Dou, J. Chen, Y. Zhang, X. Wang, D. Cui, Y. Song, L. Jiang, Anti-icing Coating with an Aqueous Lubricating Layer, Applied Materials and Interfaces, Vol. 6, No.10, 2014, pp 6998–7003.

[116] G. Momen, R. Jafari, M. Farzaneh, Ice repellency behaviour of superhydrophobic surfaces: Effects of atmospheric icing conditions and surface roughness, Applied Surface Science, vol. 349, 2015, pp. 211–218.

[117] J.B. Boreyko & P. Collier, Delayed frost growth on jumping-drop superhydrophobic surfaces. ACS Nano, Vol. 7 No.2, 2013, pp. 1618-1627.

[118] A. J. Meuler, G. H. McKinley, R. E. Cohen, Exploiting topographical texture to impart icephobicity, ACS nano, Vol. 4, No. 12, 2010, pp. 7048–52.

[119] K. K. Varanasi, T. Deng, J. D. Smith, M. Hsu, N. Bhate, Frost formation and ice adhesion on superhydrophobic surfaces, Applied Physics Letters, Vol. 97, No. 23, 2010, pp. 19–21.

[120] C. Peng, S. Xing, Z. Yuan, J. Xiao, C. Wang, J. Zeng, Preparation and anti-icing of superhydrophobic PVDF coating on a wind turbine blade, Applied Surface Science, Vol. 259, 2012, pp. 764–768.

[121] D. Yu, Y. Zhao, H. Li, H. Qi, B. Li, X. Yuan, Preparation and evaluation of hydrophobic surfaces of polyacrylate-polydimethylsiloxane copolymers for anti-icing, Progress in Organic Coatings, Vol. 76, No. 10, 2013, pp. 1435–1444.

[122] M. Susoff, K. Siegmann, C. Pfaffenroth, M. Hirayama, Evaluation of icephobic coatings—Screening of different coatings and influence of roughness, Applied Surface Science, Vol. 282, 2013, pp. 870–879.

[123] A. Lazauskas, A. Guobienė, I. Prosyčevas, V. Baltrušaitis, V. Grigaliūnas, P. Narmontas, J. Baltrusaitis, Water droplet behavior on superhydrophobic SiO2 nanocomposite films during icing/deicing cycles, Materials Characterization, vol. 82, 2013, pp. 9–16.

[124] Y. He, C. Jiang, X. Cao, J. Chen, W. Tian, W. Yuan, Reducing ice adhesion by hierarchical micro-nano-pillars, Applied Surface Science, Vol. 305, 2014, pp. 589–595.

[125] M. Ruan, W. Li, B. Wang, B. Deng, F. Ma, Z. Yu, Preparation and Anti-icing Behavior of Superhydrophobic Surfaces on Aluminum Alloy Substrates, Langmuir, Vol. 29, No. 27, 2013, pp.8482-8491.

[126] C. Laforte & A. Beisswenger, Icephobic Material Centrifuge Adhesion Test, IWAIS XI, Montreal, Canada, 2005.

[127] Solid surface energy data (SFE) for common polymers. 2015. webpage. Available(Accessed 21.9.2015): http://www.surface-tension.de/solid-surface-energy.htm

[128] R. Karmouch & G. G. Ross, Superhydrophobic wind turbine blade surfaces obtained by a simple deposition of silica nanoparticles embedded in epoxy, Applied Surface Science, Vol. 257, No. 3, 2010, pp. 665–669.

[129] H. Banitalebi Dehkordi, M. Farzaneh, P. Van Dyke, L. E. Kollar, The effect of droplet size and liquid water content on ice accretion and aerodynamic coefficients of tower legs, Atmospheric Research, Vol. 132–133, 2013, pp. 362–374.

[130] C. Laforte and J. Laforte, Deicing Strains and Stresses of Iced Substrates, Journal of Adesion Science and Technology, Vol. 26, 2012 pp. 603–620.

[131] S. Noormohammad, Nanostructured Thin Films for Icephobic Applications, Université du Québec à Chicoutimi, 2009, 159p. Available: http://constellation.uqac.ca/172/1/030112137.pdf

[132] E.M. Yorkgitis, K.C. Melancon, A.M. Hine, S.M. Giaquinto. Glaciphobic Polymer Materials. Journal of Adhesion Science and Technolog, Vol. 26, 2012, pp.681-699.

[133] Z. Ghalmi &M. Farzaneh, Durability of nanostructured coatings based on PTFE nanoparticles deposited on porous aluminum alloy, Applied Surface Science, Vol. 314, 2014, pp. 564–569.

[134] L. Makkonen, Back to the basics : Wettability , icing and ice adhesion, IWAIS 2015, Uppsala, Sweden, 2015.